Coherent Backscattering from Free-Flying Insects

Implications for Remote Species Identification

Li, Meng

2024

Coherent Backscattering from Free-Flying Insects

Implications for Remote Species Identification

MENG LI
DEPARTMENT OF PHYSICS | FACULTY OF ENGINEERING | LUND UNIVERSITY

Coherent Backscattering from Free-Flying Insects

Coherent Backscattering from Free-Flying Insects

Implications for Remote Species Identification

Meng Li

DOCTORAL DISSERTATION

by due permission of the Faculty of Engineering, Lund University, Sweden.

To be defended at Rydbergsalen, The Department of Physics, Professorsgatan 1.

4th of October 2024 at 09.15.

Faculty opponent

Prof. Pete Vukusic, Department of Physics and Astronomy,

School of Physics, Exeter University, UK

Organization: LUND UNIVERSITY

Document name: DOCTORAL DISSERTATION **Date of issue:** 2024-10-04

Author: Meng Li **Sponsoring organization**

Title and subtitle: Coherent Backscattering from Free-Flying Insects

Implications for Remote Species Identification

Abstract: The alarming decline in global insect populations and diversity calls for improved monitoring methods with species specificity. Conventional trapping techniques are labor-intensive and fail to provide real-time *in situ* data on species composition. In response, novel remote and automated monitoring methods have emerged, offering the potential for high-resolution and efficient data collection. However, existing remote sensing techniques, which primarily focus on wingbeat frequencies or direct insect imaging, have inherent limitations. These include the overlap of wingbeat frequencies between species and image challenges of focusing on rapid-moving free-flying insects.

To address these challenges, our research group has developed an entomological lidar, using the Scheimpflug principle to acquire signals across various distances. This approach captures detailed spectroscopic and dynamic features. Lidar could be a realistic photonic solution for monitoring the state of insect populations and diversity. My Ph.D. research investigates how the unique optical properties of insects, as characterized through infrared hyperspectral imaging, can enhance their identification *in situ* through lidar with multiple spectral bands or photonic methodologies. Specifically, I'm exploring how wing reflectance, interference patterns, surface roughness, and polarimetry can improve insect species differentiation. This research also investigates promising methodologies like dual-band and hyperspectral lidar, which could identify insects in flight by their micro- and nanoscopic features.

Entomological Lidar, combined with innovative photonic techniques, could complement or transform insect monitoring. This transformation can enhance pest control strategies, strengthen biodiversity studies, and deepen our knowledge of these crucial organisms.

Keywords: lidar, insect, WIP, fringe, thin-film, hyperspectral, remote sensing, entomology

Classification system and/or index terms (if any) Supplementary bibliographical information

Language: English **ISSN and key title**: 1102-8718

ISBN: 978-91-8104-153-8 (Print) 978-91-8104-154-5 (PDF)

Recipient's notes **Number of pages**: 323

.

Coherent Backscattering from Free-Flying Insects

Implications for Remote Species Identification

Meng Li

LUND
UNIVERSITY

Front cover photos by Meng Li

Back cover photos by Meng Li, Hampus Månefjord, Lauro Müller, Mikkel Brydegaard

Department of Physics, Faculty of Engineering

Lund University

ISBN 978-91-8104-153-8 (Print) 978-91-8104-154-5 (PDF)

LRCP: 257

ISSN 1102-8718

ISRN: LUTFD2/TFCP-257-SE

Printed in Sweden by Media-Tryck, Lund University

Lund 2024

"It's your road and yours alone. Others may walk it with you,
but no one can walk it for you."

- Rumi
Persia, 13th century

Credits: Harry Biggs

Table of Contents

Abstract

The alarming decline in global insect populations and diversity calls for improved monitoring methods with species specificity. Conventional trapping techniques are labor-intensive and fail to provide real-time *in situ* data on species composition. In response, novel remote and automated monitoring methods have emerged, offering the potential for high-resolution and efficient data collection. However, existing remote sensing techniques, which primarily focus on wingbeat frequencies or direct insect imaging, have inherent limitations. These include the overlap of wingbeat frequencies between species and image challenges of focusing on rapid-moving free-flying insects.

To address these challenges, our research group has developed an entomological lidar, using the Scheimpflug principle to acquire signals across various distances. This approach captures detailed spectroscopic and dynamic features. Lidar could be a realistic photonic solution for monitoring the state of insect populations and diversity. My Ph.D. research investigates how the unique optical properties of insects, as characterized through infrared hyperspectral imaging, can enhance their identification *in situ* through lidar with multiple spectral bands or photonic methodologies. Specifically, I'm exploring how wing reflectance, interference patterns, surface roughness, and polarimetry can improve insect species differentiation. This research also investigates promising methodologies like dual-band and hyperspectral lidar, which could identify insects in flight by their micro- and nanoscopic features.

Entomological Lidar, combined with innovative photonic techniques, could complement or transform insect monitoring. This transformation can enhance pest control strategies, strengthen biodiversity studies, and deepen our knowledge of these crucial organisms.

Popular Science

Gotta Catch 'em All: A Real-Life Pokédex for Insect Identification

Does the iconic Pokémon slogan spark a sense of adventure? What if there was a tool that could instantly identify insects like a real-world Pokédex? Scientists are working to turn this dream into reality, and it all starts with understanding the challenges we face.

Conventional methods of insect study can be time-consuming, intrusive, and impractical to scale up. That's why we need new tools to quickly identify these vital creatures without disturbing their natural behaviors. New technologies like automation, remote sensing, and machine learning are being implemented to identify insects. However, challenges exist – insects in flight are hard to track and identifying them using wingbeat frequencies alone has limitations. With millions of insect species on Earth, the task is complex!

To overcome these challenges, our team has developed a specialized tool: entomological lidar. This system uses laser light to monitor insects in flight over distances in the landscape. We can then analyze backscattered light to differentiate species and collect vast amounts of data—imagine recording up to 100,000 insect observations in a single day! This is about 1,000 times more than a standard insect trap can manage. Our technology could be used to track changes in biodiversity and understand insect migration patterns.

Despite the potential, even lidar has trouble pinpointing the exact identity of every insect. That's where my Ph.D. research comes in. I'm exploring how the unique ways in which insect wings interact with light can help with identification. Imagine each species having invisible "fingerprints" on their wings – patterns of color and reflection that hold the key to who they are. Even seemingly dull moth wings exhibit surprising colors and shine when viewed at specific wavelengths. Transparent wings, like those of a fruit fly, display vibrant, soap-bubble-like colors due to a phenomenon called thin-film interference. My research focuses on understanding how the thickness and structure of insect wing membranes scatter light. By enhancing the properties of the light reflected from insect wings, we can improve our systems' ability to detect and identify these insects even at longer ranges.

Our team is actively developing specialized lidar systems to detect these patterns. This tool could transform how we study insects, with far-reaching impacts on precision pest control and conservation efforts and, ultimately, helping us better understand and protect these essential creatures.

Populärvetenskaplig sammanfattning på Svenska

Måste fånga fler: En riktig Pokédex för att identifiera insekter

Föreställ dig ett verktyg som kan identifiera levande insekter direkt i fält, precis som en Pokédex i verkligheten. Ny teknologi kan göra denna dröm till verklighet, och börjar med att förstå de utmaningar vi står inför.

Konventionella metoder för att studera insekter kan vara tidskrävande, svåra att skala upp och ger sällan realtidsinformation, ofta kräver de att vi fångar in eller till och med avlivar individer. Därför behövs nya verktyg för att snabbt identifiera dessa viktiga varelser utan att störa deras naturliga beteende. Banbrytande teknik som automatisering, och fjärranalys, samt datorseende, och maskininlärning utvecklas för att övervaka och identifiera insekter. Men utmaningar finns – insekter i flykt är svåra att fokusera på, och identifiering baserad på vingfrekvens har begränsningar. Med miljontals insektsarter på jorden är snabb bedömning av biologisk mångfald och övervakning av insekter en komplex uppgift.

För att möta behovet av mindre arbetskrävande, kostnadseffektiva, icke-invasiva och storskaliga metoder för långsiktig insektsövervakning, har vårt team utvecklat ett specialiserat verktyg: entomologisk lidar. Detta system använder en laserstråle för att räkna insekter på avstånd i luften. Vi kan sedan analysera det reflekterade ljuset för att skilja arter och samla in enorma datamängder – tänk dig att registrera 100 000 insektsobservationer på en enda dag! Det är 1 000 gånger mer än en vanlig insektsfälla klarar. Vår teknik ger en enorm fördel för att mäta förändringar i biologisk mångfald och förstå insektsmigrationsmönster.

Även lidar har svårt att exakt identifiera varje insekt. Här kommer min forskning in. Jag undersöker hur insektsvingar sprider ljus för att förbättra identifieringen. Tänk dig att varje art har osynliga "fingeravtryck" på sina vingar – mönster av färg och ljusreflektion som avslöjar deras identitet. Till och med bruna nattfjärilsvingar visar överraskande färger med skimmer vid specifika våglängder. Genomskinliga vingar, som hos bananflugor, uppvisar skiftande färger som påminner om såpbubblor på grund av tunnfilmsinterferens. Min forskning fokuserar på hur vingmembranens tjocklek påverkar dessa ljusinteraktioner. Genom att förstå vingars ljusspridning kan vi förbättra identifieringen av insekter på avstånd i fält.

Vårt team utvecklar specialiserade lidarsystem för att detektera dessa mönster. Detta verktyg kan revolutionera insektsstudier med långtgående effekter på skadedjursbekämpning, bevarandeinsatser och vår förståelse av dessa avgörande varelser.

Popular Science in Chinese

《神奇宝贝》图鉴不再是梦：昆虫识别新科技 (科普简介)

还记得《神奇宝贝》的经典口号“Gotta Catch 'em All”吗？这激起了多少人探索大自然的热情！如果真有一款工具能像神奇宝贝图鉴那样，瞬间识别出昆虫种类，那该有多酷？科学家们正努力让这个梦想照进现实。

传统的昆虫研究费时费力，往往需要捕捉甚至杀死样本。我们需要的是既能快速识别这些小生命，又不打扰它们生活的工具。科学家们想到了自动化、遥感和机器学习等先进技术，希望能实现非接触式识别。然而，昆虫飞行轨迹难以追踪，仅凭翅膀振动频率识别种类也有局限性。地球上昆虫种类繁多，要准确识别它们绝非易事。

为了解决这些难题，我们的团队开发了昆虫激光雷达。这个系统利用激光远距离监测昆虫飞行，通过分析反射光来区分不同物种，还能收集海量数据。想象一下，它一天能记录多达 10 万次昆虫观测，是普通诱虫陷阱的 1000 多倍！这将成为追踪生物多样性变化和昆虫迁徙规律的有力工具。

尽管激光雷达很强大，但要精确识别每一种昆虫仍有难度。这时，我的博士研究就派上用场了。我研究昆虫翅膀与光的独特互动方式，希望能改进昆虫识别技术。你可以把每种昆虫的翅膀想象成拥有独特的“指纹”——那些颜色和反射光的纹理就是识别它们的线索。即使看似普通的飞蛾翅膀，在特定波长的光照下也能呈现出令人惊叹的颜色和光泽。透明的翅膀，如果蝇的翅膀，也会因“薄膜干涉”现象而呈现出类似肥皂泡的鲜艳色彩。我的研究重点关注昆虫翅膀膜的厚度和结构如何影响这种独特的光学互动。如果能增强昆虫翅膀反射光的一些特性，我们就能让昆虫识别系统更灵敏，甚至实现远距离精准探测。

我们的团队正积极开发专用激光雷达系统来检测这些特征。这必将给昆虫研究带来革命性变革，造福于精准虫害防治和益虫保护工作，最终帮助我们更好地理解和保护这些重要的小生物。

List of Papers

Paper I

M. Li, S. Jansson, A. Runemark, J. Peterson, C. Kirkeby, A. M. Jönsson, M. Brydegaard, Bark Beetles as Lidar Targets and Prospects of photonic Surveillance, Journal of Biophotonics (2020) (Front page feature).

Paper II

H. Chen†, **M. Li**†, H. Månefjord, P. Travers, J. Salvador, L. Müller, D. Dreyer, J. Alison, T. T. Høye, G. Hu, E. Warrant, M. Brydegaard, Lidar as a Potential New Tool for Monitoring Migratory Insects: A Field Case Study in Sweden, iScience (2024).

† *These authors contributed equally as the first authors.*

Paper III

H. Månefjord, A. S. D. Yamoa, Y. A. Gbogbo, L. Müller, A. Runemark, B. K. Kouakou, R. Boateng, A. A. Huzortey, I. K. Badu, N. Wahlberg, M. Brydegaard, J. T. Zoueu, B. Anderson, **M. Li**, Stratification of Insect Diversity and Daily Activity Patterns in Taï Virgin Forest assessed by Entomological Lidar (Manuscript in preparation) (2024).

Paper IV

D. Bernenko, **M. Li**, H. Månefjord, S. Jansson, A. Runemark, C. Kirkeby, M. Brydegaard, Insect Diversity Estimation in Polarimetric Lidar (Submitted) (2024).

Paper V

D. Dreyer, **M. Li**, H. Månefjord, A. S. D. Yamoa, Y. A. Gbogbo, L. Müller, A. Runemark, B. K. Kouakou, R. Boateng, A. A. Huzortey, J. T. Zoueu, B. Anderson, M. Brydegaard, Dual-Band Lidar and Statistical Moment-Based Assessment of Insect Diversity and Abundance in the Taï Virgin Rainforest (Manuscript in preparation) (2024).

Paper VI

H. Månefjord, L. Müller, **M. Li**, J. Salvador, S. Blomqvist, A. Runemark, C. Kirkeby, R. Ignell, J. Bood, M. Brydegaard, 3D-Printed Fluorescence Hyperspectral Lidar for Monitoring Tagged Insects, IEEE Journal of Selected Topics in Quantum Electronics 28 1-9 (2022).

Paper VII

H. Månefjord, **M. Li**, C. Brackmann, N. Reistad, A. Runemark, J. Rota, B. Anderson, J. T. Zoueu, A. Merdasa, M. Brydegaard, A Biophotonic Platform for Quantitative Analysis in the Spatial, Spectral, Polarimetric, and Goniometric domains, Review of Scientific Instruments 93 (2022).

Paper VIII

M. Li, C. Seinsche, S. Jansson, J. Hernandez, J. Rota, E. Warrant, M. Brydegaard, Potential for Identification of Wild Night-flying Moths by Remote Infrared Microscopy, Journal of the Royal Society Interface (2022) (Featured by National Geographic Society and *Nature*).

Paper IX

M. Li, A. Runemark, N. Guilcher, J. Hernandez, J. Rota, M. Brydegaard, Feasibility of Insect Identification Based on Spectral Fringes Produced by Clear Wings, IEEE Journal of Selected Topics in Quantum Electronics 29 1-8 (2022).

Paper X

M. Li, A. Runemark, J. Hernandez, J. Rota. R. Bygebjerg, M. Brydegaard, Discrimination of Hover Fly Species and Sexes by Wing Interference Signals, Advanced Science (2023) (Front page feature).

Paper XI

H. Månefjord[†], **M. Li**[†], J. Hernandez, L. Müller, C. Brackmann, A. Merdasa, C. Kirkeby, M. D. Bulo, R. Ignell, M. Brydegaard*, The Deadliest Animals with the Thinnest Wings – Near Infrared Properties of Tropical Mosquitoes, Laser & Photonics Reviews (Submitted) (2024).

† These authors contributed equally as the first authors.

Paper XII

L. Müller, **M. Li**, H. Månefjord, J. Salvador, N. Reistad, J. Hernandez, C. Kirkeby, A. Runemark, M. Brydegaard, Remote Nanoscopy with Infrared Elastic Hyperspectral Lidar, Advanced Science (2023) (Featured by NKT).

Paper XIII

M. Li, H. Månefjord, M. Brydegaard, Resolving fast Wingbeat Flashes in situ with Entomological Lidar, IEEE IPC Proceedings (Accepted) (2024).

Related work

A

M. Li, M. Tsuboi, A. Runemark, E. Svensson, M. Brydegaard, Spectral Mating Preferences in Damselfly Species with Potential Evolutionary Implications.

B

M. Li, V. Feng, H. Månefjord, B. K. Kouakou, R. Meier, M. Brydegaard, Integrating Lidar, Computer Vision, and Genetic sequences for Comprehensive Insect Biodiversity Monitoring.

C

J. Salvador, M. Li, H. Månefjord, A. Runemark, C. Kirkeby, S. Jansson, M. Brydegaard, Initial Investigation of Range Dependence of Coherent Backscatter from Free Flying Insects.

Paper Summaries and Author's contribution

Paper I: Bark Beetles as Lidar Targets and Prospects of Photonic Surveillance

M. Li, S. Jansson, A. Runemark, J. Peterson, C. Kirkeby, A.M. Jönsson, M. Brydegaard, Journal of Biophotonics (2020) (Front page feature).

In this paper, we investigated the potential of entomological lidar for monitoring free-flying bark beetles, a destructive pest posing a significant threat to spruce forests and the timber industry. By studying light scattering characteristics, optical properties, wing thickness, and wingbeat frequency of captured beetles, we demonstrated lidar's potential for monitoring both insects and pheromone plumes in a Swedish forest. Specific polarimetric- and spectral properties for pinned bark beetles are presented.

My contributions to this paper included participation in the lidar field campaigns, preparing the samples for scanning, capturing *ex vivo* and *in vivo* data using the entomological chamber, goniometer, and hyperspectral camera, assisting in the analysis of *in situ* data, creating data visualizations, and drafting the manuscript.

Paper II: Lidar as a Potential New Tool for Monitoring Migratory Insects: A Field Case Study in Sweden

H. Chen†, **M. Li**†, H. Månefjord, P. Travers, J. Salvador, L. Müller, D. Dreyer, J. Alison, T. T. Høye, G. Hu, E. Warrant, M. Brydegaard, iScience (2024).

† These authors contributed equally as the first authors.

In this study, we evaluated the feasibility of using lidar technology to monitor migratory insects. We conducted continuous lidar observations in southern Sweden from May to July, coinciding with the insects' yearly northward migration. These observations provided detailed information on insect heights, flight directions, size, and vertical velocities. By implementing polarization bands, we could successfully differentiate moths from other insects despite the challenge of low wingbeat frequencies and short transit times. The challenges and opportunities for our lidar to study their nocturnal flight patterns near the ground are outlined.

My contributions to this paper included designing and conducting the field experiment, helping set up the lidar, developing analysis code, visualizing data, and drafting the manuscript.

Paper III: Stratification of Insect Diversity and Daily Activity Patterns in Taï Virgin Forest assessed by Entomological Lidar

H. Månefjord, A. S. D. Yamoa, Y. A. Gbogbo, L. Müller, A. Runemark, B. K. Kouakou, R. Boateng, A. A. Huzortey, I. K. Badu, N. Wahlberg, M. Brydegaard, J. T. Zoueu, B. Anderson, **M. Li** (Manuscript in preparation) (2024).

In this paper, we conducted a study in the Taï forest of Côte d'Ivoire to investigate the crucial role of virgin rainforests in supporting insect diversity and the effectiveness of the lidar application to assess this. We employed a lidar system and insect trapping to study the distribution and abundance of insects within the forest canopy, revealing distinct activity patterns across different layers. This approach enabled us to monitor insect populations and identify a variety of species based on their optical properties. Multiple beam elevations were employed to decouple lidar range biasing from height over ground preferences. Our findings highlight the ecological significance of undisturbed forests and lidar's potential to assess insect diversity non-intrusively in challenging conditions.

I proposed and obtained a research grant to conduct this expedition. This grant covered participation in the field experiment, instrumentation, and upgrades to the Ivorian lidar, traps, and field equipment. I was responsible for planning the field campaign, proposing several experiments, and participating in the campaign with responsibility for trap sampling, mounting, and documenting species. I calibrated, analyzed, and clustered entomological lidar data, contributed visualizations, and directed and drafted the manuscript together with the first author.

Paper IV: Insect Diversity Estimation in Polarimetric Lidar

D. Bernenko, **M. Li**, H. Månefjord, S. Jansson, A. Runemark, C. Kirkeby, M. Brydegaard (Submitted) (2024).

In this study, we developed an unsupervised method for estimating insect diversity using lidar observations. We applied hierarchical clustering (HCA) and Gaussian Mixture Models (GMM) to group observations based on modulation power spectra derived from retrieved entomological lidar waveforms. To estimate diversity, we propose a criterion based on HCA linkage and use instrument noise as a negative control. Additionally, we explored the potential benefits of incorporating polarization for improved specificity. We investigate to what extent distinct signals are encountered at distinct ranges and hours of the day.

My contributions to this paper included collaborating on the project's planning, participating in the field experiment, supervising an MSc student, and actively engaging in discussions and manuscript contributions.

Paper V: Dual-Band Lidar and Statistical Moment-Based Assessment of Insect Diversity and Abundance in the Taï Virgin Rainforest

D. Dreyer, **M. Li**, H. Månefjord, A. S. D. Yamoa, Y. A. Gbogbo, L. Müller, A. Runemark, B. K. Kouakou, R. Boateng, A. A. Huzortey, J. T. Zoueu, B. Anderson, M. Brydegaard (Manuscript in preparation) (2024).

In this study, we investigated a robust and straightforward method for interpreting lidar signals to directly reflect the biological properties of target insects. We used statistical moments to analyze the behavior and trends within lidar observations, with specific examples provided. Our study employed a dual-band lidar at 980nm and 808nm. We provide reflectance values for wild ensembles of insects, confirming that while melanization explains body reflectance, coherent scatter is necessary to explain wing scatter.

My contributions to this paper included participating in the project's planning, obtaining the grant to conduct an expedition, taking part in the field experiment, assisting with insect trapping, and contributing to manuscript development.

Paper VI: 3D-Printed Fluorescence Hyperspectral Lidar for Monitoring Tagged Insects

H. Månefjord, L. Müller, **M. Li**, J. Salvador, S. Blomqvist, A. Runemark, C. Kirkeby, R. Ignell, J. Bood, M. Brydegaard, IEEE Journal of Selected Topics in Quantum Electronics 28 1-9 (2022).

In this paper, we developed and field-tested a compact, inexpensive hyperspectral fluorescence lidar system designed for studying insect dispersal. Unlike coherent scatter methods, our system relies on fluorescence to identify tagged insects. Our 3D-printed system successfully identified auto-powder-tagged honeybees and free-flying mosquitoes (which had fed on fluorescent-dyed sugar water) under field conditions. This technique offers efficiency and broad applicability, allowing for parallel monitoring of multiple insect groups and facilitating novel ecological experiments.

My contributions to this paper included collaborating on project planning, participating in the field experiment, assisting with insect capture by CO_2 traps, handling and releasing, and contributing to the manuscript.

Paper VII: A Biophotonic Platform for Quantitative Analysis in The Spatial, Spectral, Polarimetric, and Goniometric Domains

H. Månefjord, **M. Li**, C. Brackmann, N. Reistad, A. Runemark, J. Rota, B. Anderson, J. T. Zoueu, A. Merdasa, M. Brydegaard, Review of Scientific Instruments 93 (2022).

In this paper, we describe the development of BIOSPACE (Biophotonics, Imaging, Optical, Spectral, Polarimetric, Angular, and Compact Equipment), a low-cost,

versatile biophotonic instrument. Designed to be accessible for hands-on learning in education and research in low-income countries, BIOSPACE uses multiplexed light-emitting diodes and a synchronized camera for high-quality quantitative analysis of biological targets. We detail the instrument's construction, calibration, evaluation, and diverse functionalities.

My contributions to this paper included participating in planning, assisting with time-of-flight measurements, and writing the manuscript.

Paper VIII: Potential for identification of wild night-flying moths by remote infrared microscopy

M. Li, C. Seinsche, S. Jansson, J. Hernandez, J. Rota, E. Warrant, M. Brydegaard, Journal of the Royal Society Interface (2022) (Featured by National Geographic Society and *Nature*).

In this paper, we investigated the specular infrared reflectance spectra of moth species using polarimetric hyperspectral imaging in the short-wave infrared region. We found that wings exhibited glossy and specular properties at longer wavelengths, revealing distinct optical signatures between species. Our comprehensive modeling and parametrization demonstrated that microscopic wing surface features could be inferred from these infrared properties. These findings hold the potential to significantly improve remote identification of free-flying moths, possibly enabling sensing over considerable distances.

My contributions to this paper include acquiring hyperspectral images during a trip to Norsk Elektro Optikk, Oslo. I also developed analysis and statistical code, visualized data, and drafted the manuscript.

Paper IX: Feasibility of Insect Identification Based on Spectral Fringes Produced by Clear Wings

M. Li, A. Runemark, N. Guilcher, J. Hernandez, J. Rota, M. Brydegaard, IEEE Journal of Selected Topics in Quantum Electronics 29 1-8 (2022).

In this paper, we explored the potential of differentiating insects based on spectral fringes, or interference signals, reflected from their clear wings. We conducted a survey study focusing on 87 common pollinator species in Skåne, Sweden. Using a hyperspectral camera to capture wing interference patterns, we accurately determined wing thickness. Our results demonstrate that distinct modulation patterns and wing thickness can significantly improve species identification using photonic sensors.

My contributions to this paper included designing and collecting hyperspectral data in Norway, visualizing data, and drafting the manuscript.

Paper X: Discrimination of Hover Fly Species and Sexes by Wing Interference Signals

M. Li, A. Runemark, J. Hernandez, J. Rota, R. Bygebjerg, M. Brydegaard, Advanced Science (2023) (Front page feature).

In this paper, we investigated the potential of spectral approaches for remote and automatic insect species identification. We analyzed unique light patterns, known as wing interference signals (WISs), generated by the wings of free-flying insects that could be used for this purpose. Our extensive study of 600 wings from 30 hoverfly species revealed that factors such as wing thickness and heterogeneity, influenced by factors like larval diet and mimicry, could differentiate between species and sexes. Using just five parameters, we achieved 91% accuracy for the differentiation of sexes and closely related species. This highlights the potential of WIS-based surveillance for enhancing our ability to identify and protect insect diversity.

My contribution to this paper included remoistening, spreading, and mounting hundreds of museum specimens. I also traveled to Oslo to acquire infrared hyperspectral data, developed the analysis code, visualized statistics, and drafted the manuscript.

Paper XI: The Deadliest Animals with the Thinnest Wings – Near-Infrared Properties of Tropical Mosquitoes

H. Månefjord†, **M. Li**†, J. Hernandez, L. Müller, C. Brackmann, A. Merdasa, C. Kirkeby, M. D. Bulo, R. Ignell, M. Brydegaard, Laser & Photonics Reviews (Submitted) (2024).

† These authors contributed equally as the first authors.

In this study, we employed photonic monitoring via hyperspectral imaging and laser multiplexing to investigate the spectroscopic properties of mosquitoes. We developed models that could deduce nanoscopic- and microscopic features like wing thickness and absorption paths of melanin and water. The investigation revealed extremely thin mosquito wings of 174 nm with high precision, which could be implemented for lidar and remote sensing of wild insects.

In this paper, my contributions included participating in the hyperspectral imaging, preparing and mounting sub-micron wings of dead mosquitoes as well as immobilizing fresh specimens for scanning. I contributed to the manuscript text and figures.

Paper XII: Remote Nanoscopy with Infrared Elastic Hyperspectral Lidar

L. Müller, **M. Li**, H. Månefjord, J. Salvador, N. Reistad, J. Hernandez, C. Kirkeby, A. Runemark, M. Brydegaard, Advanced Science (2023) (Featured by NKT).

In this paper, we explored the potential of infrared hyperspectral lidar, a type of laser remote sensing, for long-distance insect monitoring and species identification. We developed an infrared hyperspectral lidar system with 64 spectral bands, capable of detecting unique, species-specific wing interference patterns in free-flying insects. As a proof of principle, we successfully retrieved coherent scatter from a damselfly wing, accurately determining its membrane thickness. We also captured signals from free-flying insects, estimated their wing thickness, and detected their wingbeat frequency, demonstrating the potential of this method for differentiating insect species.

My contributions to this paper included participating in fieldwork, preparing samples for scanning, visualizing hyperspectral imaging data, and contributing to manuscript figures and text. MSc student supervision.

Paper XIII: Resolving fast Wingbeat Flashes in situ with Entomological Lidar

M. Li, H. Månefjord, M. Brydegaard, IEEE IPC Proceedings (Accepted) (2024).

In this study, we evaluated the necessary sampling frequency to accurately capture wing modulation across various insect species using a kHz entomological lidar system. By systematically increasing the sampling rate, we assessed the resolution improvements in wing modulation measurements. Additionally, we collected data on environmental factors to understand their impact on the activity patterns of each classified insect group.

My contributions to this paper included discussing the planning, setting up the field experiment, acquiring the experimental data, visualizing and illustrating the figures, and drafting the manuscript.

Abbreviations

BIOSPACE	Biophotonics, Imaging, Optical, Spectral, Polarimetric, Angular, and Compact Equipment
DoLP	Degree of Linear Polarization
eDNA	Environmental DNA
EHSL	Elastic Hyperspectral Scheimpflug Lidar
FPA	Focal Plane Array
HCA	Hierarchical Cluster Analysis
HSI	HyperSpectral Imaging
LED	Light-Emitting Diode
Lidar	Light Detection and Ranging
NBC	Naive Bayes Classifier
NIR	Near-Infrared (in this thesis: 700-1000 nm)
SEM	Scanning Electron Microscope
SWIR	Short-Wave InfraRed (in this thesis: 1000-2500 nm)
ToF	Time-Of-Flight
UV	UltraViolet (in this thesis: 200-400 nm)
VIS	VISible (in this thesis: 400-700 nm)
WBF	WingBeat Frequency
WIS	Wing Interference Signal

1.Introduction

A single bumblebee, its fuzzy body dusted with pollen, might not seem remarkable, yet its tireless flights from flower to flower are vital for the reproduction of countless plant species. But the bumblebee is just one of millions of insect species, each playing a crucial role in the intricate dance of life. From pollinating our crops to recycling nutrients, these tiny creatures are the unsung heroes of our planet, quietly working to maintain the delicate balance of our ecosystems.

1.1. Insects in Ecosystems

1.1.1. Insects' ecological significance

Insect, known as the most abundant and diverse animals on Earth [1-3], and are often overlooked despite playing an undeniably crucial role in the ecological processes that sustain our natural world [4]. Animal pollinators, particularly insects like wild bees and hover flies, are essential for ensuring global food supply. These

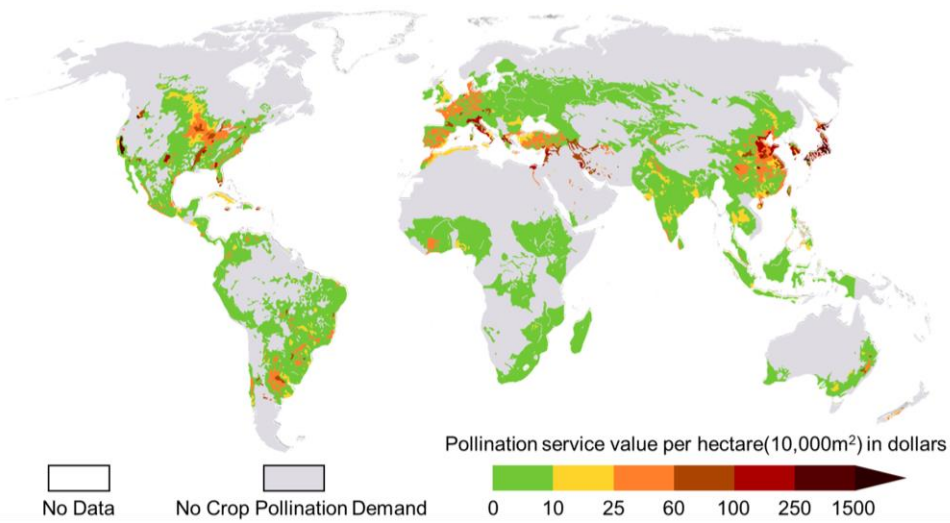

Fig. 1.1: Global map of pollination benefits (2000). The figure is adapted from ref [5].

pollinators underpin the reproduction of roughly 75% of the world's leading food crops [6, 7]. Among them, bees are the most vital group, visiting over 90% of the leading 107 global crop types [8]. This pollination activity has a direct impact on our diets, with 5-8% of our intake by volume being attributable to their work [9]. The global map of pollination benefits shown in Fig. 1.1 highlights the far-reaching economic stability derived from robust pollination services.

As decomposers, insects break down organic matter, which releases essential nutrients into the soil, boosting plant growth [4, 10] and forming the base of food chains [11, 12]. Additionally, many insects are natural pest control agents. Parasitoid wasps, for example, lay eggs inside other insects, controlling populations of crop-damaging pests [13].

However, the relationship between insects and humans is not always mutually beneficial. Some insects are considered serious agricultural and forestry pests, causing significant crop [14-17] or tree farm [18, 19] damage and economic hardship [20]. The spruce bark beetle (*Ips typographus*) is a major pest in European forests, capable of killing millions of trees during outbreaks. This destruction impacts both the forest ecosystem and the timber industry [21-23]. Others, like mosquitoes and disease-carrying flies, represent major public health threats. As illustrated in Fig. 1.2, where the mortality caused by insect-transmitted diseases far exceeds that caused by larger, more traditionally feared animals such as crocodiles or lions. Mosquitoes alone stand out as the world's deadliest animals due to diseases like malaria, dengue, and Zika. Malaria alone caused approximately 627,000 deaths in 2020 [24], disproportionately affecting poorer regions like Africa and Southeast Asia [24-26].

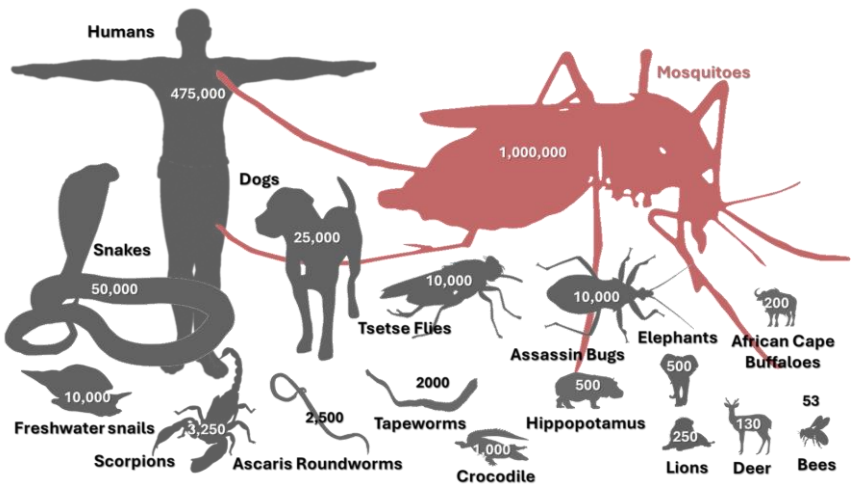

Fig. 1.2: Top 17 of the deadliest animals in the world based on the number of human deaths as of 2016. In the ranking of animals by annual human fatalities, the mosquito holds the grim title. Data is adapted from ref [27].

1.1.2. Biodiversity monitoring and conservation challenges

The monitoring of insect biodiversity is crucial for both the purposes of pest and disease vector control and pollination conservation, yet it faces numerous challenges. Insects are under-represented in general in biodiversity assessments compared with birds, mammals, and plants [29]. This is likely due to insects' small size and the high degree of knowledge necessary for identification often requiring

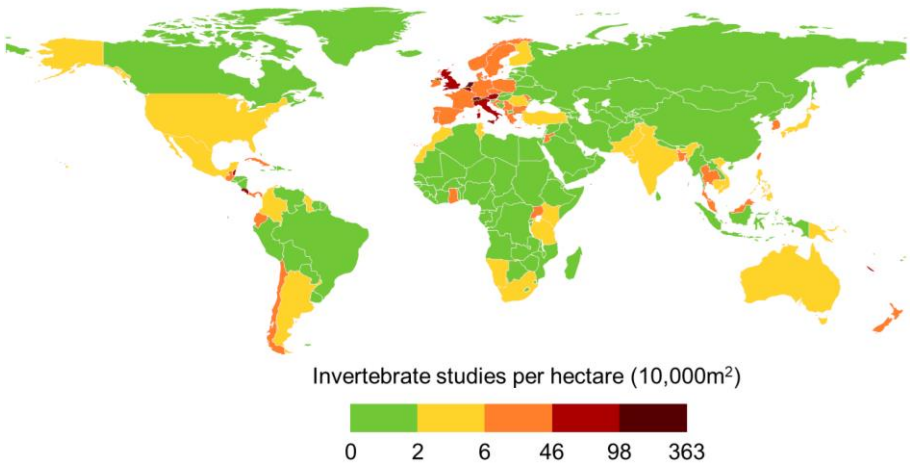

Fig. 1.3: Global map of invertebrate studies. The figure is adapted from ref [28].

experts with a narrow focus on a single insect order or family [30]. Flies and parasitoid wasps, for example, are often overlooked in biodiversity assessments despite their ecological importance [31, 32], simply due to the difficulty of identifying them. These challenges in accurately monitoring insect populations and diversity likely contribute to the significant lack of biodiversity data from highly biodiverse regions such as Africa and South America (as shown by the heterogeneity in research effort depicted in Fig. 1.3. A lack of comprehensive and long-term monitoring policies and methods further hinders conservation efforts [33].

1.2. Existing Approaches to Insect Detection and Identification

1.2.1. Conventional monitoring methods

Conventional methods, long considered the gold standard for monitoring and managing insect populations, often rely on various trapping systems to capture

insects under diverse environmental conditions. In our field campaigns, we utilized several conventional trapping systems to capture insects (see Fig. 1.4).

While conventional insect monitoring systems provide valuable data, they possess inherent limitations. These systems frequently result in insect mortality and offer restricted catching capacities [34]. Additionally, they necessitate specialized taxonomic knowledge for analysis, which is both time-consuming and expensive. Consider the case of a comprehensive study conducted in the San Lorenzo Forest, Panama [35-37], which sought to quantify arthropod species richness within a tropical rainforest. This collaborative effort involved 102 taxonomists and a total of 24,354 trap- (or person-) days of sampling. A total of 300,000 US$ was spent solely on fieldwork to acquire the sample. Despite substantial investment, only 23.7% of the 129,494 arthropods collected from a 0.48-hectare site could be identified to the species level after an 8-year interval, resulting in the identification of 6144 species [37]. This highlights the urgent need for more efficient collection and identification methods, as the time and cost of traditional taxonomy methods severely hinder our ability to develop timely management plans.

Fig. 1.4: Overview of conventional insect trapping methods used in our field campaigns. a-b) Malaise traps: a - canopy, b – ground-based. c) Sweep netting. d) Window trap with soapy water collection box. e) Pheromone trap for bark beetles. f-h) Pan traps in three colors to attract pollinators. i) UV light moth trap. j) Rotational light trap for various timeslots. k) CO_2 and light bait traps for catching blood-sucking insects. l-m) Mosquito traps with CO_2 generation from yeast l) and dry ice m).

1.2.2. Insect identification using wingbeat frequency

Acoustic [38] or electronic traps (E-traps) [39] offer a non-invasive way to capture and identify insects. These devices use sensors to detect and analyze the wingbeat frequencies (WBFs) of flying insects [39-42]. However, a significant challenge for both methods is their limitation in analyzing only one insect at a time, potentially causing bottlenecks in data collection. Additionally, there is considerable overlap in WBFs among different insect species, which can complicate species identification. As shown in Fig. 1.5, The 50 to 200 Hz range is crowded for WBFs, with significant overlap across various orders. This overlap is even more pronounced when considering species-level variations. Environmental factors such as temperature [43-45] and humidity [45, 46], along with biological factors like age [47, 48] and weight loading [49, 50], can also influence WBFs. Even within controlled laboratory environment, individual insects of the same species can display up to 25% variability in their WBFs [51], further complicating the analysis.

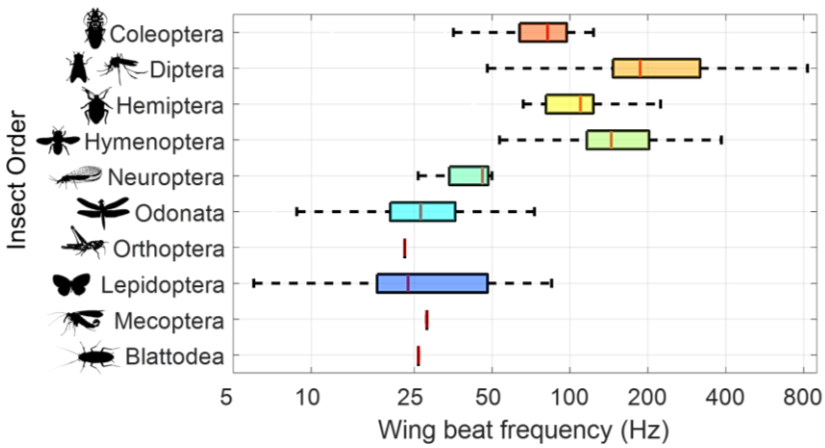

Fig. 1.5: Distribution of WBFs across major insect orders. This data was compiled through a massive literature review by *Noélie Guilcher*. See the accompanying Excel sheet for data sources and values [52].

1.2.3. Machine vision identification

Machine vision offers a practical solution to the challenges of manual insect identification. It can be a non-invasive method that captures images of insects without causing them harm. Camera traps, some equipped with light bait [53] and others without [54], are strategically placed in natural habitats to capture detailed images of insects in their environment. The images are then analyzed using a trained convolutional neural network (CNN) for accurate identification. An example of a camera trap with light bait is shown in Fig. 1.6. CNNs have shown the capability to identify insects down to the family level [55-57] and even species level [58, 59].

These systems can distinguish insects with remarkable precision. However, direct image-based machine vision systems face limitations: image clarity suffers with subject movement or focus issues, and light baits can introduce behavioral bias. These challenges underscore the need for continued refinement of detection techniques, potentially be those aimed at mitigating motion artifacts and reducing reliance on bait, to achieve accurate and unbiased insect identification.

Fig. 1.6: Operation of a machine vision-equipped moth light trap [53]. a) Weather-resistant system with UV light ring, camera, and white sheet. b) Operated at night for optimal moth attraction. c) Attractions of many moths, demonstrating effectiveness. d) Captured high-resolution image.

1.2.4. Genetic methods

Genetic-based techniques are revolutionizing insect biodiversity assessment, providing researchers with powerful new tools and insights.

eDNA analysis involves detecting traces of insect DNA present in their environment [60-62], as animals naturally shed traces of DNA, by collecting samples of air, soil, or even flowers, researchers can identify related species without the need for direct observation. This non-invasive method enables efficient biodiversity surveys, cataloging a wide range of species from environmental samples [60]. However, eDNA degrades quickly [63], and its concentration does not always reflect organism abundance. Contamination risks present additional challenges.

DNA barcoding offers another approach, using a short, standardized DNA sequence from a specimen and comparing it against a reference database [64] to accurately identify the species. Metabarcoding extends this approach to identify multiple species within a mixed sample [65-67]. However, metabarcoding often lacks detailed population-level information, while individual DNA barcoding [68, 69], provides more precise abundance and diversity data while being labor-intensive.

The effectiveness of both techniques relies heavily on the availability of comprehensive and accurate reference databases [64]. Additionally, the DNA extraction process destroys part of the sample. Importantly, neither eDNA nor DNA barcoding directly measures species biomass, a crucial metric for understanding ecological dynamics, abundance, distribution, and the effects of environmental changes. Therefore, integrating these genetic techniques with other methods and continued innovation are crucial to fully utilize their potential for understanding and conserving insect populations.

1.2.5. Radar & Lidar

Since the mid-20th century, radar technology has been used to track the migration patterns of birds, revealing valuable insights into their movements and behaviors [70]. Decades later, this technology was adapted and applied to the study of insect migration [71]. Radar systems, such as the one illustrated in Fig. 1.7, operate by emitting radio waves and analyzing their reflections to detect and monitor large insect swarms within a range of several kilometers [71-77]. This method provides data on migration routes, swarm sizes, and the altitudinal distribution of flying insects, enriching the understanding of their ecological impact. However, traditional radar has difficulty differentiating between insect species and generally works best for larger insects with a substantial radar cross-section [78]. A newer technology, Frequency-Modulated Continuous-Wave (FMCW) radar, allows for even more detailed monitoring of insect movement at lower altitudes (between 0 and 150 m) [79, 80]. FMCW radar's potential for insect detection is promising, but its full capabilities and limitations remain to be seen, as it has not yet been widely deployed in field testing.

Fig. 1.7: Examples of radar and lidar in field research. a) Radar at Stensoffa field station in Sweden generates data on bird migration patterns. b) Lidar in the Tai virgin rainforest, Ivory Coast, provides insights into insect behavior and populations.

While radar technology has proven effective for tracking insect swarms, its limitations in species identification and the detection of smaller insects have spurred the development of alternative remote sensing techniques. Entomological lidar [81-86], a specialized form of Light Detection and Ranging (Lidar), offers a unique and powerful remote sensing approach for detecting insects with improved sensitivity and accuracy [87, 88]. By measuring backscattered laser light, entomological lidar gathers detailed biometric data such as WBF, wing size, and body size. This data provides valuable insights for insect identification [87, 89-91]. The Scheimpflug configuration developed for lidar systems expands their capabilities, enabling the monitoring of insects throughout diverse habitats and over long distances (see *Paper I* and reference [92]). Additionally, ongoing enhancements like polarimetric capabilities (see *Paper II-IV*) and dual-band features (see *Paper V*) are significantly improving precision, allowing us to better estimate diversity indices [92] and gain detailed biological information about the insects.

However, entomological lidar does face certain challenges. The narrow beam can limit its effectiveness for tracking large insects or their swarm migrations. Additionally, pinpointing observations down to the species level remains difficult, as insects can intersect the lidar beam at various angles (see *Papers I* and *VII*). To address this, laboratory systems are used to develop a database of reference signals from insect specimens (see *Paper I* and *VII-XI*). Studies demonstrate that insect features like melanin absorption, body size (affected by gravidity), surface roughness, and nanoscopic wing thickness can aid identification (see *Paper VII-XI* and references [93, 94]). Variables like changes in water and chitin levels reveal valuable information about an insect's state, potentially helping to determine species, sex, gravidity, and age (see *Paper XI*). Multiband lidar can differentiate between these features, and by carefully selecting the correct wavelength for a specific insect species, lidar can maximize the signal reflected from their wings.

Hyperspectral lidar offers a complementary and promising approach for advancing entomological lidar in species identification (see *Paper VI* and *XII* and reference [95]). By capturing spatial, temporal, and spectral characteristics simultaneously, this technology enables the utilization of spectral data, such as wing interference signals, for more accurate species identification of in-flight targets. In addition, ongoing exploration of higher sampling frequencies in lidar systems, as shown in *Paper XIII*, coupled with continuous advancements in hardware and analytical methods, promises to further enhance the capabilities of entomological lidar. This multifaceted approach holds the potential to unlock valuable insights into insect populations, behaviors, and their essential roles within ecosystems.

1.3. Thesis Outline

Paper I lays out the foundational techniques for using entomological lidar to track and monitor insects. It outlines the basic setup and early methodologies developed to differentiate insects based on their biometric data such as body and wing size, as well as wingbeat frequency. This paper sets the stage for subsequent enhancements and applications of lidar technology.

Papers II-IV focus on integrating polarimetric capabilities into entomological lidar systems. These papers explore how polarization enhances detection specificity and identification accuracy across diverse habitats and distances.

Paper V explores the implementation of dual-band features in lidar systems. It enhances the detection of insect biometrics by leveraging different wavelengths to maximize signal reflection from insect wings.

Paper VI introduces the use of fluorescence lidar for detecting specifically tagged insects, expanding the scope of lidar applications in tracking and monitoring ecological behaviors of marked targets.

Paper VII presents BIOSPACE, a cost-effective biophotonic instrument designed to empower research and education in low-resource settings. Demonstrate how BIOSPACE can be used to build a comprehensive insect database, directly enhancing the accuracy and capabilities of our lidar insect identification ability.

Papers VIII-XI explore how stable features such as melanin absorption, surface roughness, and nanoscopic wing thickness enhance species identification for lidar technique. Additionally, variable properties like changes in water and chitin provide valuable information about an insect's state, aiding in the determination of species, sex, gravidity, and age.

Paper XII introduces hyperspectral lidar technology, capturing spatial, temporal, and spectral data simultaneously. This paper focuses on how hyperspectral data can be utilized for detailed species identification, particularly through the analysis of wing interference patterns related to wing thickness.

Paper XIII extends the capabilities of lidar by incorporating high sampling frequencies, pushing the boundaries of detection and analysis of rapid and subtle changes in insect wing modulation.

2.Light-Insect Interactions

Light plays a crucial role in insect behavior and physiology, influencing everything from thermoregulation and signaling to camouflage and warning. When light interacts with insects, it undergoes a complex interplay of reflection, absorption, and scattering. These interactions can be categorized as either incoherent or coherent interactions. Incoherent interactions randomize light's properties, while coherent interactions preserve properties such as directionality and phase to some extent. A deep understanding of these light-insect interactions is essential for developing advanced remote sensing technologies such as entomological lidar. In this chapter, we delve into how the properties arising from the interaction between light and insects can be used to assist in the development of species-specific detection methods.

2.1. Incoherent Phenomena

Imagine shining a flashlight through your hand - you see a reddish glow, but not the details of your bones. This is due to incoherent light-matter interactions. As light passes through your hand, it scatters and diffuses, losing its original direction, polarization, and phase. This randomization of light properties is caused by absorption and scattering within a medium. The interplay of incoherent interactions enables the development of systems that can either reduce unwanted incoherence for improved signal strength or leverage these unique scattering characteristics for a variety of applications, such as differentiating insect species based on their water content and scattering coefficients.

2.1.1. Absorption

Insects are primarily defined by their exoskeleton, a crucial external structure that provides support and protection and facilitates movement [96]. This exoskeleton, composed mainly of chitin, a biopolymer, exhibits a strong absorption band around 280 nm in the ultraviolet spectrum [97, 98] (Fig 2.1a). This absorption decreases towards the visible and infrared ranges, where it becomes transparent.

In addition to chitin, melanin (eumelanin) is a key factor component influencing the varied coloration of insects. It is the predominant pigment in the animal kingdom [99] and plays a significant role in determining the colors seen in insects [100], especially within the visible spectrum. Melanin exhibits broad absorption, and it is responsible for dark coloration in animals, see Fig. 2.1b. In the case of insects, melanin is generally highly concentrated in the dark spots of the eyes, legs, or patches on the body [100]. For butterflies, melanin helps thermoregulation by absorbing solar radiation across a wide range of wavelengths [101, 102]. Melanin also provides protection against UV light to mitigate the harm it potentially does to DNA [103].

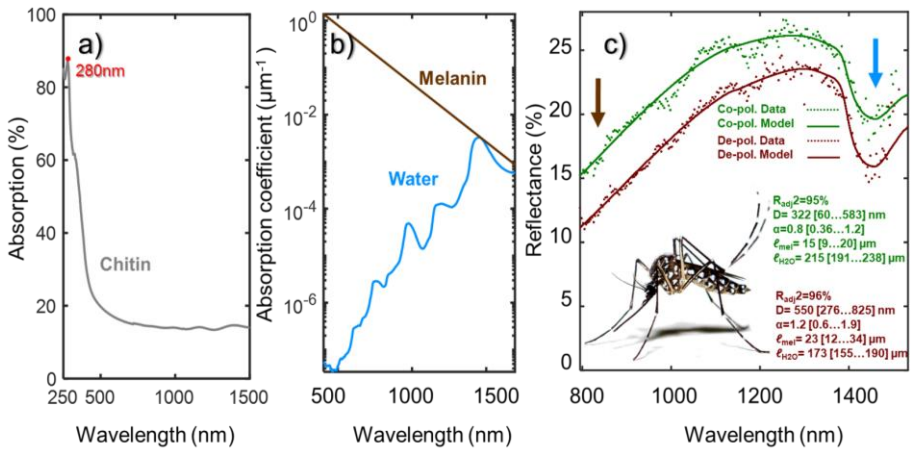

Fig. 2.1: Optical properties of Insect. a) Absorption spectrum of chitin, data originally from reference [98]. b) Absorption spectra of melanin (eumelanin) and water, data originally from references [104, 105]. c) Reflectance spectrum of live mosquitos measured with a hyperspectral camera, revealing strong melanin and water absorption features, highlighted by brown and blue arrows in the graph (adapted from *Paper XI*).

Another strong absorber within insects is water, which is also a dominant absorber within most biological tissues [104]. Water is a major component of the insect body, particularly concentrated in the thorax. This high water content greatly affects an insect's overall weight, as demonstrated in a study [106] where wet insects were found to be 2.1 times heavier than their dry mass. In the NIR wavelength region, water displays strong absorption bands around 1450 nm due to the vibrational modes of the water molecule [105]. This 1450 nm water absorption is evident in the hyperspectral reflectance scan of live mosquitoes, see Fig. 2.1c. The water characteristic has been used as a critical factor in remote sensing before, such as in environmental monitoring for detecting water content in leaves [107] or used in radar cross-section measurements of birds and insects to estimate their weight [108, 109]. Additionally, variations in water content can serve as indicators of different physiological states of insects, such as dehydration or feeding status [110], aiding in ecological studies and pest management strategies.

The Beer-Lambert Law, a fundamental principle in spectroscopy, quantifies the relationship between light absorption and the path length through an absorbing medium. It states that the transmitted light intensity decreases exponentially with increasing path length and concentration of the absorber,

$$I(\lambda) = \mathrm{I}_0(\lambda)\mathrm{e}^{-\mu(\lambda)\ell} \tag{2.1}$$

where $I(\lambda)$ is the intensity of the transmitted light, $I_0(\lambda)$ represents the initial light intensity, $\mu(\lambda)$ is the wavelength-dependent absorption coefficient, and ℓ is the effective path length. To take into consideration the absorption caused by both the water and eumelanin, the term 'Absorbance' $A(\lambda)$ was introduced into the study to describe the absorption in the insects,

$$A(\lambda) = \ell_{H_2O}\mu_{H_2O} + \ell_{mel.}\mu_{mel.} \tag{2.2}$$

where ℓ_{H2O} and ℓ_{mel} are the equivalent water and melanin path lengths. μ_{H2O} and μ_{mel} is the wavelength-dependent absorption coefficients for water [111] and melanin [112].

Insects have evolved to leverage these absorption characteristics for camouflage, mating signals, and mimicry, enhancing their survival [113] and reproduction [114, 115]. Insect absorption characteristics are key to developing tools and models that quantify and predict their properties. For example, dual-band lidar systems utilizing wavelengths differentially indexing the melanin absorption (e.g., 808 nm and 980 nm) enable remote estimation of melanin content (see *Paper V*). Additionally, models can be developed to describe and estimate the effective path lengths of melanin and water within insects (Fig. 2.1 c and *Paper XI*).

2.1.2. Incoherent scattering

Incoherent scattering occurs when light is randomized, losing its dependence on direction, phase, and polarization prior to target interaction. When absorption is absent, this often results in a white matte appearance. This suggests that the white parts of an insect, such as the body or legs, or in the case of a gravid mosquito, the eggs within its abdomen, likely result from incoherent scattering of light (Fig. 2.2a). Polarimetric studies offer another way to investigate the origin of incoherent scattering. The image in Fig. 2.2b, showing de-polarized incoherent light signals from a pinned dried specimen, reveals that these signals predominantly originate from its veins and body.

The scattering coefficient is used to quantify the degree of scattering caused by the insect. The scattering properties of insects vary with several factors. For example, the amount of light scattered by mosquitos varies when they are gravid [94]. Additionally, insects with more water in their bodies scatter light differently than dehydrated insects. The scattering properties of insects can also change significantly

in their early development during the first few days after hatching, gradually stabilizing as the insect ages [116].

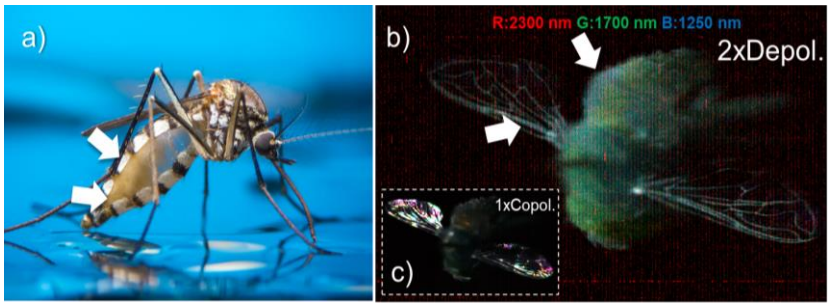

Fig. 2.2: Examples of incoherent scattering sources. a) An image of a pregnant mosquito, with its abdomen and setae on the body and legs displaying white colors (originally from reference [117]). b-c) False color polarimetric image of a hover fly (*Eristalis arbustorum* male), highlighting incoherent (de-polarized) signals originating from the veins and body. De-polarized component amplified 2x (1x Copol) for clarity.

To model light transport within a scattering medium like an insect body, the Kubelka-Munk theory was employed for diffuse reflectance (equation 44 from reference [118]). This theory is particularly suitable for '*thin specimens of poorly scattering material*.' In biological tissue, scattering is generally described sufficiently by a power law [119, 120]. In analogy with the term *Absorbance* the term '*Scatterance*' *S(λ)* was introduced, to represent the spectral dependent scattering:

$$S(\lambda) = \left(\frac{D_{½}}{\lambda}\right)^{\alpha} \tag{2.3}$$

Here, $D_{½}$ is the wavelength at which half of the light is reflected without absorption or transmission, acting as a gain factor for diffuse reflectance. The dimensionless parameter α governs the spectral shape of the scattering, allowing for adjustments in the spectral response. Based on Kubelka-Munk theory, the total diffuse reflectance from an insect can be described by the formula R_{diff},

$$R_{diff}\,(\lambda) = \frac{S}{1+S+A} \tag{2.4}$$

where A denotes the absorbance, as previously defined in equation 2.2. R_{diff} approaches 100% as S becomes very large and R_{diff} approaches 0% as A becomes very large. Additionally, R_{diff} is 0 when S is 0. This model effectively describes the spectral signal in Fig. 2.1c, with the resulting parameter values shown in the same figure.

The diffuse reflectance equation was simplified by setting A=0 to investigate the white spots present on the yellow fever mosquito (*Aedes aegypti*) in *Paper XI*. White coloration in thin objects is an unusual phenomenon, primarily because photons tend to escape before undergoing multiple scattering events [121-123]. Moreover,

nanostructures that strongly scatter visible light typically scatter less in the infrared range when their size is smaller than the wavelengths. Through the analysis, the reflectance characteristics of these white spots of *Aedes aegypti* can be accurately described using a short-pass filter function.

$$R_{spot(\lambda)} = \frac{1}{1+\left(\frac{\lambda}{D_{½}}\right)^{\alpha}} \tag{2.5}$$

In *Paper XI*, the parameter $D_{½}$ is found to be 1215 nm, and the parameter α is determined to be 4.2. This model confirms that the white spots on the *Aedes aegypti* mosquito exhibit high reflectance within the visible range (below 600 nm) and a gradual decline in reflectance at longer wavelengths.

2.1.3. Anisotropy factor g and phase function

When considering insects as lidar targets, it is essential to analyze how an insect as a whole interacts with and scatters light. This involves determining whether more light is scattered forward (in the original direction of travel) or backward (towards the light source). The anisotropy factor g is a useful parameter for quantifying the directional preference of scattered light from an object. It ranges from -1 (pure backward scattering) to 1 (pure forward scattering), with 0 indicating isotropic scattering (equal scattering in all directions). Larger objects typically exhibit forward scattering ($g > 0$), while smaller particles may show backward scattering ($g < 0$). The anisotropy factor g is defined [124] as:

$$g = \int_0^{\pi} p(\theta)\cos(\theta)\mathrm{d}\theta \tag{2.6}$$

where $p(\theta)$ represents the phase function, describing the angular distribution of scattered light, and θ is the scattering angle. The anisotropy factor summarizes scattering behavior, but directly measuring the phase function is more informative. This function reveals the precise pattern of light scattering at various angles. In *Papers I* and *VII*, the phase function of examined insect species was recorded using a goniometric system.

An example of a phase function measurement is shown in Fig. 2.3. This figure illustrates how light scatters off a target insect, with the resulting patterns for co-polarized and de-polarized light indicating whether scattering is predominantly forward or backward. In this specific case, strong forward scattering is observed for co-polarized light at the given wavelength, even when wings and elytra are removed (Fig. 2.3j, k). This persistent forward scattering might be attributed to the relatively small size of the bark beetle body, resulting in fewer scattering events that would otherwise randomize the light's direction. For de-polarized light, when the insect is turned sideways, the strong forward scattered signal is reduced (Fig. 2.3l, m). Insects with strong forward or backward light scattering are best studied using experimental setups with detectors positioned accordingly. Forward scattering is suited for

extinction measurements (e.g., eBOSS system in the study [106]) while backscattering benefits from single-ended systems such as entomological lidar [125, 126]. This matched configuration maximizes signal capture while using lower-intensity light sources for eye safety.

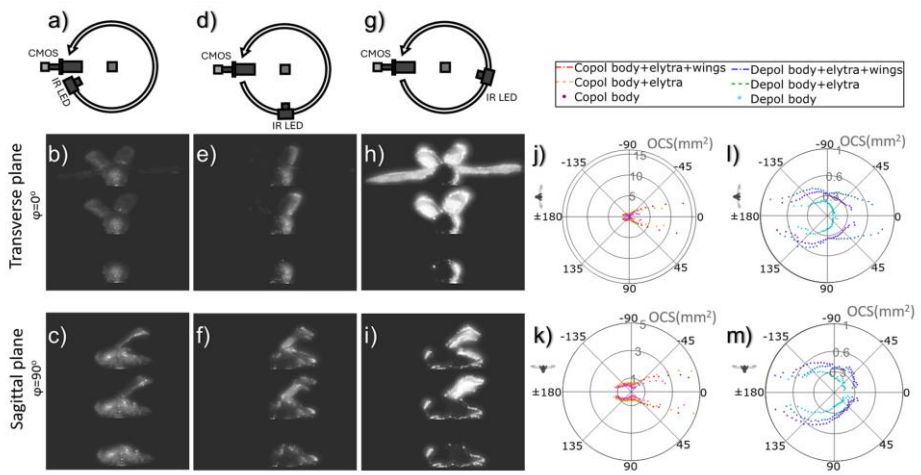

Fig. 2.3 illustrates the scattering phase function of a bark beetle, with and without wings and elytra, under co- and de-polarized light (808 nm). The experiment involved rotating the illumination source around the mounted sample, capturing images at various angles with the camera, including backscatter a), side scatter d), and near-extinction g). Images b, e, h) show the beetle illuminated along its transverse plane at positions a), d), and g) respectively, while images c, f, i) show illumination along the sagittal plane at the same positions. The recorded phase functions for two specimens at different anatomical planes are shown, differentiating between co-polarized j, k) and de-polarized l, m) signals. Data adapted from *Paper I*.

2.2. Partially Coherent Phenomena

Random organized biological tissues lack a dominant spatial frequency and thus primarily contribute to incoherent scattering [104, 124]. The organized, periodic structure of biological tissue with dominant spatial frequencies leads to contributions to coherent scattering [127-129], which can result in various optical effects depending on the symmetry and orientation of these frequencies, including iridescent [130], non-iridescent [131], grating [132], or thin-film [133, 134] patterns.

This relationship between structural organization and light scattering behavior in biological tissue is revealed through 2D Fourier analysis [135]. Fig. 2.4 illustrates this relationship between structural color and the arrangement of collagen fibers in

birds. Examples in Fig. 2.4a-d show the highly organized arrangement of fibers within green caruncles, producing a Fourier transform with distinct peaks. This frequency pattern indicates a clear, repeated structure in certain directions, demonstrating the regular spacing and alignment of the collagen fibers, see Fig. 2.4d. In contrast, less organized but still patterned fibers within light blue caruncles in Fig. 2.4e-h result in a ring-shaped transformation. Broader peaks in the 1D Fourier power spectra in Fig. 2.4h reflect this less defined structure, resulting in a spread in spatial frequency and some diffuse signal from the non-organized parts. In the case of diffuse white tissue Fig. 2.4i, lacking organized structure, the Fourier transform power spectra are characterized by a continuous distribution of spatial frequencies with a gradual decrease in power at higher frequencies. While 2D Fourier analysis is informative, this approach can be extended to 3D using electron tomography, albeit at a higher computational cost.[128].

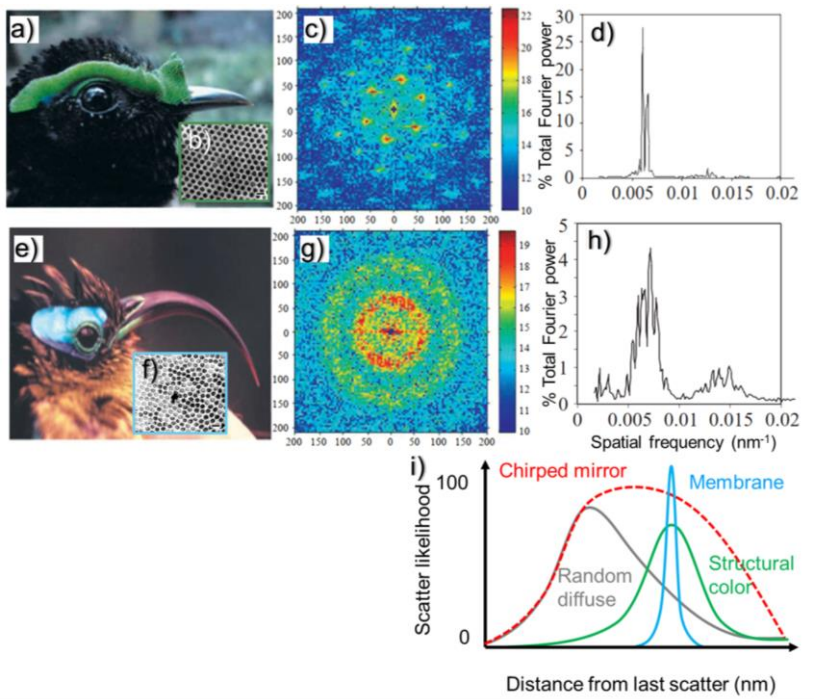

Fig. 2.4: Structural coloration in birds, arising from the organization of collagen arrays within their caruncles. Shown are: a,e) *Philepitta castanea* (green caruncles) and *Neodrepanis coruscans* (light blue caruncles) with their respective structurally colored caruncles; b,f) Transmission electron micrographs of color-producing collagen arrays from these caruncles; c,g) Corresponding 2D Fourier power spectra, revealing the spatial organization of the collagen; and d,h) Normalized radial averages of single quadrants of the power spectra. (All figures from a-h) adapted from reference [135]) i) Illustration of Fourier power spectra differences between organized (structural color) and unorganized (diffuse white) tissues.

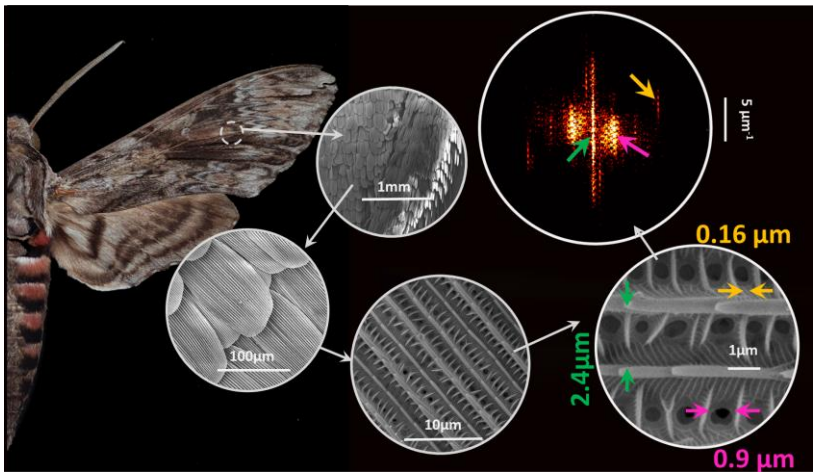

Fig. 2.5: Scanning electron microscope (SEM) study of the surface structure of a brown moth (*Agrius convolvuli*) wing scale. The 2D Fourier power spectrum reveals multiple periodicities across the surface, with each corresponding periodicity pattern marked.

Just as the structural organization of collagen in birds affects how it scatters light, the same principle applies to the varied colors found in insects. The composition of chitin, water, and melanin, along with the arrangement of biological structures, gives rise to both incoherent (diffuse) [122, 136] and coherent (specular) reflectance [125, 137]. In those studies (*Papers III*, *VII*, *VIII*, *X*, *XI*), BIOSPACE and a polarimetric hyperspectral camera were utilized to separate incoherent and coherent signals from insect wings. In *Paper VIII*, the repetitive patterns on rough brown moth wing scales were investigated using 2D Fourier power spectra analysis of SEM images (one example is shown in Fig. 2.5, examining the lateral, XY frequencies across the surface.). The dominant spatial frequencies identified in the Fourier transform of the SEM images were then correlated with the spectroscopic features deduced from the infrared properties of the wing scales, highlighting the relationship between surface structural arrangement and infrared reflectance properties.

2.2.1. Surface roughness

The wings of both clear-winged and diffuse-winged insects can exhibit a rough surface, particularly evident at visible wavelengths [138, 139]. While insect wings may appear as a thin, flat layer of chitin, their uneven surfaces arise from various factors. For instance, the clear wings of the female mosquito (*Aedes aegypti*), as shown in Fig. 2.6, have veins and hair-like structures [140] that scatter light, leading to a reduction in the specular signal [141]. Other factors contributing to the roughness of clear wings include refractive indices gradient within the membrane

[132] leading to anti-reflection. The deformation during downstrokes [142], further reduces specular scattering and enhances diffuse reflectance. In Lepidoptera, the wings are covered in scales see Fig. 2.6c, d, which are chitinous biological structures with micro and nano-scale features [139, 143, 144]. These scales can significantly increase surface roughness, leading to incoherent scattering if they lack organized structures.

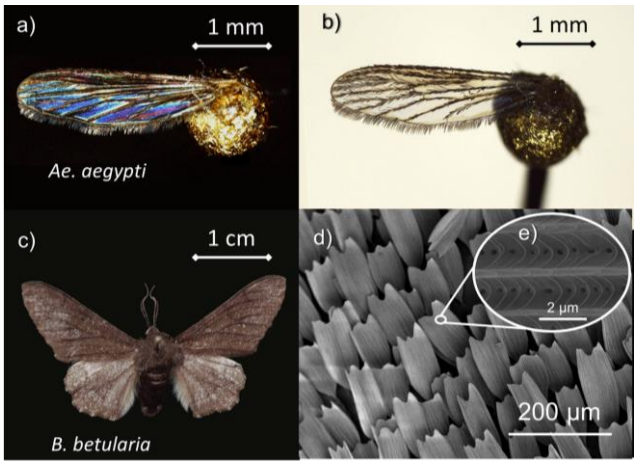

Fig. 2.6: Both clear and diffuse wings do not have a flat, perfect membrane chitin surface. a, b) Microscopic images of the *Aedes aegypti* female mosquito wing. A strong wing interference pattern is visible when the wing is placed against a black background. c) Photograph of a *Biston betularia*. d,e) SEM image of the microstructure on the surface of the moth wing.

The perceived roughness of insect wings can decrease as the wavelength of light used to observe them increases. If the wavelength is not short enough to resolve the lateral (XY) micro and nano-scale structures, the wings could appear specular (smooth) at certain wavelengths. Imagine illumination with a short wavelength as ping-pong balls scattering randomly off a rough surface (diffuse reflection), while longer wavelengths, like basketballs, bounce predictably (specular reflection), see Fig.2.7.

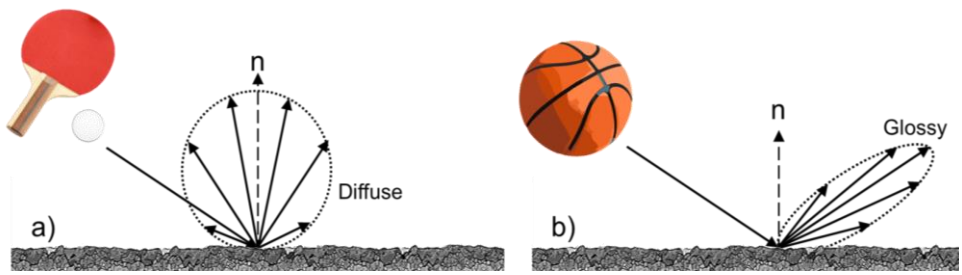

Fig. 2.7: Wavelength influences light reflection on a rough surface. a) short wavelengths scatter diffusely off a rough surface (like ping-pong balls bouncing off an uneven floor). b) longer wavelengths exhibit more focused, specular reflection (like basketballs maintaining a predictable trajectory on the same surface).

This wavelength-dependent scattering phenomenon has implications for lidar detection of insects, particularly those with rough wing structures like Lepidoptera.

A wing with low roughness makes a flash in lidar during wingbeat when the surface normally aligns with the beam. Therefore, smooth wings produce many harmonics. By translating lidar to mid- or long-wave infrared wavelengths, the apparent roughness of these wings can be reduced, as shown in *Paper VIII*, which can effectively mitigate the reduction in specular reflection caused by wrinkles, scales, or index gradients. This results in a stronger and more focused backscatter signal, enhancing detection capabilities and enabling species identification through the analysis of unique scattering patterns and resonant backscattering bands with lidar. This approach has been used in optical engineering and metrology since the invention of the CO_2 laser at 10.6 μm used to make unpolished surfaces appear specular [145, 146].

2.2.2. Bidirectional reflectance distribution function

The Bidirectional Reflectance Distribution Function (BRDF) was used to investigate how the perceived roughness of insect wings changes with varying wavelengths of incident light [147, 148]. The BRDF quantifies light reflection from a surface, considering incident and reflected light directions and wavelength, as the ratio of reflected radiance to incident irradiance. The BRDF has found applications in various fields, including digital imaging of heritage sites [149] and satellite imaging [150]. This function follows the principles of reciprocity and energy conservation [151],

$$R_\lambda(\theta_\mathrm{i}, \varphi_\mathrm{i}, \theta_\mathrm{r}, \varphi_\mathrm{r}) = \frac{I_\mathrm{r}(\theta_\mathrm{r},\varphi_\mathrm{r})\mathrm{d}\omega_\mathrm{r}}{I_\mathrm{i}(\theta_\mathrm{i},\varphi_\mathrm{i})\cos\,\theta_\mathrm{i}\mathrm{d}\omega_\mathrm{i}} \tag{2.7}$$

here, $I_r(\theta_r,\varphi_r)$ is the reflected light intensity within solid angle $d\omega_r$, and $I_i(\theta_i,\varphi_i)$ is the incident light intensity within solid angle $d\omega_i$, see Fig. 2.8.

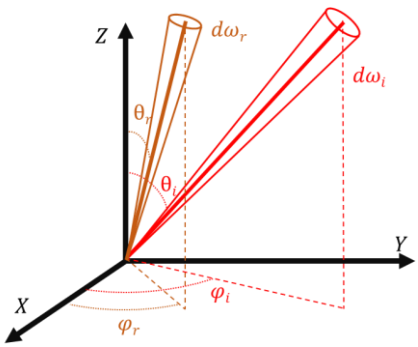

Fig. 2.8: The relationship between the reflected light intensity $I_r(\theta_r,\varphi_r)$ and the incident light intensity $I_i(\theta_i,\varphi_i)$. The figure is adapted from ref [151].

To model diffuse reflectance using the BRDF [149], the standard model is Lambertian scattering. In a Lambertian distribution, the BRDF, denoted as $R_\lambda(\theta_i,\phi_i,\theta_r,\phi_r)$, as the surface appears equally bright from all viewing angles. To

account for surfaces that deviate from ideal Lambertian behavior, this model can be modified with a 1/*r* term.

$$I = I_0 \cos^{\frac{1}{r}}(\theta) = I_0 \sqrt[r]{\cos\theta} \tag{2.8}$$

where *r* represents surface roughness. Here, *r* = 1 is a perfect Lambertian diffusor, and *r* = 0 is a perfect mirror. Note that conservation of brightness prevents the exponent from being less than 1, so *r* must always be between 0 and 1. The relationship between the BRDF definition of surface roughness and the angular spread of the scattered light lobes is illustrated in Fig. 2.9 with examples of different surface roughness.

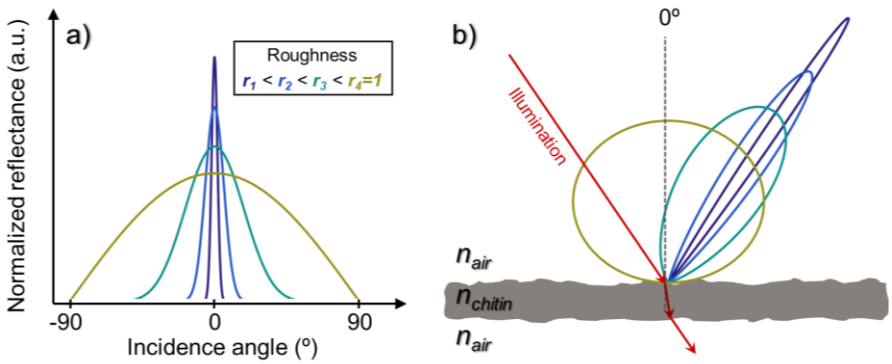

Fig. 2.9: How the bidirectional reflectance distribution function (BRDF) defines surface roughness. a) BRDF definition of surface roughness ($r_1 < r_2 < r_3 < r_4$), the smaller the *r* is, the less rough the surface is. b) The angular scatter lobe for different degrees of surface roughness. The figure is adapted from ref [152].

The specular reflectance model builds upon the diffuse model in equation 2.8. To capture the dependency of specular reflectance lobes on incident light, a symmetric link function, $F_{link}(\theta, \theta_0)$, with the property $F_{link}(\theta, -\theta) = 0°$ (maximum of the cosine function) was incorporated. This guarantees that incident and reflected light angles are symmetrical. Moreover, θ_0 was scaled by 1 – r, ensuring that the reflectance lobe of a perfect diffuser aligns with the surface normal, thus becoming equivalent to Lambertian reflectance:

$$I(\theta, \varphi) = I_0 \left(\cos\left(F_{\text{link}}(\theta, (1-r)\theta_0) \cos\left(F_{\text{link}}(\varphi, (1-r)\varphi_0) \right) \right) \right)^{1/r} \tag{2.9}$$

$$r \in 0 \ldots 1$$

$$F_{\text{link}}(\theta, \theta_0) = 90° \left(\left(\frac{\theta + 90°}{180°} \right)^{\frac{-\log(2)}{\log\left(\frac{90° - \theta_0}{180°}\right)}} - \left(\frac{90° - \theta}{180°} \right)^{\frac{-\log(2)}{\log\left(\frac{\theta_0 + 90°}{180°}\right)}} \right) \tag{2.10}$$

$$\theta, \theta_0 \in -90° \ldots + 90°$$

$$\int_{-90^\circ}^{+90^\circ} I(\theta,\varphi)d\theta d\varphi = 1 \tag{2.11}$$

The BRDF model was used to calculate the 180° backscatter from a moth using a vertically positioned polarization lidar in *Paper VIII*. The dynamic wing roll and pitch were adopted from a previous study [153]. The backscattered reflectance during the wingbeat was multiplied by the ventral projected wing area during the wingbeat, and the optical cross-section was obtained as a function of time. The de-polarized signal is modeled with r = 1. This model does not account for light diffraction and directional reflectance caused by the grating-like structures on the scales. These periodic features likely vary in alignment across the wing.

The BRDF model was also employed to investigate the surface roughness of clear wings in a recent master's project [152], to examine the relationship between the surface roughness of clear wings and the spectral fringes (calibrated as an optical cross-section in this example), see Fig. 2.10. The project revealed an inverse correlation between surface roughness and spectral fringe characteristics, specifically the intensity and spacing, especially in visible wavelengths. Wing veins were identified as the primary contributors to diffuse scattering, while wing membranes were mainly responsible for specular reflection.

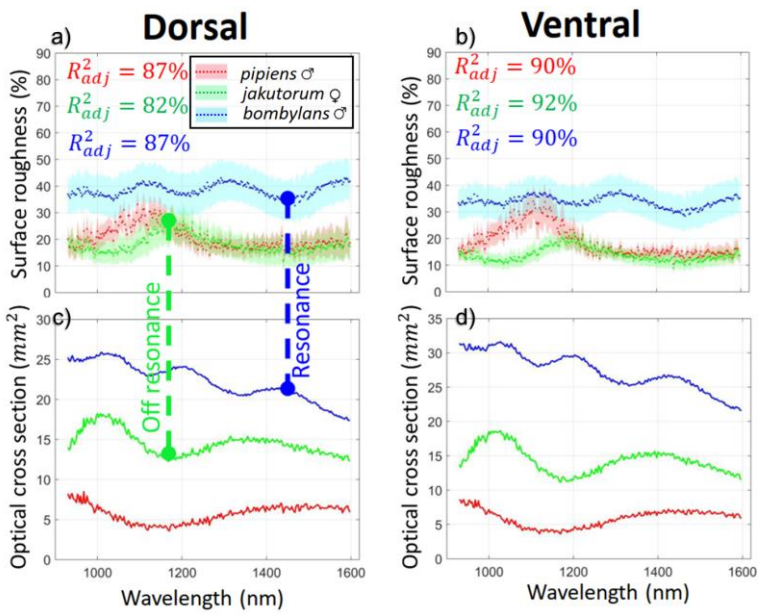

Fig. 2.10: Relationship between the estimated surface roughness and reflectance of hover flies clear wing. a) Estimated surface roughness on the dorsal (top) side of the wing. b) Estimated surface roughness on the ventral (bottom) side of the wing. c) Reflectance spectra from the dorsal side of the wing. d) Reflectance spectra from the ventral side of the wing. Surface roughness increases off-resonance. The figure is originally from [152].

2.2.3. Specular and diffuse reflection

Insect reflectance can be separated into incoherent (diffuse) reflectance, R_{diff}, and coherent (specular) reflectance, R_{spec}. Diffuse reflectance arises from light undergoing multiple scattering events within the insect's body, such as within the abdomen or eggs. Specular reflectance, on the other hand, occurs when light interacts minimally with the insect's body, as in reflections from the thin membrane wings or tiny legs. Although specular reflection from insect surfaces is rare, it can far exceed diffuse reflection when the surface normally aligns with the light source and detector. Notably, while average insect reflectance in the NIR is around 20% [137, 154], specular components can be partially collimated, enabling detection over greater distances than diffuse reflectance [98, 155]. All work included in this thesis primarily focused on the NIR and SWIR regions, where melanin [112, 156] and water [111, 157] are the main absorbers in insects.

To quantify both specular and diffuse reflectance, a Kubelka-Munk model was previously employed [118], where *Absorbance A* (equation 2.2), *Scatterance S* (equation 2.3), and total reflectance (combining specular and diffuse components) are expressed as:

$$R_{\text{spec.}} = \left| R_{\text{copol. }(\lambda)} - R_{\text{depol. }(\lambda)} \right|_{\text{median}} \tag{2.12}$$

$$\hat{R}_{\text{body}}(\lambda) = R_{\text{spec.}} + R_{\text{diff}}(\lambda) = R_{\text{spec.}} + \frac{S}{1+S+A} \tag{2.13}$$

$$\hat{R}_{\text{body}}(\lambda) = R_{\text{spec.}} + \frac{\left(\frac{D_{½}}{\lambda}\right)^{\alpha}}{1+\left(\frac{D_{½}}{\lambda}\right)^{\alpha} + \ell_{H_2O}\mu_{H_2O(\lambda)} + \ell_{\text{mel}}\,\mu_{\text{mel }(\lambda)}} \tag{2.14}$$

where $D_{½}$ is the wavelength of 50% reflectance, α adjusts the spectral shape, ℓ_{H2O} and ℓ_{mel} represent absorption in water and melanin respectively, and $\mu_{H2O(\lambda)}$ [111] and $\mu_{mel(\lambda)}$ [112] are the respective absorption coefficients, all of which were fitted to the measured diffuse reflectance using a numerical search algorithm.

2.2.4. Surface roughness vs lidar signal harmonics

Surface roughness determines whether reflected light is incoherent (diffuse) or coherent (specular), directly impacting the number of harmonics observed in entomological lidar signals [98, 125, 158].

The glossy wings of certain insects exhibit specular reflectance, producing bright flashes of light as their wing surface normal coincides with the source-detector midpoint. These specular flashes, captured as spikes in lidar observations, contribute to a greater number of harmonics compared to rough surfaces [87, 94, 137, 159], as illustrated in Fig. 2.11a, b. This is because spike signals contain higher frequencies, requiring more harmonics to accurately represent the waveform.

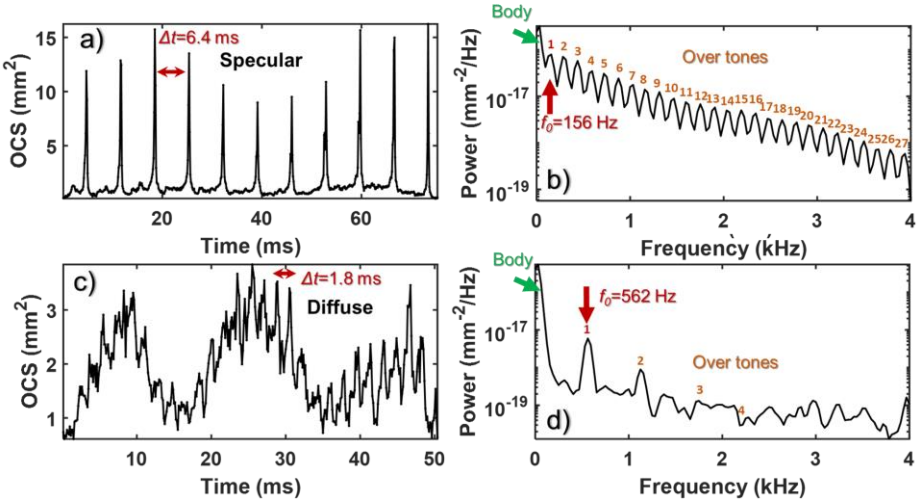

Fig. 2.11: Comparison of lidar signals from insect wings with varying surface roughness. a, b) Specular (glossy) wing generates a significantly larger number of harmonics compared to c, d) Diffuse (rough) wing. The laser used for these observations was an 808 nm continuous wave laser with co-polarized light.

Modulation spectra (Fig. 2.11 b and d) are composed of a non-oscillatory body contribution, a fundamental tone f_0, and multiple overtones. These spectra have been utilized for species recognition through modulation spectroscopy [42, 160-164]. The first few harmonics are particularly informative for identification as they relate to wing shape, dynamics, and observation aspects [165]. However, challenges arise due to the fundamental tone's variability with insect weight and temperature [43, 44, 166, 167], and its inconsistent signal strength [82, 158, 168]. To address these challenges, Scheimpflug lidar offers a promising solution. Its flexible band selection [88, 169, 170], ability to capture spectral fringes [171, 172], and integration with modulation spectroscopy [87] capture both modulation properties and spectroscopic properties. Instruments can be built with sensitivity to features such as surface roughness, wing thickness, and signal modulation. Improvements can be made to Scheimpflug lidar to reduce reliance on WBF, enabling the identification of a broader range of insect species.

2.2.5. Insects as polarimetric lidar target

Polarization describes the orientation of a light wave's oscillating electric field and its relationship with the magnetic field [148, 173]. This oscillation can be linear, circular, elliptical, or random, with the electric field's amplitude (E) indicating strength and its angle denoting direction. The relative phase between the electric and magnetic fields determines the handedness (right- or left-hand circular) of the polarization.

Polarization is used in various biomedical studies to gather detailed information about tissue [174-176]. It enhances imaging techniques, improving contrast for detailed tissue analysis [177, 178], such as separate superficial and deeper scatter contributions in biomedical imaging [176]. Animals use polarization for various functions [148, 179], including communication and vision [180-182]. Mantis shrimp possess specialized eyes that detect polarized light, aiding in hunting and social interactions [183]. Insects like field crickets [184] and dung beetles [185] use polarized light patterns for navigation [185-187]. Certain beetles reflect circularly polarized light [188-190], which enhances color and contrast, benefiting their communication and camouflage [148].

In entomological lidar studies, polarization was utilized to aid in insect identification based on the degree of polarization (DoLP) of backscattered light. Polarization lidar has previously been developed for atmospheric measurements [191]. Other research groups have also explored polarization lidar for insect studies [192, 193]. In the laboratory setting, polarization has been successfully applied to differentiate between gravid and non-gravid mosquitos [94].

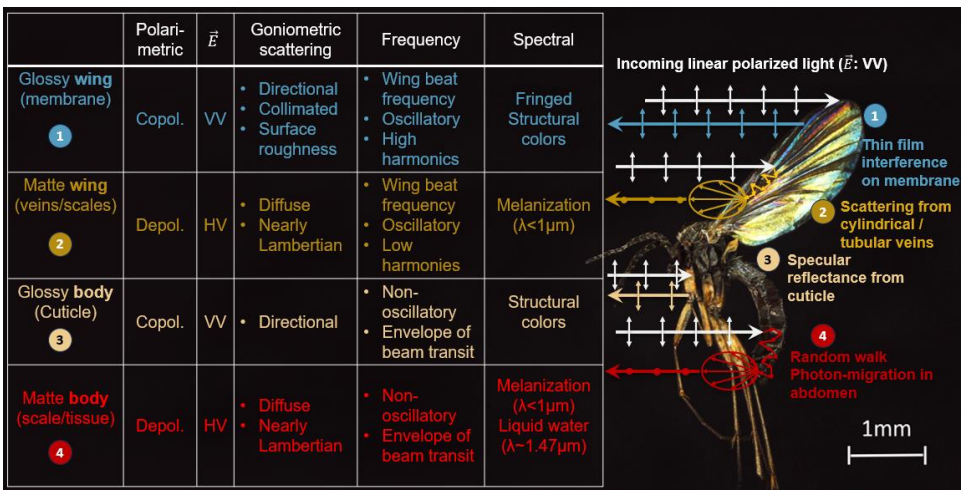

Fig. 2.12: Contributions to backscattered polarimetric signals from insect anatomical features. H and V represent horizontal and vertical polarization. The first letter in each combination (HV, VV) denotes the transmitted polarization, while the second letter denotes the detected polarization. The image is inspired by the reference [194].

The polarization of light reflected from various insect species was investigated in the laboratory (see references [106, 170] and *Papers I*, *III*, *VII-XII*). The experimental observations and measurements show that co-polarized and de-polarized backscatter can differentiate between coherent reflection (mainly due to thin-film interference [93, 195]) and incoherent scattering (originating from random photon migration in tissue [174, 176, 177]).

When linearly polarized light (Fig. 2.12) interacts with an insect in flight, the backscattered signal contains both co-polarized and de-polarized components. Co-polarized backscatter results from coherent specular reflections, while de-polarized backscatter arises from incoherent diffuse reflections. The lidar signal includes an oscillatory component resulting from wing flapping and a non-oscillatory component from the insect's body. The non-oscillatory signal generally resembles the lidar beam's transit envelope. Thin-film interference with insect membranes results in backscattered co-polarized light, maintaining a high DoLP. The DoLP is defined as the ratio of light maintaining its original polarization I_{co} to the total light intensity I_{co} + I_{de}, ranging from 50% (completely unpolarized) to 100% (fully linearly polarized), although instances below 50% were observed, suggesting additional de-polarization mechanisms to be detailed in the following section. The equation for DoLP is given by

$$\mathrm{DoLP} = \frac{\mathrm{I_{co}}}{\mathrm{I_{co}+I_{de}}} \tag{2.15}$$

Veins, scales, and abdomen tissue display low DoLP due to the random walk and photon migration of light entering these structures, leading to a loss of polarization, phase, and direction. Other factors like changes in scattering and absorption by melanin and water also contribute to this DoLP drop, as de-polarized photons undergoing longer migrations are more likely to be absorbed (time-of-flight phenomenon [120, 174]). The same insect can exhibit a DoLP change before and after consuming water/blood or becoming engorged with eggs [94] due to this.

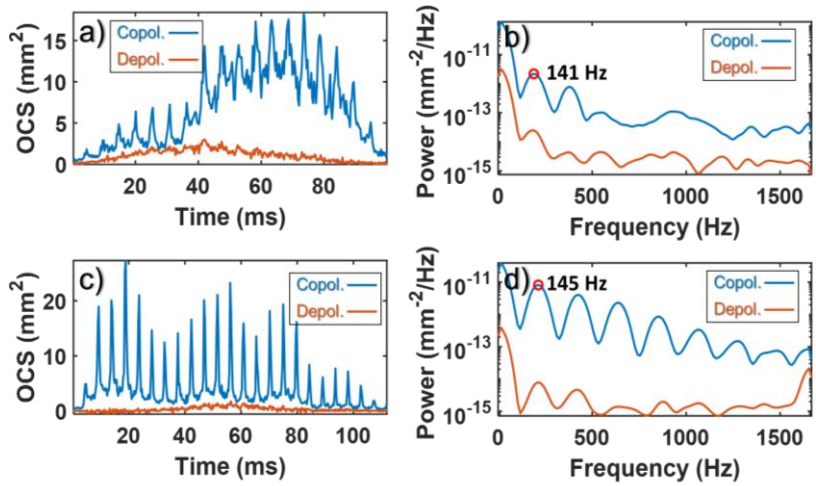

Fig. 2.13: Example of insects displaying different specularity and polarization and their lidar signal. a) An insect with a less specular surface and higher DoLP, and its corresponding power spectrum b). c) An insect with a more specular surface and lower DoLP, along with its power spectrum d).

Typical polarization lidar signals are shown in Fig. 2.13. The insect signal is separated into co-polarized and de-polarized components. The insect in Fig. 2.13a exhibits greater overall de-polarization and a less specular wing signal compared to the insect in Fig. 2.13c. This difference could potentially be attributed to a rough wing texture in a) and a glossy wing texture in c). The power spectra in Fig. 2.13b and d show that the rough-winged insect signal with lower overall DoLP has less pronounced overtones in the co-polarized component, consistent with rough surfaces leading to fewer harmonics. The glossy-winged insect's co-polarized signal instead shows many overtones. In both cases, the de-polarized signal in the power spectra exhibits oscillation, indicating that it contains both body signal and de-polarized wing signal, contributing to the oscillatory behavior.

2.2.6. Brewster angle at the air-chitin interface

The Brewster angle, calculated as θ_B=56° for an air-chitin interface, assumes a step-function change in the refractive index using the formula below,

$$\theta_{\mathrm{B}} = \tan^{-1}\left(\frac{n_{chitin}}{n_{air}}\right) \tag{2.16}$$

The Fresnel equations (to be discussed in Section 2.3.3) are used to calculate the reflectance for s- and p-polarized light at this interface, as shown in Fig. 2.14, illustrating their dependence on the incidence angle. When light strikes the chitinous surface at the Brewster angle, the p-polarized component is fully transmitted into the insect's exoskeleton, while the s-polarized component is partially reflected [173]. The transmitted p-polarized light undergoes multiple scattering events within the insect, leading to de-polarization and a mixed s- and p-polarized signal upon re-emergence. Analyzing this reflected light reveals the properties of the insect's exoskeleton structures.

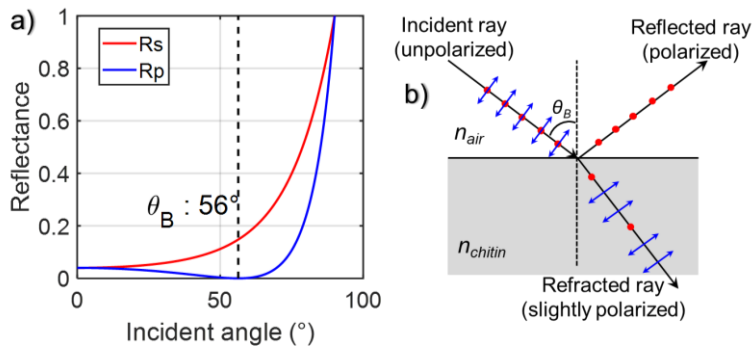

Fig. 2.14: Fresnel reflection coefficients and Brewster angle effects at an air-chitin interface (n_{air} = 1, n_{chitin} = 1.53). a) Reflectance differences for s- and p-polarized light. b) Behavior of incident light at Brewster angle (56°), no p-polarized light is reflected.

2.2.7. Polarization and surface roughness

Polarization has been used to study surface structure in radar [196, 197], microwave remote sensing [198], infrared [199, 200], and photometric [201]. Surface roughness influences the backscattering coefficients of electromagnetic waves, with the degree of influence depending on the incidence angle, frequency, and polarization of the waves [198, 201].

The relationship between surface roughness and polarization is most pronounced near the Brewster angle [198]. Smooth surfaces at this angle primarily reflect s-polarized light, yielding a high polarization ratio (p-polarized to s-polarized light), see Fig. 2.14. However, surface roughness disrupts this, causing increased p-polarized reflection, making the polarization ratio a sensitive indicator of even slight roughness changes.

The surface roughness of insect wings was investigated at the Brewster angle (in *Paper VIII-X*). For instance, the specular reflectance of a matte butterfly wing (illustrated in Fig. 2.15) can be modeled using a long-pass function.

$$R_{spec.} = R_{\text{long}} \frac{(\lambda/\lambda_0)^{\alpha}}{1+(\lambda/\lambda_0)^{\alpha}} \tag{2.17}$$

where R_{long} represents the asymptotic maximum reflectance, λ_0 the cut-on wavelength or surface roughness, and α the slope steepness of the spectrum. This model is valid for specular reflectance at large incident angles. As shown in Fig. 2.15 (specular wing pixel and entire wing), specular reflectance typically increases and plateaus towards the infrared region. However, in a previous study (*Paper VIII*), it was observed some moth species with reflectance that continued increasing without reaching a plateau within the 900-2500 nm spectral range, suggesting their surfaces were too rough for accurate assessment with the SWIR hyperspectral camera with wavelength range 900-2500 nm. The wavelength-dependent polarization changes for specific regions or the entire matte wing can be expressed using the following formula:

$$\text{DoLP} = \frac{I_{\text{co}}}{I_{\text{co}}+I_{\text{de}}} = \frac{1+\text{e}^{-(\lambda_{\text{p}}/\lambda)^{\gamma}}}{2} \tag{2.18}$$

where I_{co} and I_{de} represent co-polarized and de-polarized reflected intensities. The wavelength at which wings become co-polarized is denoted as λ_p, and the spectral dependence of DoLP is given by γ. A higher λ_p indicates a more diffuse wing (see the comparison between the specular and diffuse wing pixel in Fig. 2.15f), while a higher γ means DoLP increases with wavelength more rapidly. The matte body in Fig. 2.15 exhibits a DoLP below 50%, suggesting factors beyond simple diffuse reflection. Moth scales and hairs may trap specular co-polarized light, leaving primarily de-polarized light to escape, thus lowering the observed DoLP.

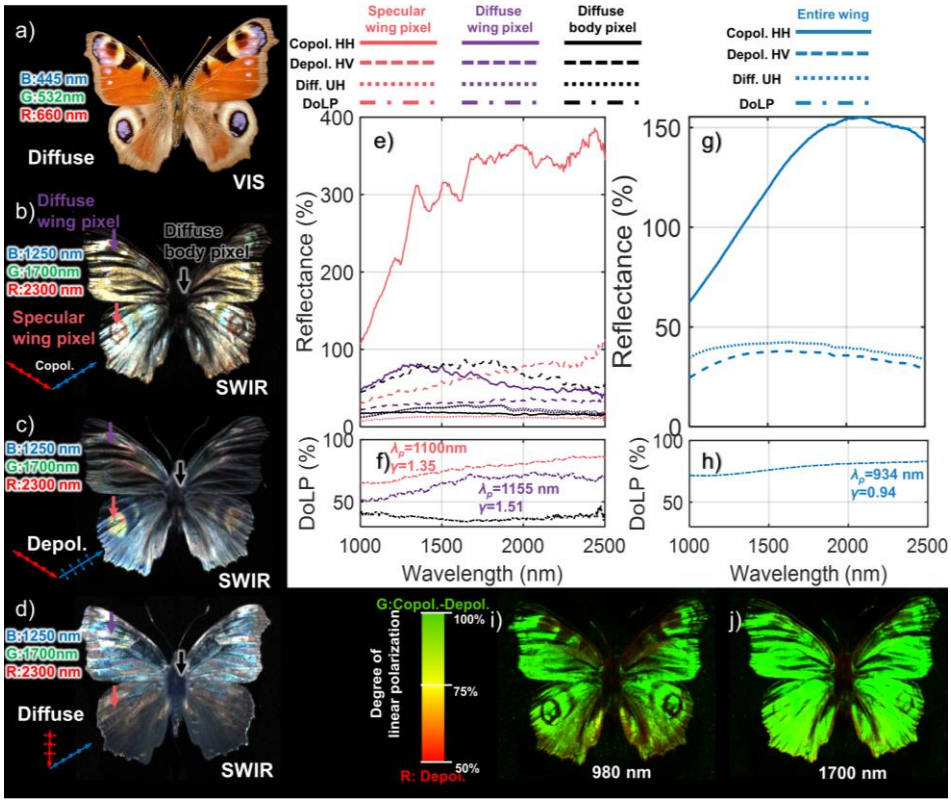

Fig. 2.15: Example of hyperspectral polarimetric imaging used to study surface roughness in matte-winged insects. a) A commercial camera image of a European peacock butterfly (*Aglais io*) under normal diffuse sunlight. b) Co-polarized false-color image of the same butterfly under specular illumination with Brewster angle. c) De-polarized false-color image of the butterfly under specular illumination with Brewster angle. d) False-color image under diffuse illumination. Red and blue arrows in b-d) show illumination and detection configurations. Polarization is denoted as HH, HV, or UH, with the first letter indicating transmitted and the second received polarization. e) Reflectance of selected specular wing pixel, diffuse wing pixel, and body pixel from b) under three different illumination and detection configurations (HH, HV, UH). f) DoLP calculated for all three pixels from the matte wing, showing their polarization ratio to wavelength. g) Reflectance from the entire wing under three different illumination and detection configurations (HH, HV, UH). h) DoLP of the entire wing over wavelength. i, j) DoLP images of the same butterfly at two wavelengths, showing increased linear polarization at higher wavelengths.

2.3. Coherent Phenomena

Coherent interactions preserve the original optical properties of light: direction, phase, and polarization. For instance, when light reflects off a thin insect membrane, which essentially acts like a mirror, it changes direction but maintains the light's initial phase and polarization.

2.3.1. Refractive index

The refractive index *n* of a material quantifies how light interacts with it by altering its group velocity *v* and wavelength λ compared to a vacuum (*c* and λ_0): $v = c/n$ and $\lambda = \lambda_0/n$. The refractive index varies with wavelength, a phenomenon called dispersion, leading to the separation of different wavelengths. Materials commonly found in insect structures, such as chitin [202], melanin [203], or water [157], exhibit dispersion in the visible wavelength range, see Fig. 2.16a. The Cauchy equation models dispersion as:

$$n(\lambda) = k_0 + \frac{k_1}{\lambda^2} \tag{2.19}$$

Where $n(\lambda)$ is the refractive index at a specific wavelength λ. k_0 and k_1 are constants specific to the material. Typical values in the case of insect chitin are $k_0 = 1.517$ and $k_1 = 8800$ nm² [202]. When developing models to quantify insect microscopic features and structures, it is important to consider the changes in refractive index with wavelength, as different values could lead to varying results.

To add complexity, insect microscopic surface structures can have complex compositions resulting in a gradient refractive index. For example, when considering light interacting with a membrane as shown in Fig. 2.16b, an air-chitin-air interaction is simplified, assuming a step function change in refractive index.

However, the complex composition of the membrane, with its uneven surface and varying density, results in refractive index gradients. Calculations [132] reveal that transitioning from a step function refractive index profile to a gradient profile reduces reflectance, especially in the shorter wavelength region where photons experience a smoother gradient in relation to their wavelength (see Fig. 2.16c). Furthermore, the gradient profile flattens the spectral fringe modulation (potentially suppressing spectral fringe production in biological films). This can lead to low overall reflectance across the visible spectrum. This phenomenon is also observed in the *Papilio ulysses* butterfly, which appears "blacker than black" due to structurally enhanced blackness [151]. The cuticle spike structure in Fig. 2.16g not only efficiently scatters incident light towards the diffusely distributed pigmentation [151] but also creates a gradient surface refractive index, as illustrated in Fig. 2.16h, leading to exceptional light absorption.

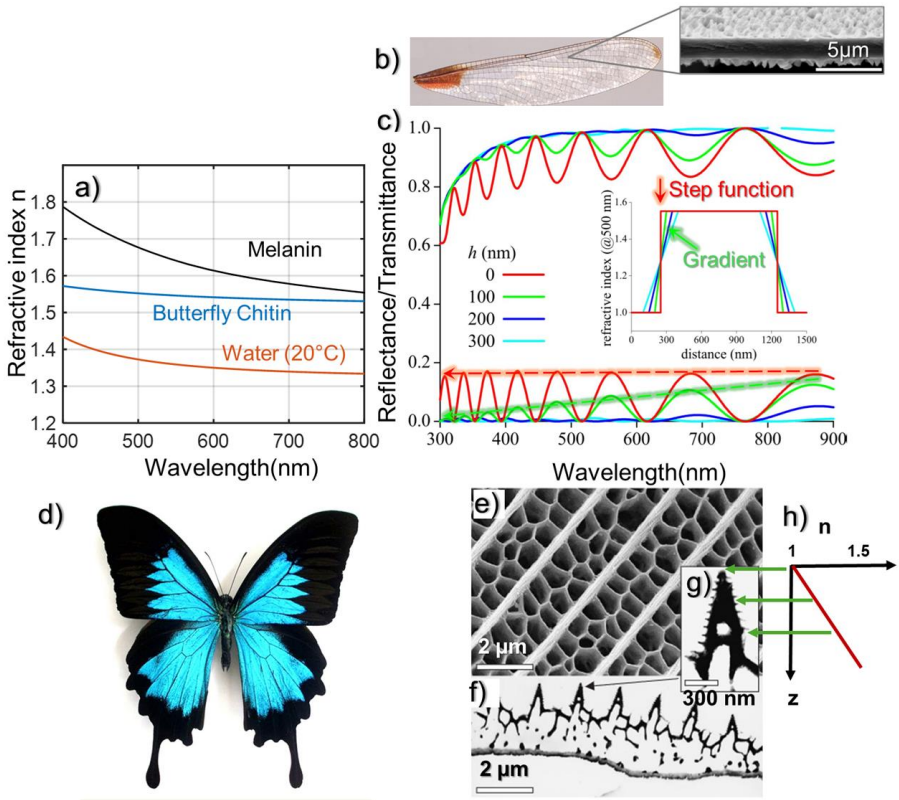

Fig. 2.16: Refractive indices of common insect materials and the impact of structure on gradient refractive index surface. a) Refractive index of melanin [203], chitin [202] and water [157]. Data were extracted from the corresponding references. b) Scanning electron micrograph of a section of *Hetaerina americana* damselfly wings, the photo is cited from [132]. c) Calculated transmittance and reflectance spectra for a thin film with an average thickness of 1000 nm. The refractive index was assumed to change linearly in surface layers with thicknesses h = 0, 100, 200, and 300 nm; the figure is cited from [132]. d) Image of *Papilio ulysses* butterfly. e) SEM image of the surface of a single scale from the matte black region of the butterfly shown in d). f) TEM image of the cross-section of a single scale from the matte black region of the butterfly shown in d). g) Zoomed-in view of one of the spikes shown in f). h) Sub-wavelength structures lead to a gradient refractive index surface. Images e-g) are from reference [151].

2.3.2. Snell's law

Snell's law describes the change in direction of light as it passes from one medium to another with a different refractive index. This change in direction, known as refraction, is caused by the mismatching of refractive indices of the two media and the angle at which the light strikes the interface. Snell's law is expressed as:

$$n_1 \sin(\theta_i) = n_2 \sin(\theta_t) \tag{2.20}$$

where n_1 and n_2 are the refractive indices of the two media, θ_i is the angle of incidence, and θ_t is the angle of refraction.

Some beetles and weevils possess intricate multilayer structures within their exoskeletons, composed of thin parallel layers of chitin with distinct refractive indices [127, 204, 205]. When light interacts with these multilayered structures, it undergoes refraction at each interface according to Snell's law. This repeated refraction, combined with subsequent interactions between the refracted light waves, can produce vibrant colors.

2.3.3. Fresnel equations

While Snell's Law describes how light changes direction at an interface due to refractive index mismatch, the Fresnel equations quantify the amount of light that is reflected and transmitted at this boundary [206]. For a single thin film, the analysis is simplified compared to the matrix formalism typically employed for multilayer structures [132, 207]. Importantly, the Fresnel equations distinguish between the light's polarization, whether it is p-polarized (parallel) or s-polarized (perpendicular) to the plane of incidence. The equations for a single thin film are [173]:

$$R_s = \left|\frac{n_1 cos(\theta_i) - n_2 cos(\theta_t)}{n_1 cos(\theta_i) + n_2 cos(\theta_t)}\right|^2, \quad T_s = 1 - R_s \tag{2.21}$$

$$R_p = \left|\frac{n_2 \cos(\theta_i) - n_1 \cos(\theta_t)}{n_2 \cos(\theta_i) + n_1 \cos(\theta_t)}\right|^2, T_p = 1 - R_p \tag{2.22}$$

here, R_s and R_p is the reflectance of s-polarized and p-polarized light, respectively, while T_s and T_p represent the corresponding transmittance values, n_1 and n_2 is the refractive index of the first medium (from which the light is coming), and the second medium (into which the light is going), θ_i is the angle of incidence, and θ_t is the angle of transmission, which can be found using Snell's law. In the case of lidar with normal incidence (the light beams perpendicular to the surface), the angles of incidence and refraction are zero. The Fresnel equation for an air-chitin interaction then simplifies to:

$$R_{Fresnel} = \left|\frac{n_1 - n_2}{n_1 + n_2}\right|^2 = \left|\frac{n_{air} - n_{chi.}}{n_{air} + n_{chi.}}\right|^2 \tag{2.23}$$

where $R_{Fresnel}$ represents the reflectance determined by the refractive indices of air (n_{air}, typically approximated as 1) and chitin n_{chi}. The refractive index of chitin, n_{chi}, is wavelength λ dependent, as described in equation 2.19.

While the Fresnel equations provide the magnitudes of reflected and transmitted light separately, they do not directly give us the combined effect, as this depends on the complex interaction (interference) between the reflected and transmitted waves.

To account for the effective reflectance, the Fresnel equations need to be combined with thin-film equations [130], which will be discussed in a later section.

2.3.4. Kramers-Kronig-relation

The refractive index of a material is a complex quantity consisting of a real part ε_1, which determines the degree of refraction, and an imaginary part ε_2, which signifies absorption. The Kramers-Kronig (KK) relations [208] reveal a fundamental connection between these components: a material's absorption characteristics directly shape its refractive properties, and vice versa. This connection is rooted in causality, the principle that a material's response to light must adhere to the cause-and-effect relationship inherent in physical phenomena [209].

Mathematically, the KK relations are expressed as integral transforms, demonstrating the interdependence of the real and imaginary parts of the refractive index:

$$\varepsilon_1(\omega) = 1 + \frac{2}{\pi}\mathcal{P}\int_0^\infty \frac{\omega'\varepsilon_2(\omega')}{\omega'^2-\omega^2}d\omega' \tag{2.24}$$

$$\varepsilon_2(\omega) = -\frac{2\omega}{\pi}\mathcal{P}\int_0^\infty \frac{\varepsilon_1(\omega')-1}{\omega'^2-\omega^2}d\omega' \tag{2.25}$$

where *P* denotes the Cauchy principal value. At frequencies much higher than the material's resonance ($\omega >> \omega'$), the real part of the dielectric function ($\varepsilon_1(\omega)$) approaches 1, indicating negligible dispersion. However, at resonance ($\omega = \omega'$), the real part of the dielectric function ($\varepsilon_1(\omega)$) approaches infinity, necessitating the use of the principal value method. This signifies a strong coupling between the real (ε_1) and imaginary (ε_2) components of the dielectric function, resulting in significant absorption and pronounced changes in the refractive index, see example in Fig. 2.17. Water shows strong absorption peaks in the infrared spectrum and refractive

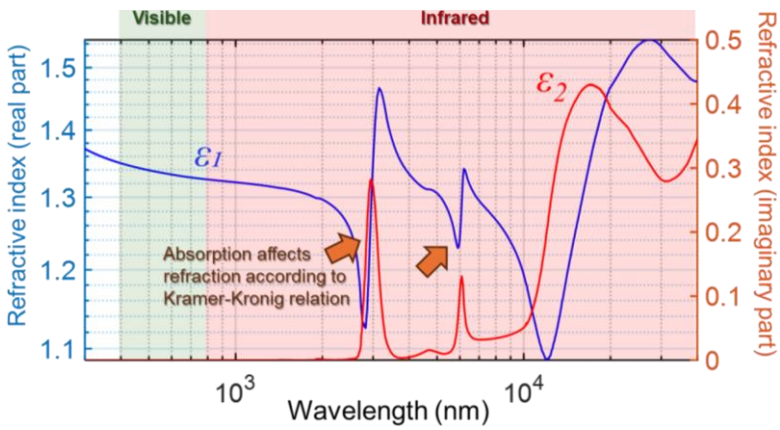

Fig. 2.17: The complex refractive index of water. Data from reference [111]. The figure is inspired by reference [212].

index derivation. Fig. 2.17 demonstrates that the refractive index of water remains relatively constant in the visible and NIR spectrum (before 2000 nm) due to the absence of strong water absorption lines in the range. However, significant variations in the refractive index are observed in the NIR (above 2000 nm) and SWIR regions. Applying the same logic, the refractive index of chitin is relatively flat in the NIR to SWIR range because its only absorption band peaks at 280 nm.

To maintain the cause-and-effect relationship described by the KK relations, the real and imaginary parts of a material's refractive index must be related. Dispersion, which refers to the dependence of a material's refractive index on the wavelength of light, results in changes in the phase velocity of light as it propagates through the material. This means that the speed of light varies with wavelength, leading to phenomena such as the separation of white light into its constituent wavelengths. Dispersion is crucial for comprehending the complex phenomenon of structural coloration in insects, where intricate nanoscale structures interact with light to produce vibrant colors [210, 211].

2.3.5. Thin film interference

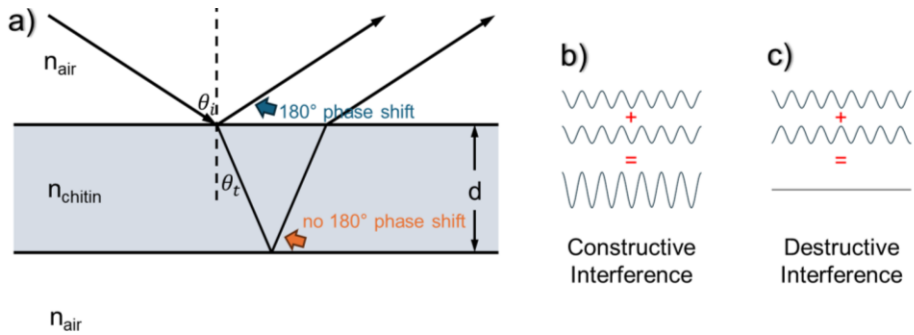

Fig. 2.18: Illustration of thin film interference conditions of uniform thickness. a) Showcasing angle of incidence θ_i, angle of transmission θ_t, refractive index of the medium n, and film thickness d. b-c) In constructive interference, waves with aligned phases amplify each other. In destructive interference, waves with opposite phases cancel each other out.

Thin-film interference, illustrated in Fig. 2.18, is a phenomenon arising from the interaction of light waves reflected at the upper and lower boundaries of a thin-film [173]. This interference can result in the selective amplification or attenuation of specific wavelengths, producing iridescent colors often observed in nature [132, 213, 214]. A 180° phase shift occurs when a wave reflects from a medium with a higher refractive index ($n_2 > n_1$), while no phase shift occurs with a lower refractive index ($n_2 < n_1$). The resulting colors depend on film thickness, refractive index contrast, and incident light angle.

Consider a thin chitin layer forming an insect's clear wing, surrounded by air. Since the refractive index of chitin n_{chitin} is greater than that of air n_{air} at the top surfaces of the wing, reflections at these boundaries induce a 180° phase shift. For constructive interference to occur, the optical path length difference (twice the wing thickness) must equal an odd multiple of half the wavelength within the chitin:

$$2dn_{chi.}\cos(\theta_t) = \left(m - \frac{1}{2}\right)\lambda_{max}, m \in \mathbb{N} \tag{2.26}$$

$$2dn_{chi.}\sqrt{1 - \frac{\sin^2(\theta_i)}{n_{\text{chi.}}^2}} = \left(m - \frac{1}{2}\right)\lambda_{max}, m \in \mathbb{N} \tag{2.27}$$

Destructive interference occurs when the optical path length difference equals an integer multiple of the wavelength within the chitin:

$$2dn_{chi.}\cos(\theta_t) = \mathrm{m}\,\lambda_{min}, m \in \mathbb{N} \tag{2.28}$$

$$2nd_{chi.}\sqrt{1 - \frac{\sin^2(\theta_i)}{n_{\text{chi.}}^2}} = m\lambda_{min}, m \in \mathbb{N} \tag{2.29}$$

where d is the wing thickness, $n_{chi.}$ is the refractive index of chitin, λ is the wavelength, θ_i is the angle of incidence, θ_t is the angle of transmission, and m is an integer. For lidar measurements, the angle of incidence θ_i is zero (like the hyperspectral lidar measurement in *Paper XII*), so the entire square root factor in equations 2.27 and 2.29 can be omitted. However, for hyperspectral scan measurements performed in Papers *I*, *VIII*, *IX*, *X*, and *XII* in a laboratory, an angle of incidence is present and must be considered to adjust for the resulting spectral shift. For example, due to the increasing incidence angle, a spectral peak at 600 nm, captured at a 56° incident angle (n=1.53), would exhibit a blue shift to 505 nm when corrected to normal incidence. Such compensation is thus crucial to ensure comparability between laboratory hyperspectral and field lidar observations.

2.3.6. Fringe model

A fringe model was developed to express the spectral fringes observed in clear insect wings. This model incorporates a thin-film equation, derived from previous research on iridescence from pigeon neck feather [130], and Fresnel equations to account for the reflection and interference of light.

$$F(\lambda, d) = \frac{4R_{Fresnel}\sin^2\left(2\pi d\frac{\sqrt{{n_{chi.}}^2 - \sin^2\theta}}{\lambda}\right)}{(1-R_{Fresnel})^2 + 4R_{Fresnel}\sin^2\left(2\pi d\frac{\sqrt{{n_{chi.}}^2 - \sin^2\theta}}{\lambda}\right)} \tag{2.30}$$

where $F(\lambda,d)$ is the fringe, λ is the wavelength of light that interacts with the wing, and d is the wing's chitin layer thickness. $R_{Fresnel}$ is from equation 2.23, and the refractive index of chitin varies with wavelength, as shown in equation 2.19.

While the model $F(\lambda,d)$, incorporating thin-film interference effects, addressed scaling and material dispersion issues, it still could not account for the overall change in reflectance over varying wavelengths due to the heterogeneous nature of the wing's chitin layer thickness [132]. To address this issue, an approach (first appearing in *Paper X*) utilizes a long-pass function for amplitude and a short-pass function for bias to weigh the spectral fringe. This leads to the evaluation of spatial thickness heterogeneity across each wing by adjusting the fringe amplitude a and bias b relative to a specific cut-off wavelength λ_0,

$$\hat{R}_{wing(\lambda)} = \frac{aF(\lambda,d)\lambda^k + b\lambda_0^k}{\lambda_0^k + \lambda^k} \tag{2.31}$$

The exponent k in these functions influences how reflectance changes with wavelength. In the hover fly study from *Paper X*, it was found that $k = e = 2.311$ to best describe all effective fringes. However, in *Paper XI*, due to thinner wings and observing only a single fringe period, k could not be determined and was set to zero. The use of short- and long-pass functions is analogous to the use of electronic filters in signal processing to selectively pass specific frequency ranges [215]

For wings that do not produce fringes, the $F(\lambda, d)$ term vanishes, and the reflectance of the wing with no spectral fringe is thus described solely by the bias term of the fringe model from equation 2.31:

$$\hat{R}_{wing(\lambda)} = \frac{b}{1+\frac{\lambda}{\lambda_0}^k} \tag{2.32}$$

How the amplitude and bias terms address the increasing fringe modulation towards infrared wavelengths, and decreasing modulation towards visible wavelengths is illustrated in Fig. 2.19. It also shows examples of thick and thin wing pixel spectral fringes. The effective fringe was obtained by XY spatially integrating all wing pixel spectral profiles. The differing degrees of modulation in these fringes can be described by the modulation depth, M, calculated using the following equation:

$$M = \frac{\sigma_\lambda(R_\lambda)\cdot\mu_\lambda(F(\lambda,d))}{\sigma_\lambda(F(\lambda,d))\cdot\mu_\lambda(R_\lambda)} \tag{2.33}$$

where R_λ denotes measured reflectance, F denotes the computed fringe, λ is the wavelength, σ_λ denotes standard deviation in the spectral domain, and μ_λ is the spectral mean value.

Thicker wing regions exhibit narrower fringes, more susceptible to dephasing with neighbor regions (XY destructive interference, not XZ which is related to thickness) in the VIS spectrum due to the chirped nature of fringe periodicity. For a thin film, the periodicity of the interference fringes is constant in the frequency domain; the

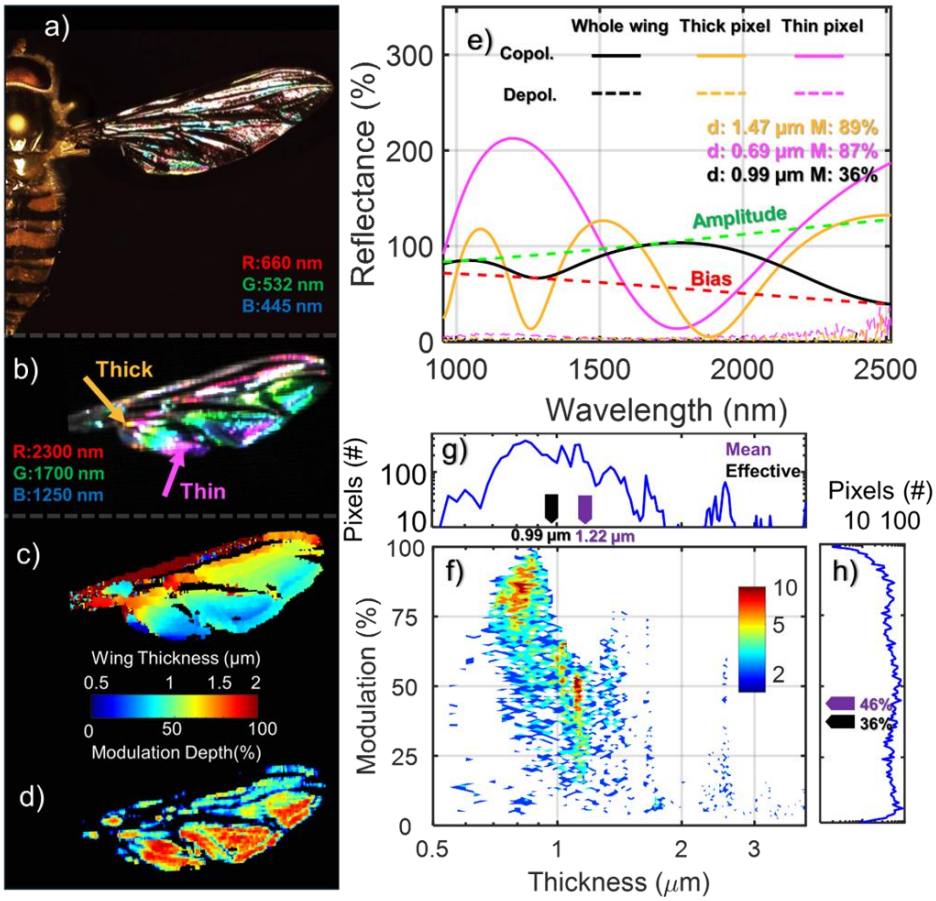

Fig. 2.19: Characterization of structural coloration in hover fly (*Episyrphus balteatus*) wings. a) Photograph of a hoverfly wing exhibiting structural coloration. b) False color image highlighting the wing's interference pattern. c) Wing thickness map derived from the interference signal. d) Fringe modulation depth map, revealing variations in the intensity of the interference signal at each wing pixel. e) Example of spectral fringes from thin and thick wing regions, as well as the effective fringe formed by spatially integrating the spectral profiles of all wing pixels within the SWIR hyperspectral camera detection range window. The fringe is weighted by the long and short pass functions to evaluate the heterogeneity of the wing; amplitude *a* and bias *b* are also illustrated in the same figure for the effective fringe. f) 2D histogram depicting the distribution of wing thickness and modulation depth across the wing surface. g, h) Demonstration that the resolved effective thickness and modulation depth are not simply the mean of all thickness or modulation values from the wing.

frequency *f* is directly proportional to the order *m* [132, 156]. Therefore, the fringes occur at regularly spaced frequencies, leading to non-uniform (chirped) spacing in the wavelength domain due to the inverse relationship between frequency and wavelength. As a result, fringes are more closely spaced at shorter wavelengths,

increasing the likelihood of dephasing with neighbor regions in the VIS compared to the SWIR range. Consequently, thicker wing membranes contribute less to the overall modulation of the effective fringe, as seen in Fig. 2.19c and d. While thinner wing regions exhibit higher modulation depths.

The effective fringe, formed by XY spatially integrating the spectral profiles of all wing pixels, has a final appearance determined by the interaction between spectral fringes from areas with varying thicknesses (XZ). When the wing is dominated by thin regions with high modulation fringes, their cumulative contribution results in the effective fringe converging towards the characteristic spectral patterns of these thinner regions. Notably, the effective thickness does not directly correspond to the mean of all wing thicknesses and fringe modulations due to the disproportionate influence of these thinner, highly modulating regions with different thicknesses.

Capturing spectral fringes using lidar is a promising method for performing remote nanoscopy and retrieving wing thickness characteristics from in-flight insects. Wing thickness has been shown in recent studies to be a feasible feature for identifying species, sex, and gravidity (*Papers IX, X, XI, XII*) and is more reliable than modulation spectra [40, 159, 160]. The wing interference pattern and signal are thermally stable [216], and consistent over time [93]. Lidar systems can be implemented with various laser bands. In Paper *XII*, in-flight insect fringes were successfully captured and retrieved wing thickness using hyperspectral lidar with a single flash. Spectral fringes can also be captured with passive lidar systems utilizing sunlight [158, 171, 217]. Additionally, employing several laser bands [88, 169, 170, 218] enables the extraction of biologically relevant nanoscale features, such as melanin content ratio in the body and wings, which can be used for insect identification with dual- or multi-band lidar systems (*Paper V*). If the chosen laser band is resonant with the insect wing's interference fringes, as demonstrated in *Papers I- III*, the degree of flash polarization can be utilized for insect identification. Furthermore, in *Paper XI*, the speed required to capture specular flashes was analyzed, enabling remote nanoscopy for improved insect identification.

3.Research Methodology

3.1. Hyperspectral camera

Hyperspectral imaging (HSI) is a technique where a camera collects detailed image data across a wide spectrum of light, extending beyond the capabilities of standard cameras, which capture images only in the three specular bands: red, green, and blue. HSI records hundreds of narrow spectral bands across a wide range of wavelengths, from UV [219, 220] to SWIR wavelengths [221, 222].

In remote sensing, satellites equipped with HSI sensors collect detailed spectral profiles [223], enabling the mapping of land cover, tracking changes in vegetation [224], identifying specific minerals based on their unique spectral signatures [225], and estimating water quality [226]. The ability of HSI to differentiate between materials based on their spectral characteristics is also being utilized in medical diagnostics. The spectral reflectance of skin tissues provides a non-invasive method for estimating optical parameters [227] or use as a diagnostic tool [228, 229]. In combination with lidar for tree height identification, the distinct spectral reflectance of different tree species results in accurate identification and classification using HSI [230, 231]. In the field of entomology, intricate details of wing patterns, body pigmentation, and physiological states can be captured and analyzed using HSI for accurate species identification and classification [232].

In all the studies included within this thesis, two different push-broom hyperspectral cameras: a visible-extended InGaAs camera (Norsk Elektro Optikk) with a spectral range of 900-1600 nm and a sterling-cooled HgCdTe SWIR camera (MCT) [221] (Norsk Elektro Optikk) covering 900-2500 nm were used. These cameras collect light through an objective lens, focusing it onto a narrow slit that acts as a spatial line selector. The transmitted light is then collimated and spectrally dispersed by a diffraction grating before being re-imaged onto a two-dimensional focal plane array (FPA). The FPA material determines the spectral range of each camera: for example, Si-CMOS FPAs typically cover 350-1100 nm, InGaAs FPAs cover 900-1700 nm, and HgCdTe FPAs cover 900-2500 nm. Different spectral filtering is also implemented to achieve the desired spectral ranges for specific experiments and to eliminate second-order effects. A fiber-coupled tungsten halogen lamp (Illumination Technologies model 2900) and a standard Philips tungsten bulb were used as light sources, both of which exhibit a blackbody-like spectrum.

Each hyperspectral image forms a 3D data cube, see Fig.3.1, with two spatial dimensions and one spectral dimension. Each camera exposure captures a continuous spectrum (288 spectral bands for the HgCdTe camera, 382 spectral bands for the extended InGaAs camera) for each pixel along the swath width. A complete hyperspectral image is built up over time by scanning the imaging scene. Typically, the camera is fixed in a stationary position, while the sample is placed on a motorized translation stage that moves it across the camera's field of view. This creates a hyperspectral data cube, a 3D dataset consisting of a 2D spatial image at each wavelength.

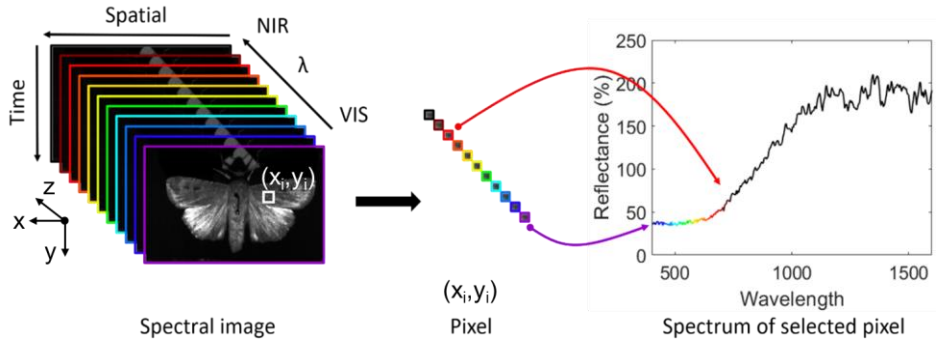

Fig. 3.1: Detailed hyperspectral data cube of a dried Bogong moth specimen. Data was acquired using a push-broom hyperspectral camera with an extended InGaAs sensor (450-1700 nm wavelength range). The cube's x-axis represents the spatial distribution, the y-axis represents the line-scan acquisition sequence, and the z-axis represents spectral profiles. Each pixel (x_i, y_i) contains a full spectrum across contiguous bands. Analysis of a selected pixel spectrum reveals a strong melanin presence in the wing scale, with intensity decreasing towards the infrared region.

Reflectance calibration is necessary due to the influence of factors such as the illumination source's spectral output, grating efficiency, detector quantum efficiency, and the angles of illumination and collection. This is accomplished by converting raw intensity into reflectance using a reference image. A standard Lambertian diffuse surface, typically Spectralon® with 50% diffuse reflectance, is used as the calibration target. However, the calibrated reflectance may sometimes exceed 100%. This is because a potentially specular signal is being calibrated against a Lambertian diffuse reference target, resulting in reflectance values that can exceed the expected range.

The visible-extended InGaAs camera is particularly suited for capturing features like melanin and water absorption bands, providing insights into insect body and wing melanization, thickness, and water content. The extended range into the infrared of the SWIR camera enables the investigation of surface roughness and polarization changes at longer wavelengths.

3.2. Polarimetric goniometry

A polarimetric goniometer is used to examine how light interacts with a target, particularly insects, by analyzing changes in light's polarization after reflection or scattering [137]. This involves precise control of illumination angles and detailed measurement of the scattered light, providing insights into the target's optical properties. Using different polarizations helps interpret how an insect's structure alters light polarization depending on the viewing angle.

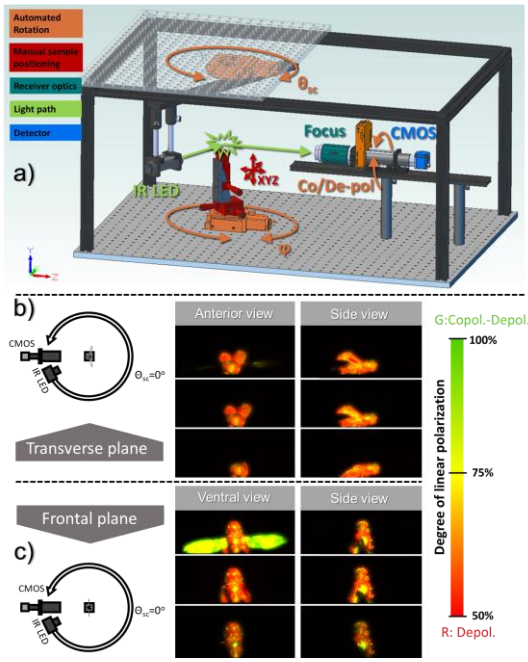

Fig. 3.2: Polarimetric goniometry analysis of an insect sample under varying conditions. a) CAD model of the SPOTIG system (image from reference [137]). b, c) Polarization changes in a bark beetle with progressively removed structures (wings intact, wings removed, wings and elytra removed) and viewed from different angles within anatomical planes. Due to the flat wing positioning, high polarization specular reflection is visible only in the frontal plane from ventral or dorsal views.

Two polarimetric goniometers have been developed to study the optical properties of insects. The first, SPOTIG (Spectral Polarimetric Optical Tomographic Imaging Goniometer) [137], features three motorized rotation stages, facilitating the manipulation of polarization filters, the camera, and the target specimen, see Fig. 3.2. This flexible setup provides insights into insect optical cross-sections and how anatomical features with varying optical properties influence lidar signatures. SPOTIG was notably employed to document the optical parameters of bark beetles in *Paper I* in detail, capturing backscattering and extinction cross-sections, along with the phase function, from three anatomical planes. The backscatter optical cross-sections were further parameterized using spherical harmonics to efficiently represent the target's complete features for lidar applications.

Building on SPOTIG's foundation, the BIOSPACE (Biophotonics, Imaging, Optical, Spectral, Polarimetric, Angular, and Compact Equipment) polarimetric

goniometer was created. Constructed primarily from LEGO components to facilitate adaptability and distribution for educational purposes due to its affordability, BIOSPACE boasts adjustable illumination spectral bands achieved through LED multiplexing, enabling the study of polarimetric signatures across diverse wavelengths. Its modular design, having free rotation of the polarization filter and either the insect sample or light source, enhances flexibility in measurement angles. BIOSPACE's wider spectral range and enhanced flexibility compared to SPOTIG have been instrumental in generating comprehensive reference databases of insect optical signatures, particularly through measurements of museum specimens. These findings have been presented in *Papers III, VII, and XI*.

3.3. Lidar

Scheimpflug lidar leverages the Scheimpflug principle, a 19th-century photographic technique [233, 234], to achieve an extended depth of field. Unlike traditional time-of-flight (ToF) lidar, relying on pulsed lasers [235], Scheimpflug lidar employs one or more continuous wave laser diodes, often multiplexed, and a line sensor to capture backscattered light from an illuminated air volume [169, 236, 237]. Scheimpflug lidar range resolution is achieved through the Scheimpflug criterion and Hinge rule [169, 238], resulting in infinite focal depth where each sensor pixel corresponds to a specific section of the laser beam.

3.3.1. Light detection and ranging

Lidar, also known as laser radar, measures distances by emitting pulses of laser light toward a target and measuring the time it takes for the light to return to the sensor [235]. The conventional ToF lidar measurement calculates distances using the following formula:

$$R = \frac{tc}{2n_{medium}} \tag{3.1}$$

Where R is the distance to the target, t is the time difference between the transmitted and received light pulses, and c is the speed of light. The resolution of a lidar system, which determines the level of detail captured in the measurements and the minimum resolvable distance between two objects (range resolution, ΔR), is crucial. Higher resolution systems can distinguish between closely spaced objects and provide more accurate distance measurements [235]. It is calculated using the formula:

$$\Delta R = \frac{\tau_p c}{2n_{medium}} \tag{3.2}$$

where τ_p is the pulse duration. ToF lidar is used in environmental monitoring (forest mapping [239, 240], biomass assessment [241]), atmospheric science (aerosol

concentration [235, 242], cloud height [243]), and pollution tracking [244]. Recent research comparing ToF and Scheimpflug lidar found them comparable in performance for aerosol sensing [245], with Scheimpflug lidar offering a more cost-effective and simpler solution.

3.3.2. Scheimpflug principle

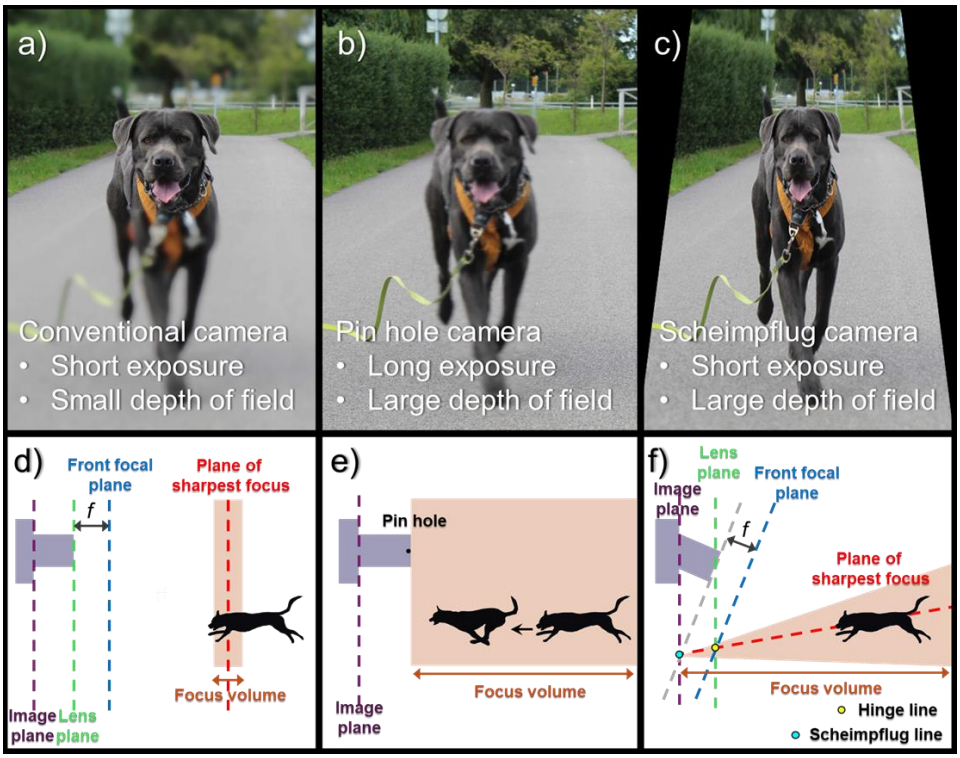

Fig. 3.3: Comparative focus mechanisms in three different camera systems: a, d) Conventional camera with limited depth of field; b, e) Pinhole camera with broad depth of field but motion blur; c, f) Scheimpflug camera with extended depth of field for simultaneous capture of near and far objects but with image distortion. Image inspired by work [194].

The Scheimpflug principle, popularized by Austrian Captain Theodor Scheimpflug [234] but discovered by Jules Carpentier [233], provides a unique approach to manipulating depth of field in photography. In conventional cameras, the lens and image sensor are parallel, limiting the range of sharp focus (as shown in Fig. 3.3a, d). Pinhole cameras (Fig. 3.3b, e) offer an extended depth of field due to their tiny aperture but often require long exposure times, causing motion blur. The Scheimpflug principle involves tilting the lens relative to the image sensor (Fig. 3.3c, f). This tilts the plane of focus and results in both near and far objects being in

sharp focus simultaneously. This technique offers greater control over depth of field compared to conventional photography, though it can introduce some distortion. The Scheimpflug principle finds applications in various fields, such as structural displacement monitoring [246].

3.3.3. Scheimpflug lidar

The application of the Scheimpflug principle to lidar systems is a relatively recent development [81, 169]. It has been used in atmospheric detection, [170, 191, 238, 247] and flame diagnostics [194], and entomology in insect study [88-91, 126, 154, 237, 248]. Fig. 3.4 illustrates the Scheimpflug condition, which requires the plane of the detector and the plane of the lens to meet at a point on the object plane. The Hinge condition further specifies that the tilted lens plane parallel to the detector, also intersects the front focal plane of the lens at this same point on the object plane. The range r to a target, can be approximated by considering the chip-normalized pixel positions (p_r and p_λ), the baseline length (ℓ_{BL} = 0.814m), the slant angle between the optical axes (Φ_{slant}), and the receiver field of view (θ_{FoV}):

$$\hat{r}(p_r, p_\lambda) = \ell_{\mathrm{BL}} \cot\left(\Phi_{\mathrm{slant}} + \theta_{\mathrm{FoV}} p_r\right) \tag{3.3}$$

This formula is originally from *Paper XII*. For a basic entomological lidar system, such as the one used in *Paper I*, one wavelength band is used and multiplexed to capture both background and laser signal reflections from in-flight insect targets,

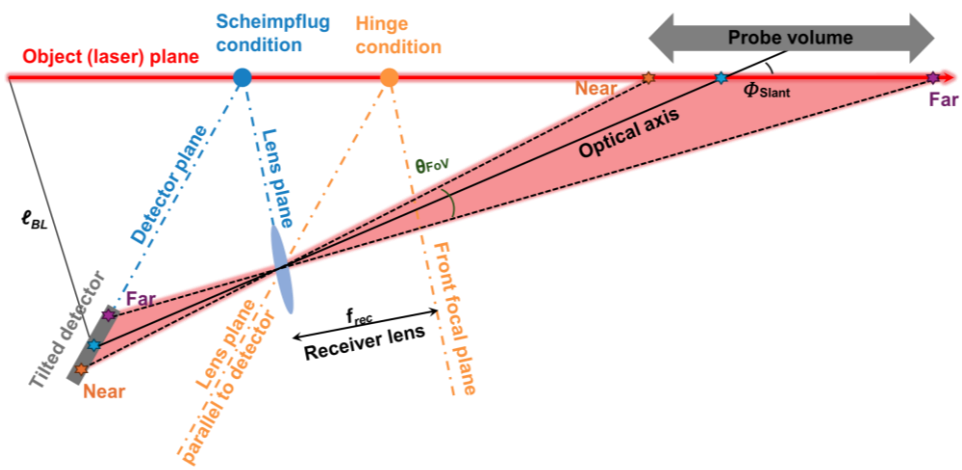

Fig. 3.4: Scheimpflug and Hinge configuration in an entomological lidar system. Varying observations along the laser beam are detected at distinct locations on the tilted detector, with each pixel corresponding to a unique distance from the lidar. The figure is based on references [86, 249] with minor modifications.

it measures the backscattered intensity as a function of range and time. This type of lidar data contains information on insect time of detection, range, optical cross-section (in mm^2), and apparent size (in mm) [125]. The optical cross-section is calibrated using a fixed target of known distance and reflectance. Typically, a neoprene flat board serves as the lidar termination and is also used for calibration. The insect signal is then calibrated to optical cross-sections based on the neoprene reference. Apparent size, derived from the pixel footprint and telescope magnification, provides an estimate of the insect's dimensions (see detailed explanation in *Paper II*). Captured lidar time series data generally reveal wingbeats of in-flight insects. Power spectral analysis via Welch's method of these modulations provides wingbeat frequency, characteristics, and surface roughness at the illumination wavelength. Depending on the insect body's orientation, the fundamental frequency may not be the strongest signal in the power spectrum [158]. For a detailed discussion of calibration and sizing calculations, see a recent study [89].

3.3.4. Backward-lasing with Scheimpflug lidar

Backward propagating lasers in lidar are desirable to circumvent the range attenuation of the signal. This can be accomplished through atmospheric lasing and filamentation. Atmospheric lasing manipulates the atmosphere itself to amplify the returning light signal, offering increased signal strength and longer detection ranges, but requires specific conditions and sophisticated systems [250-255]. Filamentation, using high-intensity femtosecond laser pulses, creates a waveguide in the atmosphere, enhancing sensitivity and probe volumes, but also necessitates complex and expensive technology [256-258]. By capturing the specular reflections from flat membranes, it is possible to achieve "backward-lasing" from atmospheric insects. The lasing approach based on optical breakdown in the medium is not feasible for insect monitoring as it is destructive. The use of flat targets presents a simpler and more practical approach to backward-lasing. This method involves directly reflecting the outgoing laser beam backward off a flat surface, maintaining its collimation, polarization, and phase while propagating in the backward direction [98, 259, 260]. This approach has found applications in gas sensing [261] and has been instrumental in achieving the longest lidar-ranging distances [262]. Snowflakes [259, 263] and insect wings [247] are naturally occurring structures that act as flat targets for lidar. The reflective properties of insect wings can be optimized by selecting a laser wavelength that resonates with the wing thickness or aligns with a specific infrared spectral band where the wing surface is most specular and reflective. This approach enhances insect wings' reflectivity for lidar systems, leveraging their natural flatness for coherent backscatter and polarization analysis. This enables specularity estimation, remote nanoscopy via thin-film interference, see *Paper XII*, and enhanced flatness in the infrared.

3.3.5. Polarization lidar

Polarization lidar was first developed for atmospheric studies utilizing a linearly polarized pulsed laser to distinguish between ice and water clouds [264]. Due to their spherical shape, liquid water drops preserve the polarization of backscattered light, only changing its propagation direction. In contrast, non-spherical ice crystals induce a change in the polarization of the backscattered light through multiple scattering events. By analyzing the polarization of the backscattered light, the lidar can thus effectively differentiate between ice and water clouds [265]. This technology has since found further applications in atmospheric research [191, 263, 266] and ecological studies [192, 193, 267].

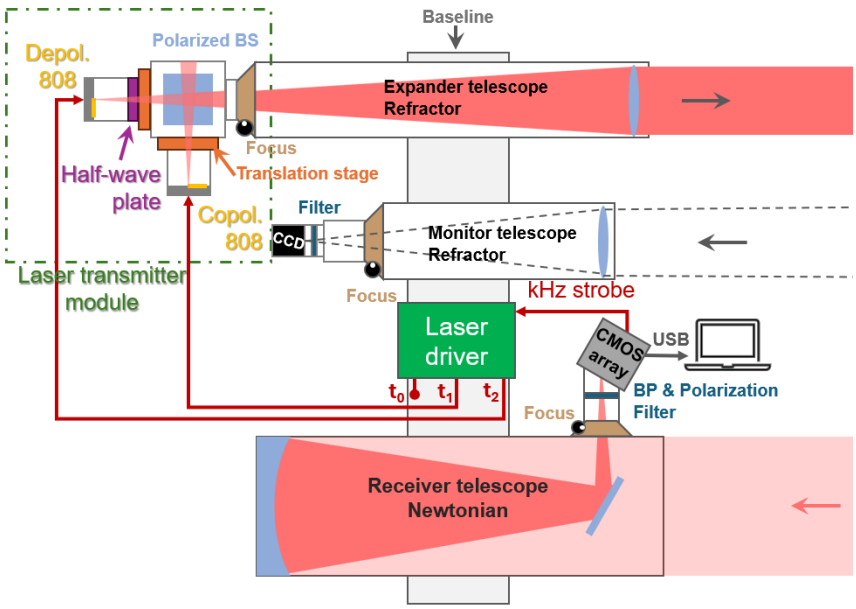

Fig. 3.5: Schematic of a polarization lidar, showcasing the key components and their function. The laser transmitter itself is integrated with two 3W TE-polarized 808 nm laser diodes. One of these laser beams is then rotated 90 ° using a wide-angle polymer half-wave plate. A polarization beam splitter combines these beams for transmission. Backscattered light is collected and passed through a polarization analyzer, separating the orthogonal components for detection and subsequent analysis of the target's de-polarization characteristics. Figure inspired by lecture slide from Biophotonics course and reference [194].

Polarization lidar for insect study (an example of the schematic is shown in Fig. 3.5) utilizes a laser module with two polarized laser diodes multiplexed into de-polarized, co-polarized, and background bands. The receiver telescope projects the collected light through a linear polarizer onto a linear detector array, enabling analysis of the backscattered light's polarization. As previously discussed, the DoLP observed in the backscattered signal from insect is influenced by several factors,

including the location of light scattering on the insect [98, 137], absorption of light by melanin, blood, or water [120, 174], and scattering effects related to the insect's body size and the influence of gravidity [94]. The differences in polarization signatures in lidar observations are effective in separating glossy wing and diffuse wing signals, as shown in *Paper II-IV*, the dependence of signal range on flash coherence and the frequency content of specular flashes was investigated, knowing that de-polarized incoherent scatter attenuates by the squared range. The findings demonstrate that the glossiness of an insect's wings directly impacts how easily it can be detected using lidar. The most detailed information about wing glossiness is obtained by analyzing the harmonic content within the co-polarized power spectra.

The polarization characteristics observed in lidar signals can be compared to a reference library of polarization signatures associated with specific insect species. This library, as demonstrated in *Papers III*, *VII*, and *XI*, can be generated using BIOSPACE scans by analyzing the varying scattering profiles produced when wavelengths and polarization are adjusted. By comparing lidar signals to this established reference library, it is possible to identify insect species in the field. This database should store quantitative data in SI units to ensure compatibility and enable meaningful comparisons across different instruments and research groups. This approach fosters an accurate understanding of light scattering from insects and allows retrieval of quantitative measures in metric units, ultimately aiding in insect species identification.

3.3.6. Dual-band lidar

Previous research has demonstrated the feasibility of retrieving kHz modulation wingbeat from free-flying insects and simultaneously retrieving dual-band signals [159]. This has enabled the separation of mosquito species and sex based on dual-band signatures. Other optical sensors using dual wavelengths have also proven effective in separating insect species [51, 162, 163]. Building upon this concept, dual-band lidar was developed and has proven valuable in various fields, including atmospheric [170, 268] and ecological research [88].

A typical dual-band lidar system, similar in configuration to polarization lidar but with a modified laser transmitter module [88], transmits superimposed laser beams at 808 nm and 980 nm with multiplexing (Fig. 3.6). Dual-band illumination enables estimation of insect melanization and wing thickness. By analyzing differences in backscattered light due to both differential absorption and thin-film interference, increased diffuse reflectance at the longer wavelength is correlated with a higher

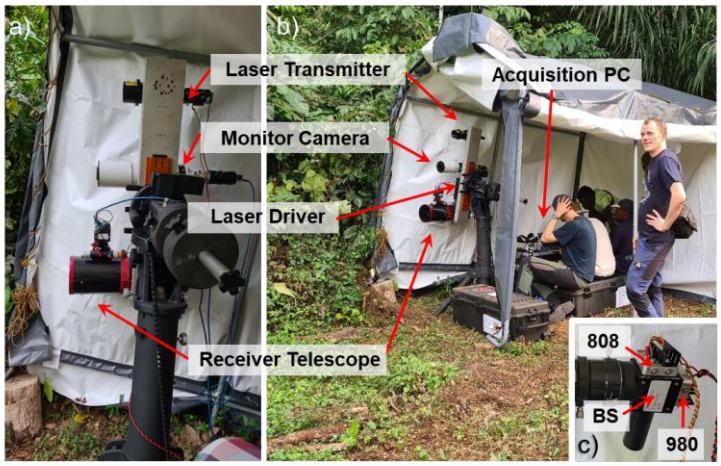

Fig. 3.6: Photos of a dual-band lidar. a-b) Lidar system and its components. c) Laser transmitter module; in this instance, there is no half-wave plate since no altering the polarization plane. Instead, combining a 980 nm and 808 nm laser beam together. BS: beam splitter.

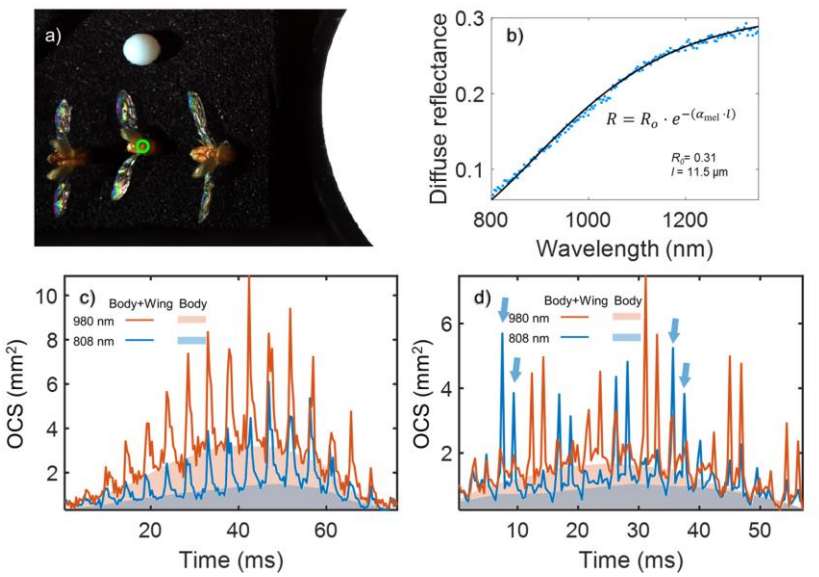

Fig. 3.7: Diffuse reflectance from a dried bark beetle abdomen, showcasing variations in wavelengths and their impact on insect specificity. a-b) Reflectance dips before 1200 nm indicate melanin presence, with a model provided to show melanin path length at the chosen pixel. c) Generally observation using dual-band LiDAR demonstrates that 980 nm is less affected by melanin, thus providing a stronger signal for body and wing analysis compared to 808 nm. d) Specific instances where the 808 nm wing signal exceeds that of 980 nm during certain wingbeats, indicating wing membrane resonance with 808 nm, a crucial clue to insect specificity.

degree of melanization [104], and wavelength-dependent variations in the intensity of specular flashes provide insights into the insect's wing thickness. An example of Dual-band lidar observations (Fig. 3.7) reveals that the 980 nm wavelength, being less absorbed by melanin, generally results in a stronger lidar signal from both the insect's body and wings compared to 808 nm. However, Fig. 3.7d shows that during certain wingbeats, the 808 nm wing signal surpasses that of 980 nm, suggesting that the wing membrane resonates more with the 808 nm wavelength at specific roll pitches. The varying response between 808 and 980 nm during different wingbeats highlights how wing structure, such as wing thickness, influences wavelength-specific interactions, potentially enabling more accurate species-specific identification.

3.3.7. Hyperspectral lidar

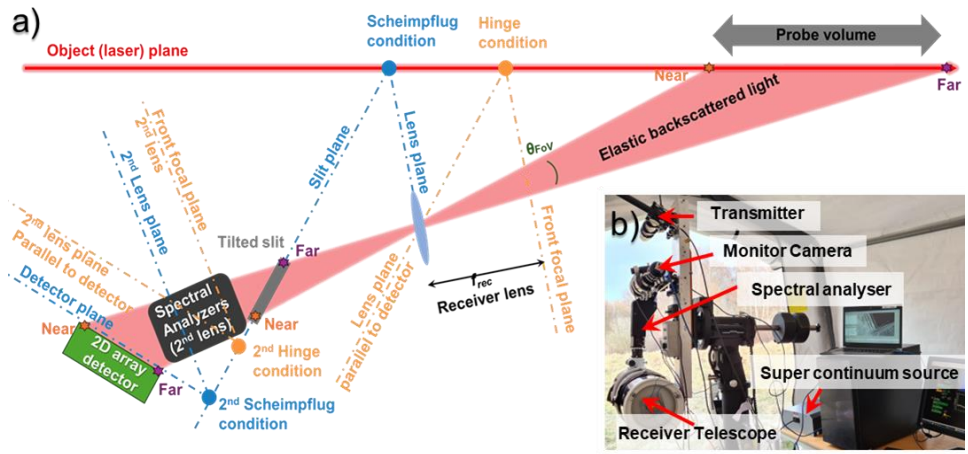

Fig. 3.8: Example of Elastic Hyperspectral Scheimpflug Lidar (EHSL). a) Scheimpflug and hinge conditions were applied twice on a hyperspectral lidar. The figure is based on references [86, 249] with minor modifications. b) Photo of the EHSL setup.

Hyperspectral lidar offers detailed spectral profiles across numerous narrow bands. With the capability to operate across various wavelength ranges, including visible (VIS) [172, 230, 269], NIR [231], and SWIR [231], hyperspectral lidar has found diverse applications. In environmental monitoring, for instance, hyperspectral lidar has been utilized for remote sensing of vegetation or forests [230, 231, 270]. Additionally, it is also used to differentiate rock in geological studies and mining operations [271, 272]. Beyond terrestrial applications, hyperspectral lidar has also extended its reach to aquatic studies [172]. Other promising applications involve monitoring powder-tagged insects, where the fluorescence of an applied powder is measured [273], and induced fluorescence [274-276].

Existing hyperspectral lidar systems typically offer around 8 spectral bands and a detection range of 20 to 30 meters [270, 272], providing valuable insights into the composition of objects and environments. A new hyperspectral lidar system (*Paper XII*) has been developed that utilizes 64 bands and achieves a detection range of up to 100 meters. The 100 meters range limitation is due to the test site meadow size, not the lidar system itself. *Paper XII*'s hyperspectral lidar system (Fig. 3.8) achieves spectral dispersion and maintains focus across scene depth and the SWIR spectral range by applying Scheimpflug and hinge conditions twice. The object plane is projected onto a tilted entrance slit, then dispersed light is projected onto a tilted 2D array detector. The system uses a supercontinuum light source with a long-pass filter to minimize insect disturbance. This unique combination of lidar and hyperspectral imaging enables the collection of detailed spectral reflectance and interference signals (Fig. 3.9) from insects, showing the potential for remote identification of insect species and advancing entomological research through remote insect studies.

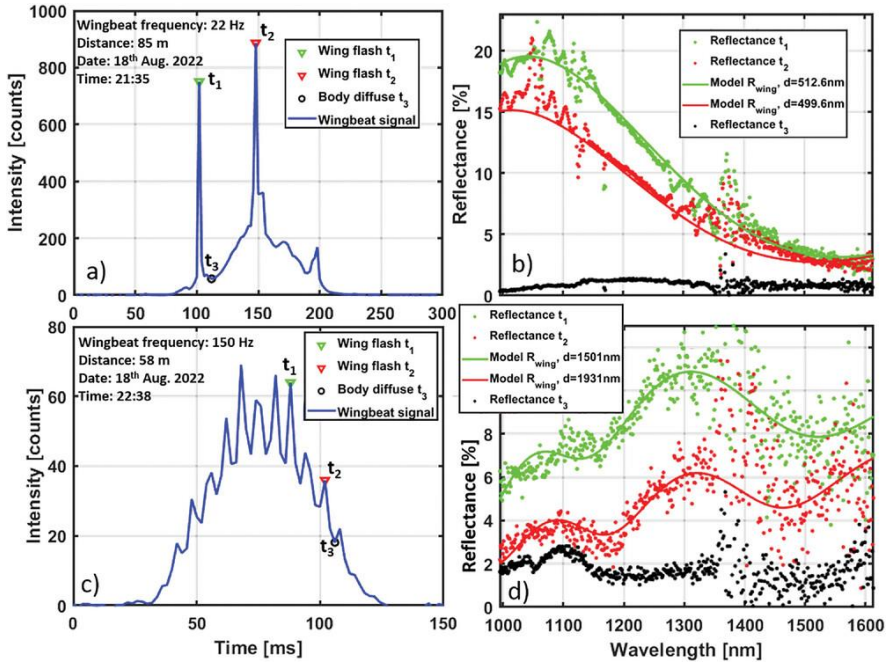

Fig. 3.9: Hyperspectral lidar signals from free-flying insects (figure originally from *Paper XII*). a) Large insect (85m): spiky waveforms, glossy wings, precise fringe model fit. b) Spectral reflectance with fringe model fit. c) Smaller insect (58m): less precise fringe model fit. d) 430 nm fringe difference.

4.Computational data processing

4.1. Scheimpflug lidar data analysis

4.1.1. Raw data visualization and initial signal identification

Entomological lidar offers flexibility for various upgrades or adjustments. It can be adapted to operate in various modes, including polarimetric, dual-band, multi-band, fluorescence, or hyperspectral. To illustrate lidar data processing, this section is focused on polarization lidar data only. Note that lidar settings are also highly customizable, the camera exposure, lines of exposure, offset, and laser module choice can all be adjusted [88, 169, 170, 236-238, 245]. Therefore, it is important to maintain careful documentation of these settings.

In polarization lidar, the laser alternates between de-polarization, co-polarization, and background modes. The lidar was set to capture 30,000 exposure lines per file. Each file takes approximately 4 seconds to record and reaches 120MB in size (sampling frequency at 9kHz). Continuous 24-hour data collection would generate approximately 2.47 TB of data. Given this volume, an initial overview of the data is crucial to monitor data quality. To create this overview, plots are generated that color-code the maximum de-polarized, co-polarized, and background readings within each file. These plots offer insights into temporal and spatial variations in insect presence (appearing as bright green dots) while also revealing atmospheric changes, such as increased cloud echoes under humid conditions.

Consider frame 3991, recorded on June 6, 2022, at 22:46:08 (Fig. 4.1a). Zooming in on this timeframe (Fig. 4.1b) shows distinct signals (later classified as insects) along with persistent aerosol plumes (clouds). Fig. 4.1c details intensity counts for this frame, including pixel-wise median and maximum values. Insect signals are isolated using a threshold defined as the median plus five times the interquartile range (IQR), or SNR=5. This SNR ratio is configurable, but it has proven effective for visually highlighting insect observations while suppressing cloud/mist signals. Fig. 4.1d illustrates how the threshold adapts based on each pixel's median and IQR, for separation of rare, localized events (insects) from continuous aerosol signals.

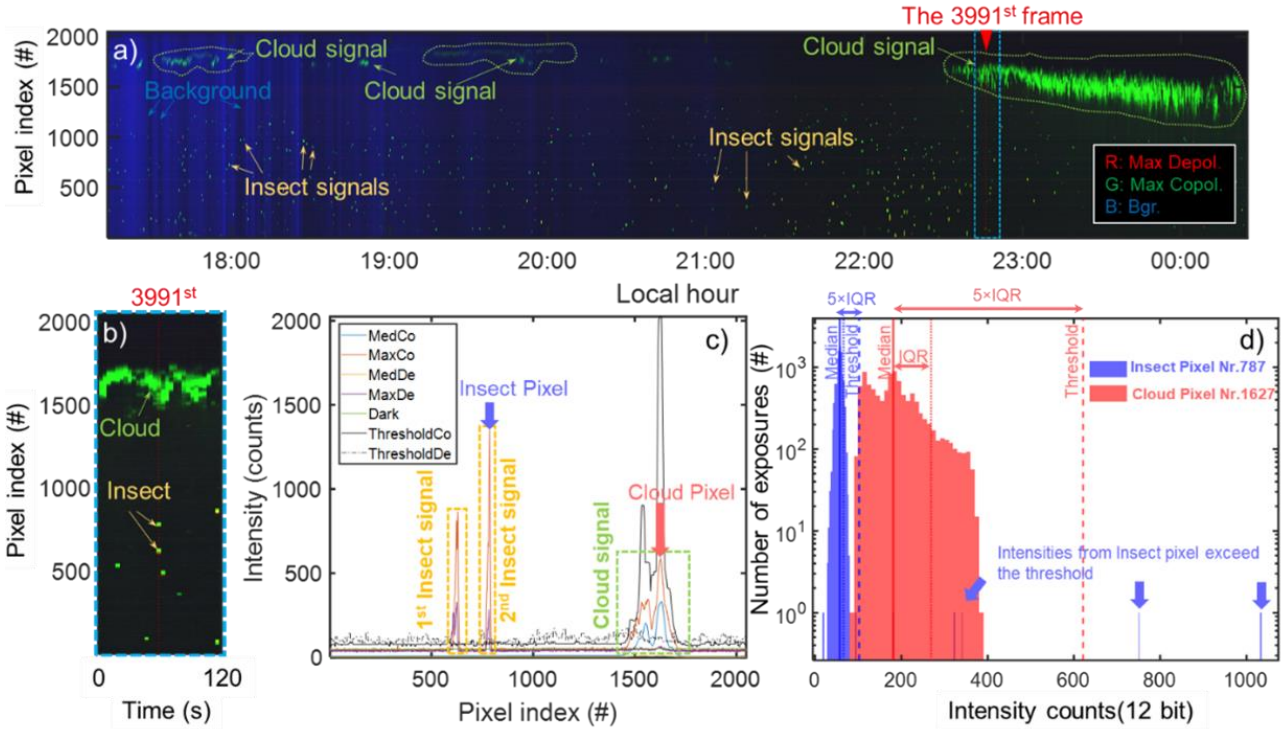

Fig. 4.1: Time-range overview map of the evening of June 6, 202. The map is color-coded to represent the maximum values of de-polarized signal, co-polarized signal, and background for each pixel in 4-second intervals. A zoomed view focuses on the time range around frame 3991. The intensity distribution on frame 3991 reveals two insect signals exceeding the SNR=5 threshold (5 times the IQR of the histogram), distinguishing them from cloud signals and leading to their exclusion. Finally, one insect pixel and one cloud pixel from frame 3991 illustrate the recorded values and demonstrate the thresholding process.

4.1.2. Observation extraction

When visualizing frame 3991 around one of these observations (Fig. 4.2a), the raw data reveals stripes due to the lidar laser's multiplexed operation. This cycling of de-polarized, co-polarized, and background modes is illustrated in Fig. 4.2b. The data was extracted for each band. The insect observation appears as shown in Fig. 4.2c-e for the different bands. After acquisition, background subtraction was performed on both the co-polarized and de-polarized signals (Fig. 4.2c, d). To isolate insect signals from noise, a detection threshold was applied, retaining only signals with an SNR of 5 or higher (Fig. 4.1d and 4.2f). Finally, the insect signals were isolated and cropped using methods detailed in previous work [125].

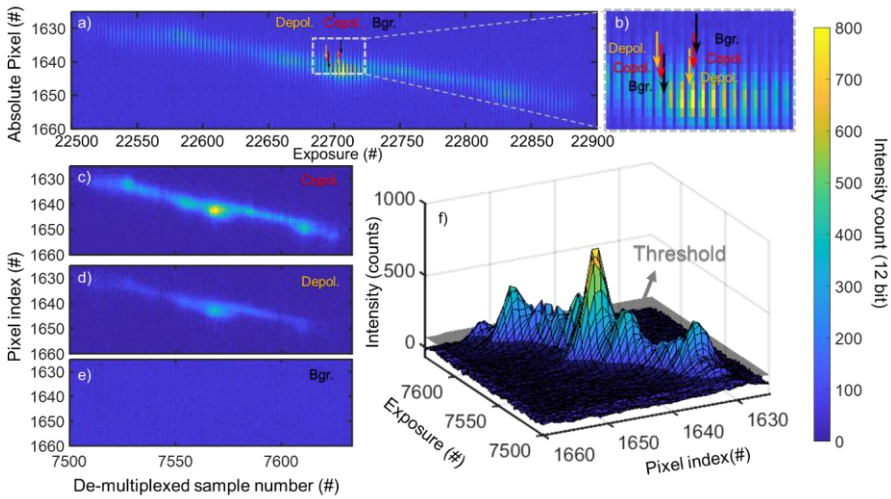

Fig. 4.2: Illustration of raw data acquisition and processing. a) and b) show the raw data captured with the laser multiplexed to de-polarized, co-polarized, and background bands. c) and d) depict the subtraction of de-polarized and co-polarized signals from the raw data, respectively. f) shows the detection mask applied to retain only signals exceeding a defined threshold of SNR=5, effectively isolating insect signals from background noise.

The data shown in Fig. 4.2f is presented as a 2D false-color image in Fig. 4.3a. This visualization employs color coding to differentiate signals: red represents de-polarization, green signifies co-polarization, and blue indicates background. This approach enables the observation of the insect's movement and heading direction within the brief period captured by the lidar. The height and apparent size of the insect were derived using lidar processing methodologies established in previous work [89, 125]. Fig. 4.3c sums all intensity pixels from Fig. 4.3a, revealing the insect's wingbeat pattern. For further calibration of the optical cross-section (mm^2), a reference target range and its corresponding optical cross-section is required. A

base calibration method involves placing a flat neoprene board in the lidar beam to serve as a reference target and termination.

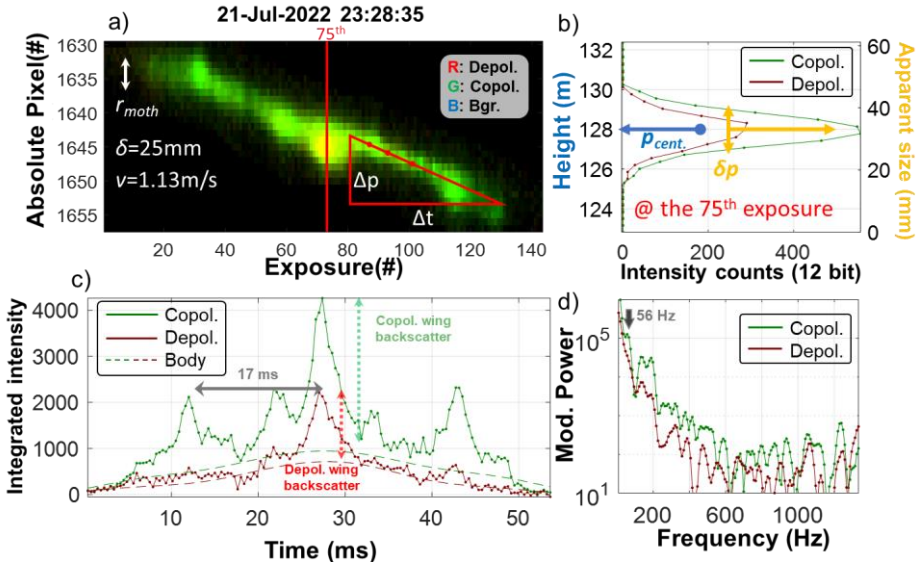

Fig. 4.3: An example of an insect observation obtained using polarization lidar technology (figure originally from *Paper II*). a) A false-color spatiotemporal display showcases the insect's presence. b) A single-camera exposure highlights the insect echo. c) The time series for both polarization bands reveal an oscillatory component due to wing movement, along with a biased envelope caused by the insect's body. d) The corresponding power spectrum identifies the fundamental frequency as the highest tone in this specific observation.

4.1.3. Hierarchical clustering & biodiversity assessment

Entomological lidar, while highly effective at quantifying insects passing through its laser beam [87, 89, 125, 277], faces challenges in associating these echoes with specific, verified taxa. This difficulty is similar to the challenge of identifying insects exclusively by their WBFs, as various factors can influence an insect's flight orientation and WBF. Both environmental conditions (temperature [43-45], humidity [45, 46]) and individual insect characteristics (age [47, 48], weight loading [49, 50]) can influence WBFs. These variations can lead to misidentification, as different insects may exhibit similar oscillatory signals and be grouped together, or the same insect may be identified as a different species due to changes in its WBF in response to environmental factors.

Despite these limitations, field data analysis using unsupervised hierarchical cluster analysis (HCA) reveals numerous distinct signal types [51, 87, 92, 277]. It is

anticipated that a diverse insect assemblage would exhibit a similarly diverse range of signals, whereas a less diverse group would display fewer distinct signals. This deterministic approach, previously applied to photonic sensors and lidar [51, 87, 93, 287], has successfully grouped observations into many groups of clusters. Some of these clusters have been associated with specific insects, like male and female mosquitoes [87, 277]. While a perfect match between the number of clusters (NoC) and species richness is unlikely, an increase in NoC is generally expected as species richness increases. A study [51] found a 67% correlation between photonic-sensed insect signals and insect families identified in Malaise traps, and the algorithm estimated higher insect diversity than was revealed by family-level trap identifications. However, malaise trap catches vary significantly depending on deployment location and time, potentially capturing vastly different species and resulting in poor correlation between individual deployments [34], suggesting that the limitations of the Malaise trap itself may be hindering a more accurate assessment of insect biodiversity.

HCA is well-suited for lidar data due to its ability to handle inconsistencies and group data points based on relative similarities rather than absolute distances or predefined labels [278]. By analyzing the power modulation spectra and calculating pairwise similarities using Euclidean distances [279], HCA organizes observations into a hierarchical structure (Z). This structure serves as a foundation for deriving clusters by setting distance thresholds or specifying the desired number of clusters. This approach enables the exploration of natural groupings within the data, aiding in the determination of distinct signal types representing different species based on their unique power modulation spectra.

An example of how this method was applied is described below. The data used in the following examples is from an unpublished study related to dual-band lidar signals (*Related Work B*). In this experiment, a dual-band lidar system was deployed to measure the population and diversity of a Swedish meadow over three consecutive days. To minimize bias and provide a negative control for biodiversity assessment, background noise captured by the lidar system was processed in the same manner as the lidar signals themselves, see Fig. 4.4. Both the lidar data and noise were normalized and compensated for slope using the data processing pipeline described in [92]. The number of compensated clusters exceeding the threshold provides an estimate of the number of species/clusters. To calculate compensated clustering, we employ a multi-step process involving the Pwelch method, logged Euclidean distances, and median slope detrending. The detailed formula and implementation can be found in the reference [92]:

$$NoC = \sum_{p}^{N-1} \left[Z_{\text{comp.(p)}} > \left(\left| Z_{\text{comp.(p)}} \right|_{\text{median}} + \left| Z_{\text{comp.}(p)} \right|_{IQR} \right) \right] \qquad (4.1)$$

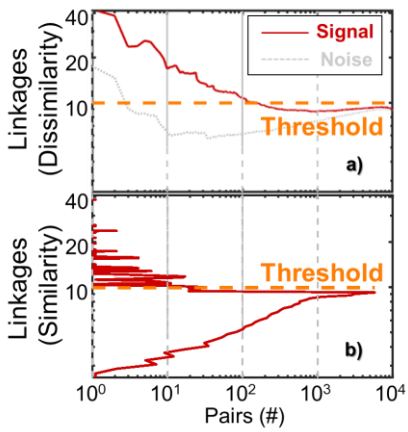

Fig. 4.4: Determination of optimal linkage threshold for biodiversity search. a) The relationship between the number of sample pairs and their corresponding compensated linkage distances, with an emphasis on dissimilarity. b) Histogram depicting the frequency distribution of linkage Z values. The vertical threshold line highlights the cutoff for significant Z values.

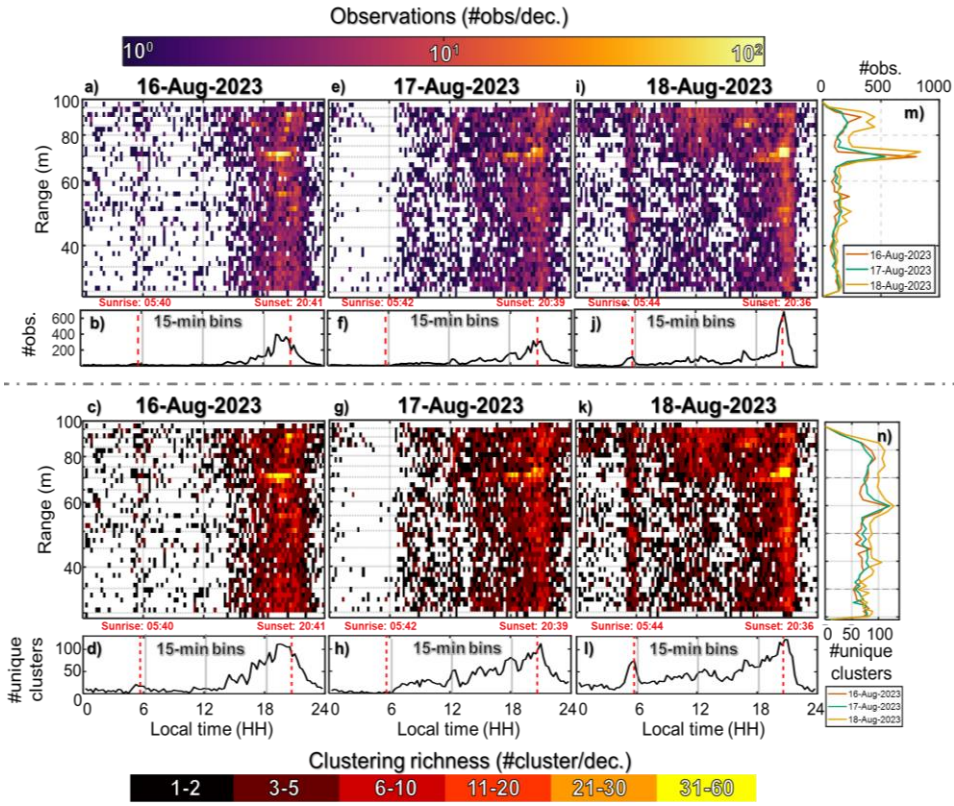

Fig. 4.5: Spatiotemporal patterns of insect activity and biodiversity across the experimental period. Heatmaps a, e, i) illustrate the spatial and temporal distribution of insect activity based on lidar observations for each experimental day, with brighter colors indicating higher activity levels within 15-minute intervals. Line graphs b, f, j) depict the overall temporal pattern of insect activity throughout each day. Heatmaps c, g, k) reveal

the variation in insect biodiversity across the three experimental days, with each decade representing the number of unique insect clustering groups within specific time and range intervals. Line graphs d, h, l) illustrate the overall temporal variation in biodiversity throughout each day. A combined line graph m) displays the total lidar-detected insect counts across the entire transect for each day, highlighting areas of higher abundance. Finally, a line graph n) shows the variation in biodiversity across the entire transect for each day, illustrating differences in group activity with respect to range.

The analysis of insect biodiversity in a Swedish meadow over three consecutive days reveals intriguing patterns in insect activity, species richness, and spatial distribution. Utilizing equation 4.1, a total of 153 unique insect species was estimated to present across the three days of observation. Heatmaps (Fig. 4.5) illustrate distinct patterns in insect activity and diversity distribution throughout the day and across different spatial zones within the meadow. Notably, the 60-100 meter range consistently demonstrated high insect activity, suggesting this area may offer favorable conditions or resources for insect populations.

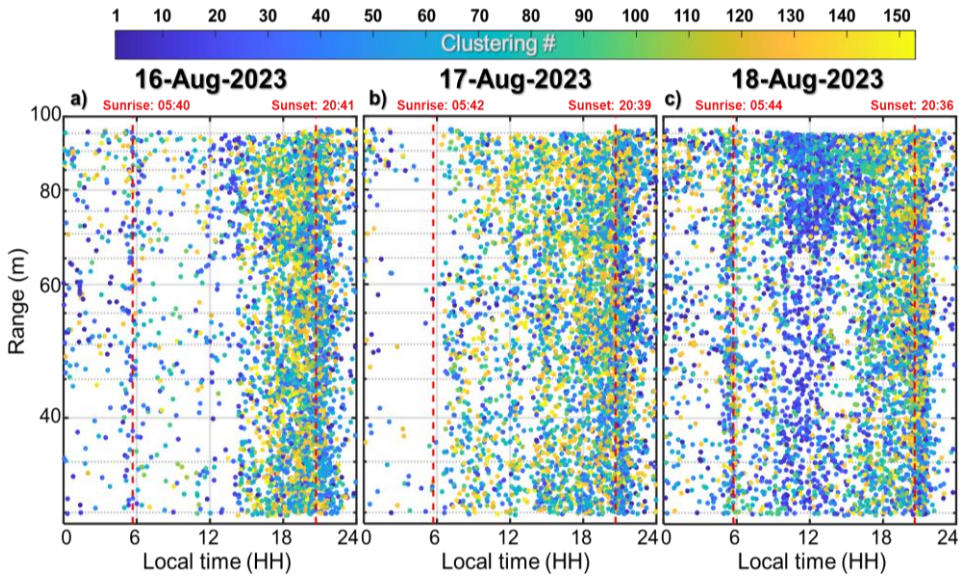

Fig. 4.6: Temporal and spatial distribution of clustering groups. Different colors represent distinct clusters

Additionally, specific clustering groups exhibited unique preferences for particular time intervals and spatial ranges, with some groups exclusively active in the late afternoon and evening, see Fig. 4.6. These findings highlight the complex dynamics of biodiversity within ecosystems and emphasize the value of advanced remote sensing techniques to visualize population and diversity distribution, enabling the possibility to correlate species distribution with habitat characteristics, activity patterns, and resource availability.

4.2. Hyperspectral data analysis

4.2.1. Reflectance calibration of hyperspectral image

The unprocessed spectral data acquired by a hyperspectral system is influenced by several instrumental factors. These encompass the spectral irradiance of the illumination source, the diffraction efficiency of the grating, the quantum efficiency of the detector, and the specific geometries of illumination and collection. Calibration using known reference standards is required to compensate for these effects. Reflectance calibration is performed using an equation derived from measurements of the sample, dark current, and a white reference. The dark current, measured in the absence of light, is important for subtracting electronic noise. In hyperspectral cameras with integrated shutters, the equation often simplifies to (Fig. 4.7):

$$R_{(y,\lambda)} = \frac{I_{S_{(y,\lambda)}}}{I_{W_{(y,\lambda)}}} \tag{4.2}$$

The choice of reference material is important. Both Teflon (approximately 99% reflectance) and a Lambertian gray Spectralon® references are good options. Note that calibrating a specular surface against a diffuse reference can result in reflectance values exceeding 100%.

Fig. 4.7: Hyperspectral scan scenario where the sample and reference are placed on the same plane. This configuration ensures close pixel-by-pixel matching between the camera's Y pixels and the reference.

4.2.2. Effective fringe and membrane thickness

Earlier discussions established that clear insect wings produce fringes due to thin-film interference. This phenomenon was elaborated upon using equations introduced in chapter 2; resonance backscatter conditions were addressed by equation 2.27, and non-resonance conditions by equation 2.29. Furthermore, each

fringe was described through equation 2.30 in conjunction with the Fresnel equations (equation 2.23) and the refractive index of chitin (equation 2.19). The method of modulation for each fringe was characterized by a formula where R represents measured reflectance, F signifies the computed fringe, λ is the wavelength, σ_λ denotes the standard deviation in the spectral domain, and μ_λ is the spectral mean value,

The model in equation 2.30, $F\ (\lambda,\ d_{pix})$ was used to calculate fringes based on membrane thickness d_{pix}. Fringe modulation was estimated using equations 2.31 and 2.33 (see equation 2.19 for examples from thick, thin, and effective thicknesses). To do this, 1000 fringes with realistic membrane thicknesses (ranging from 350 nm to 4000 nm as used in *Paper X*) were computed to ensure accurate numerical fitting within the limits of the hyperspectral camera's spectral range (950 nm to 2500 nm as used in *Paper X*). To model fringes across entire wings (including those with single thickness, d_{wing}, the function $F\ (\lambda,\ d_{pix})$ from equation 2.30 was expanded into equation 4.3. The measured fringes, R_λ, were compared with computed fringes, $F\ (\lambda,\ d_{pix})$, using the correlation coefficient C and quality parameter Q. Taking derivatives of Q helped disregard slopes and squared factors that could introduce calculation complexities. Finally, this model was applied to each wing pixel to determine membrane thicknesses and modulation depths, for example fringes.

$$C(R,F) = \frac{\int_{0.95}^{2.5}\left(F_{\lambda,d_{pix}} - \mu_\lambda\left(F_{\lambda,d_{pix}}\right)\right)\left(R_\lambda - \mu_\lambda(R_\lambda)\right)}{\sqrt[2]{\int_{0.95}^{2.5}\left(F_{\lambda,d_{pix}} - \mu_\lambda\left(F_{\lambda,d_{pix}}\right)\right)^2 \partial\lambda \int_{0.95}^{2.5}\left(R_\lambda - \mu_\lambda(R_\lambda)\right)^2 \partial\lambda}} \tag{4.3}$$

$$\mathrm{Q}\left(d_{\mathrm{pix}}\right) = C(R,F)\left(C\left(\frac{\partial R}{\partial\lambda},\frac{\partial F}{\partial\lambda}\right)\right)^2 \tag{4.4}$$

This enhanced model accounts for fringe modulation behavior, which increases with infrared wavelengths and decreases with visible wavelengths. Long-pass and short-pass functions were used to model modulation amplitude and bias. Parameters such as amplitude α, bias β, and heterogeneity λ_0 were fitted numerically across all recordings, ultimately parameterizing the fringe into just four values.

5.Conclusions and Outlook

This study builds upon advancements made during campaigns at the HySpex hyperspectral camera lab. We have conducted several field campaigns using entomological Scheimpflug lidar, progressively enhancing the system's capabilities with each endeavor. The development and validation of the polarimetric kHz lidar system enhances measurement specificity while preserving lidar's inherent ability to provide precise temporal and spatial information on detected insects. The introduction of dual-band lidar has proven invaluable in assisting with insect identification, leveraging the relationship between backscatter signals with insect membrane thickness and degree of melanization. Furthermore, the recent advancement in hyperspectral lidar technology has enabled detailed spectral analysis of insect membrane characteristics. This technology also captures detailed temporal and spatial data while still allowing for the detection of wingbeat patterns.

After examining thousands of specimens, we discovered that features such as membrane thickness, surface roughness, and polarization hold the potential for accurately identifying species and sex across diverse insect groups. Moreover, variations in melanin, chitin, and water content were found to enhance the capabilities of photonics-based systems to distinguish between gender, species, and life stages of insects.

Building upon these findings, we developed a novel, unsupervised biodiversity assessment algorithm that utilizes lidar data. Similar to acoustic indices used in ecological research, this algorithm clusters signals based on similarity, eliminating the need for a training dataset. This innovative approach enables rapid, large-scale biodiversity assessment and provides preliminary estimates of species richness without the need for time-consuming species identification. However, the accuracy of these estimations is contingent upon the algorithm and lidar instrument's ability to differentiate between the expected number of groups within a given habitat. If this criterion is not met, the accuracy of the richness estimation will be limited by the capabilities of either the algorithm or the instrument itself. The prerequisite for species differentiation is that differences in physical properties exceed within-species variation. We have established this to be true and have successfully extracted multiple quantitative micro-features from free-flying insects. This confirms that this approach can accurately and efficiently assess biodiversity using lidar technology.

Our work on the 'Farfetched Flatness' of rough-surfaced wing insects like brown moths has demonstrated the capability of longer wavelengths to enhance backscatter signal strength, effectively minimizing the loss of specular reflection caused by surface features like wrinkles, scales, and refractive gradient, potentially broadening the use of long wavelengths in ecological studies for insect detection. The future could benefit from a much larger database that utilizes tools like BIOSCAPE to augment lidar observations with scanned species data based on spectral and polarization properties. This could be achieved through parallelization, citizen science initiatives, and engaging high schools in data collection [280]. The collection of quantitative optical properties data of insects in standardized metric units is essential for building universally applicable and interpretable entomological databases.

Advancements in entomological lidar, combined with spectroscopy and polarimetry, offer transformative potential for insect identification and monitoring. This technology provides detailed insights into insect behavior and ecology, leading to improved strategies for pest control, pollination, and disease prevention. Ultimately, gaining a deeper understanding of insect populations and their interactions with the environment promises a more sustainable future.

Looking ahead, several promising directions for this research are evident. One such direction is to enhance the lidar system's capabilities by exploring the use of carefully selected laser bands to resolve insect wing thickness, potentially eliminating the need for complex setups like supercontinuum light sources. Furthermore, incorporating DNA sampling [65-67] along the lidar beam path could validate the lidar index monitor changes in insect abundance and diversity and be more cost-effective. This will enable the assessment of the correlation between captured insect species richness and lidar data, providing valuable insights into ecological dynamics. Additionally, integrating lidar with machine learning algorithms [55, 281, 282] has the potential to expand its applications in long-term ecosystem monitoring.

In the field of sustainable agriculture, lidar technology could prove invaluable. By assessing biodiversity changes under different farming systems, it could revolutionize landscape management practices. Similarly, in forestry, lidar could be utilized to monitor pest populations and their ecological impact, leading to more effective management strategies.

The future of entomological research lies in advancing these monitoring technologies and integrating them into broader ecological frameworks. A critical challenge remains in making these technologies accessible. By making lidar technology affordable and user-friendly, global biodiversity assessment can be empowered, ensuring its reach on a worldwide scale. As knowledge expands, a path is charted toward a more informed and sustainable coexistence with the natural world.

Acknowledgment

I'm extremely grateful to my tremendously revolutionary fantastic supervisor, *Mikkel Brydegaard*, for this incredible Ph.D. journey. Your dedication and passion are an inspiration. No matter the hour or the place, you've always made yourself available to answer our questions, even interrupting your holiday or evenings. I really appreciate your willingness to open up your network and help us build our own paths in the academic world. Your understanding and support during challenging moments have meant a lot to me. Thank you for everything!

I want to say a big thank you to my friend and colleague, *Hampus Månefjord*. He is extraordinarily intelligent – truly one of the smartest people I know – and always carries himself with kindness and gentlemanly grace. I have no doubt that he will achieve anything he sets his mind to because he is just that incredible. I am thankful for all the times he provided insights that helped me overcome challenges.

I am very happy and thankful for my friend and colleague, *Dolores Bernenko*. It has been super nice to share an office with you for the past half-year. You are not just incredibly kind but also a beacon of support. You listen with such care, making me feel valued and heard in ways I never have before. Whenever I'm stuck or have a question, you never hesitate to dive deep and help find the best solution, showing your dedication and kindness. Your intelligence shines in your work, matched only by your hard work and commitment.

I would like to extend my sincere thanks to my friend, colleague, and old-officemate, *Lauro Müller*. I've truly enjoyed sharing an office with you! Your knack for decorating our shared workspace made it feel like a second home. Your intelligence, handiness, and multilingual abilities are truly impressive. I still remember the day when you sent out three applications and ended up with seven job offers – a testament to your incredible value in the professional world!

I would like to extend my heartfelt gratitude to my friend and former colleague, *Samuel Jansson*. When I first joined the group, you were already deep into your Ph.D. with Mikkel. You've been an incredible mentor – always dependable, patient, and friendly. Your unique style and dedication to interesting projects and hobbies have truly inspired us all.

I'd like to express my gratitude to *Elin Malmqvist*. Even though we didn't work directly together, your cool and kind approach has always stood out. Your guidance,

especially with lidar coding, has been invaluable. As a fellow dog lover, I also deeply appreciate your passion for animals.

I am deeply grateful for my friend and former colleague, *Jonathan Peterson*. You were the one who patiently sat down with me at the start of my PhD and guided me through the complexities of lidar coding. Your kindness, patience, and willingness to share your knowledge have been invaluable to me.

A huge thanks to David Dreyer for his unwavering support, delicious treats, and infectious positivity. His dedication and kindness make him an invaluable member of our team.

My deep gratitude goes out to my co-supervisors, *Christian Brackmann* and *Jadranka Rota*. Christian, your kindness, patience, and stellar teaching have profoundly shaped my academic journey. I'm thankful for the role you've played in my development. Jadranka, your dedication, passion, and support have been a source of inspiration and comfort during challenging times. Together, you've been the bedrock of my support, offering essential help, guidance, and encouragement. The difference you've both made in my life, personally and academically, is immeasurable.

I truly appreciate your guidance, *Anna Runemark*, my career mentor. Your dedication and passion for your work are inspirational, and you stand as a role model for me. Beyond your kindness and caring nature, you openly share your ideas and experiences with us juniors. The lunches where you share your academic career journey are incredibly helpful as we navigate this world. Your success in the field, combined with your genuine kindness, makes you a treasure in academia. I'm deeply grateful for your mentorship.

I'd like to take this opportunity to thank the rest of the strategy lunch members: *Hanna Thosteman*, *Sofie Nilén*, *Erica Winslott*, and *Emma Kärrnäs*. Each of you is truly amazing, and your passion for your work is both motivating and inspiring. I feel privileged to have shared this time with you. I wish you all the very best in your research careers and hope we can continue our lunch gatherings even after I complete my Ph.D.

I want to extend a special word of thanks to *Nina Reistad*. From the moment we met at the atomic division, your kindness and support have been unwavering. Your gentle and friendly nature always encourages me to dream big, reminding me that anything is possible. Your generous offer to teach me how to drive is just one example of your caring spirit. Nina, you're an extraordinary person, and I hold a great deal of admiration for you.

My sincerest thanks go to *Jacobo Salvador*. Your care and concern during each field campaign ensured our safety and well-being. As a friend, your kindness and compassionate nature have been a source of great comfort. Jacobo, your presence was invaluable, and I am grateful to you. Your selflessness and unwavering support

have been a beacon during challenging times. Thank you for being an extraordinary person and friend.

I must extend my sincere appreciation to my colleague and friend, *Vivian Feng*. Even though we only worked together for a week, it surprisingly felt like we'd known each other forever. Vivian, your friendly character made it so easy to bond with you, and I'm extremely thankful for our friendship. Your love for bubble tea is adorable, and your interest in Swedish paper bags always brings a smile to my face. Additionally, your enthusiasm for your work and remarkable work ethic truly inspires all of us.

Julio Hernandez, I cannot thank you enough for generously allowing me to use your setup so frequently. Your friendliness and warm welcome every time we are in Oslo mean a lot, especially considering how busy you are. I know it's challenging to plan time with you, but you always make a genuine effort.

I would like to express my heartfelt gratitude to *Klas Rydhmer* and *Carsten Kirkeby*. Working with both of you has been an enjoyable experience. Klas, your warm and cheerful nature has always brought comfort to those around you. Your passion for your work and career is remarkable, along with your ambition to create a biodiversity world map. Carsten, your friendly and patient explanations have been invaluable. Your love for your career shines through, and I particularly cherish the moments when we all exchange awkward glances at Mikkel's dad's jokes. Thank you both for creating such a pleasant atmosphere during each field campaign.

I want to express my sincere appreciation to *Malin Malmsjö*, *Aboma Merdasa*, *Nils Gustafsson*, and *Sheikh Rafi* from the eye clinic for their support and generosity in lending us the hyperspectral camera. I also appreciate *Magnus Cinthio* and *Tobias Erlöv* from the ultrasound group for introducing us to the photoacoustic tomography system. Additionally, I'm grateful to my ultrasound course teacher, *Monica Almqvist*. Your inspiring teaching style makes you one of the best lecturers I've had during my time at the university. Thank you for an unforgettable learning experience.

I'm truly grateful to our department's incredible team: *Emelie Niléhn*, *Cecilia Bille*, *Minna Ramkull*, *Charlotta Åberg*, and *Igor Buzuk*. Emelie, your kindness and gentle demeanor brighten every day. Cecilia, I greatly appreciate your warmth, kindness, and immense patience. Minna, your friendly and lively spirit always brings joy to our workspace. Charlotta, thank you for always being so kind, friendly, and welcoming. Your patience and understanding are truly appreciated. Igor, your kindness is a beacon of light, and your problem-solving abilities are legendary. I deeply appreciate each of you. It's always a pleasure to see you all – you are the heart of the department, and your friendliness, care, and genuine warmth are unmatched.

I want to express my deepest thanks to *Per-Erik Bengtsson*. Your extraordinary kindness, support, and ability to notice when someone needs help, even before they realize it, speaks volumes about your care for those around you. When I was unwell, your prompt support and understanding were incredibly reassuring. I feel fortunate to be part of a division with such considerate and supportive leadership.

My heartfelt thanks go to *Joakim Bood* and *Sven-Inge Möller* for their exceptional kindness, care, and support. You have both shown incredible supportiveness, always available to discuss any matter. Your guidance and empathetic approach have enriched our division immensely.

My thanks also go to *Dina Hot* and *Xin Liu*. Their warm welcome to the department was a great comfort. When they graduated, their absence created a significant void that we all deeply felt. I would be remiss if I did not also mention *Jundie Chen*, *Emma Axebrink*, and *Yue Qiu*. It always makes me so happy to see you all; you are welcoming, kind, and always willing to listen. Yue, your constant cheerfulness is a joy to behold and uplifts everyone around you.

I must express my heartfelt admiration for *Yupan Bao* and *Emma Simpson*. You two have been a constant source of inspiration, and I can confidently say that you both are forever my idols. Your dedication, passion, and positive attitude toward everything you do are truly motivating. I am profoundly grateful for your influence on my life and for the example you set for me and others.

I would like to extend my heartfelt thanks to *Hui Chen*. It was a pleasure to work with you. I must say, it was the first time I encountered a biologist who understood our lidar so thoroughly. Your friendliness, intelligence, and hard work make you an exceptional colleague and valued friend.

To all the Bachelor's and Master's students I've had the chance to work with, thank you for the valuable time we spent together. I'm particularly grateful to *Ebba von Wachenfeldt*, whose dedication during the Stensoffa 2020 campaign was remarkable, keeping our system going even in the hottest weather. I want to extend my thanks to *Andrés Andrés* for the great companionship during the fieldwork at Nyteboda and for teaching me how to carve a spork. Special thanks go to *Noélie Guilcher* for organizing a vast amount of insect literature and to *Clara Seinsche* for her strong work ethic – your future in research looks bright! I also appreciate *Paul Travers* for his commitment in 2022, his help with the moths, and the impressive data he gathered. A huge thanks to *Zhicheng Xu* – your initiative and hard work are truly admirable, and you are such a caring, kind, sweet, and cute person. Also, a big shout-out to *Isa Hendriks*. Your dedication, and friendly vibe are amazing. It's great to see you diving into work you're passionate about (And thank you so much for feeding me cookies)! I would also like to express my sincere gratitude to *Emmanuel Kotu Robertson* for his incredible work ethic, independent spirit, and invaluable contributions. Your ability to create such beautiful and inspiring figures is truly remarkable.

I want to take a moment to express my heartfelt thanks to all my current and former colleagues and friends in our division and department. Your support and friendliness have been fundamental to my experience here. Although I can't mention each of you by name, please know that your contributions have been deeply appreciated. Thank you for being such a crucial part of my journey. And a special thanks to *Trivselgruppen* – you all do a wonderful job making our division feel friendly and supportive. Your dedication is really appreciated!

To our collaborators. I am deeply grateful to *Jérémie T. Zoueu*, *Edoukoua Jean Michel Konin*, and *Benoit Kouassi Kouakou* for their warm welcome and being a great host to the Côte d'Ivoire. I would also like to express my gratitude to the wonderful friends and colleagues who provided invaluable support and made our time in the jungle an enjoyable experience: *Assoumou Saint-Doria Yamoa*, *Yatana Adolphe Gbogbo*, *Rabbi Boateng*, and *Andrew Atiogbe Huzortey*. Your constant support and companionship made the impossible possible. Un grand merci à *Doria* pour m'avoir constamment nourri. Ta nourriture est très bonne.

I want to express my deep gratitude to *Tidiane Ouattara*. In the dense jungle, you were like our 'Dad', the one who could miraculously fix everything and extinguish any challenges. We faced a couple of daunting situations, but your skills and knowledge helped us navigate through them all. Without you, I genuinely doubt we could have completed the experiment in the jungle successfully. Your contributions were critical to our success, and for that, I am profoundly grateful. Je souhaite remercier *Tidiane Ouattara* pour son aide dans la jungle. Il était notre mentor et savait toujours comment résoudre les problèmes. Son expertise a été essentielle à notre succès et je lui suis profondément reconnaissant(e).

I want to say a huge thank you to *Sofia Mouchard*, my high school teacher from IHGR. When I first came to Sweden, I was lost in a world of new languages and cultures. But you were there for me, not just as a teacher, but as a friend. You showed me patience and kindness and believed in me when I was unsure of myself. You never made me feel like a burden but always treated me as someone who could reach their goals. You helped me to believe in myself and gave me the courage to chase my dream. Your influence on my life has been so important, and I carry that confidence you gave me every day. Thank you from the bottom of my heart.

I want to extend a big thank you to my Bachelor's and master's thesis supervisors, *Stefan Andersson-Engels* and *Stefan Kröll*. Your knowledge and professional attitude have truly inspired me. Your passion and dedication towards photonics have revealed its beauty and excitement to me, compelling me to pursue a path in Biophotonics. I genuinely appreciate the time I spent working under your guidance. Thank you for your mentorship and for inspiring me to continue in this fascinating field.

I want to express my deepest thanks to all my friends. Honestly, I can't imagine trying to fit all my gratitude for you all into this text – we'd end up with more pages

of acknowledgments than the thesis itself! I apologize in advance if I've inadvertently missed anyone on this list, as so many of you have touched my life in meaningful ways. So, let's catch up soon and celebrate together. Special thanks to *Alsu Zubairova, Armand Dominguez, Bonnie Wu, Daniel Dannymannen Cheveyo, Daniel Nastasijevic, David Sanned, Friederike Koerting, Hafsa Syed, Hang Yin, Harry Biggs, Hasti Yavari, Isabelle John, James Harkonnen, Josefin Lindström Månefjord, Justine Le Douaron, Kerstin Bergentz, Khanh Trinh, Lisa Rämisch, Madeleine Burheim, Martin Guvå, Megha Prakash, Meena Raveesh, Mohammed Μοχαμεντ Ghanem, Qiaoyin He, Sabrina Gericke, Senfeng Li, Stelios Στέλιος Gakis, Timothy Lewis, Timothé Ramboazanaka, Tina Lorentzon, Vanessa Skällenäs, Vibha Kumra Ahnlide, Vidar Flodgren, Yamin Zhang, Yanhong Cai, Yoana Ilarionova,* and *Yousef Namazi*. Your companionship, laughter, assistance, and support have been incredibly vital to me, providing comfort and resilience during challenging times. I may not have been able to spend as much time with you all lately due to other obligations, but each moment we share is treasured and reminds me of the warmth and support our friendships provide. To all my friends, named here or not, thank you for being such a significant part of my life and my journey. You've enriched my experiences in countless ways, and for that, I am eternally grateful. <3

I would like to express my sincere admiration for *Selma Flodgren*, undoubtedly the best artist in the world. Your professionalism, kindness, efficiency, and exceptional skill are truly inspiring. I deeply appreciate your assistance with my front cover designs.

I wish to take a moment to extend my deepest appreciation and gratitude to my old gaming family from *Final Fantasy 14*, our beloved group, the Meme Raiders. I hold each and every one of you in high regard – *Jen Jen*, *Lin*, *Saro*, *Zel*, *MB*, *Mazee*, *Aphelios*, *Seth*, and our honorary raider, *Coach*, *Kumen*, Saudi Princess *Uleena*, and Saudi Prince *Fahad*. I'm sorry I couldn't play games with you as much due to my busy schedule, but I truly cherish every moment we've shared – gaming, singing, or simply chatting. A special thank you to Saro: When Karl found himself stranded in England, you went above and beyond the call of friendship. Driving for hours to rescue him in the middle of the night showed incredible kindness, and we are eternally grateful. You're a beacon of light, and we couldn't ask for a better friend. We love you, man; thank you so much!

I am deeply grateful for the love and support from my second family, *Marketa Adamek Bastos*, *Adriano Bastos*, *Marina Bastos*, *Jana Wettermark*, and *Gunnar Wettermark*. Your encouragement means so much to me. Jag är så tacksam för all kärlek och stöd jag fått från Marketa Adamek Bastos, Adriano Bastos, Marina Bastos, Jana Wettermark och Gunnar Wettermark. Era uppmuntrande ord betyder jättemycket för mig.

I want to express my deepest gratitude to my family - Mom, Dad, Grandma, Grandpa, Niuniu, Uncle, and Aunt. Your love and support are the most precious

gifts in my life. Mom, your hard work and selfless dedication have touched me deeply. You not only gave me life but also taught me wisdom and courage. Your diligence, optimism, and resilience are my eternal role models, and you have shown me that with effort, women can also achieve great success in their careers. Dad, you are the most important male figure in my life. You have always been there for me, guiding and supporting me. Your love has provided me with the safest harbor and your dedication has taught me the profound meaning of fatherly love, which is a solid foundation for my growth. Grandpa, you taught me how to treat others with kindness and patience. I have benefited greatly from your words and deeds, and I will pass on these valuable qualities. Grandma, you are my mentor in life. You have watched over my growth with love and companionship. Your wisdom and strength are my lifelong role models, and your kind smile and warm embrace are my most cherished childhood memories. Niuniu, you little cheeky, you've grown up so much! Your company, tenderness, and support have always warmed my heart. Thank you, caring boy. Uncle and Aunt, thank you for your care and concern. Your love and support are also indispensable to my growth. Thank you all, you are the most important people in my life. You have taught me to love and be loved, and have shaped me into the person I am today.我想要深深感谢我的家人们 - 妈妈、爸爸、姥姥、姥爷、牛牛、舅舅、舅妈。你们的爱和支持是我生命中最宝贵的礼物。妈妈，您的辛勤付出和无私奉献令我永生难忘和感激。您不仅给予我生命，更教会我生活的智慧与勇气。您的勤劳、乐观和坚韧是我永远的榜样，也让我明白，只要努力，女性同样可以在事业上大放异彩。爸爸，您是我生命中最重要的男性角色。您总是陪伴我、教导我，您的爱让我拥有了最安全的港湾，您的付出让我明白，父爱如山，厚重而深沉，是我成长路上坚实的依靠。姥爷，您教导我如何待人接物，让我学会了善良和耐心。您的言传身教让我受益匪浅，我也会将这份珍贵的品质传承下去。姥姥，您是我人生的导师，您用爱和陪伴守护着我成长。您的智慧和坚强，是我一生学习的榜样，您用慈祥的笑容和温暖的怀抱守护着我，您是我童年最美好的回忆。牛牛，你这个小机灵鬼，不知不觉中你都长这么大了。这些年来，你的陪伴、温柔和支持也一直温暖着我。谢谢你，小暖男。舅舅、舅妈，感谢你们一直以来对我的关心和照顾。你们的爱和支持也是我成长路上不可或缺的力量。感谢你们，你们是我生命中最重要的人，你们教会我爱与被爱，让我成为今天的自己。

My deepest gratitude goes to the most important person in my life, my love, *Karl Bastos*. We've been together a long time, and every day, you shower me with care and support. From late-night pizza deliveries during my bachelor's thesis to ice cream runs after 4 am lab sessions for my master's degree, you've always been there. When I had to drive 2 hours at midnight to some middle-of-nowhere place for field work, I was very scared, but you would come with me and sleep on the floor of the Lumbo while I was operating the lidar. Whether I'm abroad or in the field, you take over at home, making sure everything runs smoothly and caring for Ace. You tell me you love me constantly, and while I playfully try to quiet you sometimes, it never

stops you from expressing your affection. You have an uncanny ability to sense my emotions, always offering solutions when I'm down and a safe haven during storms, literally and figuratively. Your strength and caring nature are a constant source of comfort. I apologize for neglecting you and Ace at times when I was consumed by work. Thanks to you, I've learned the true importance of family, especially during Ace's illness. You're my rock, my ADC, tank, and healer in games – roles you effortlessly fulfill in real life. You shield me from worries, mend my sadness, and always give your all. Karl, your unwavering support is my pillar of strength. You've made countless sacrifices to ensure my well-being, and I'm eternally grateful. Your love is my guiding light, leading me through dark times and towards a brighter future. Your kindness, compassion, and dedication are unmatched. I am beyond lucky to have you by my side. Thank you for everything, my love.

In the end, to the memory of *Jens Rydell*. You were a brilliant scientist and a truly wonderful person. Thank you for inspiring me.

Funding

European Research Council (ERC) under the European Union's Horizon 2020 research and innovation program (Grant Agreement No. 2019-850463 Bug-Flash).

Grant holder Mikkel Brydegaard

The Royal Physiographic Society of Lund. (Grant Agreement No. 151277 - Kungl Fysiogr-22 Ivorian Lidar)

Grant holder Meng Li

The African Spectral Imaging Network (AFSIN) is funded by the International Science Program (ISP, Uppsala University) by the Swedish Development Agency (SIDA).

Grant holders Jeremie Zoueu & Carla Puglia

FORMAS. (Grant Agreement No. 2018-01061)

Grant holder Mikkel Brydegaard

References

[1] C. W. Sabrosky, "How many insects are there?," *Systematic Zoology,* vol. 2, no. 1, pp. 31-36, 1953.

[2] A. D. Chapman, "Numbers of living species in Australia and the world," 2009.

[3] N. E. Stork, "How many species of insects and other terrestrial arthropods are there on Earth?," *Annual review of entomology,* vol. 63, pp. 31-45, 2018.

[4] E. O. Wilson, "The little things that run the world (the importance and conservation of invertebrates)," ed: JSTOR, 1987, pp. 344-346.

[5] S. Lautenbach, R. Seppelt, J. Liebscher, and C. F. Dormann, "Spatial and temporal trends of global pollination benefit," *PloS one,* vol. 7, no. 4, p. e35954, 2012.

[6] S. G. Potts *et al.*, "Safeguarding pollinators and their values to human well-being," *Nature,* vol. 540, no. 7632, pp. 220-229, 2016/12/01 2016, doi: 10.1038/nature20588.

[7] A.-M. Klein *et al.*, "Importance of pollinators in changing landscapes for world crops," *Proceedings of the royal society B: biological sciences,* vol. 274, no. 1608, pp. 303-313, 2007.

[8] R. PRESCOTT‐ALLEN and C. PRESCOTT‐ALLEN, "How many plants feed the world?," *Conservation Biology,* vol. 4, no. 4, pp. 365-374, 1990.

[9] M. A. Aizen, L. A. Garibaldi, S. A. Cunningham, and A. M. Klein, "How much does agriculture depend on pollinators? Lessons from long-term trends in crop production," *Annals of botany,* vol. 103, no. 9, pp. 1579-1588, 2009.

[10] K. Y. Barragán-Fonseca *et al.*, "Insect frass and exuviae to promote plant growth and health," *Trends in Plant Science,* vol. 27, no. 7, pp. 646-654, 2022.

[11] L. H. Yang and C. Gratton, "Insects as drivers of ecosystem processes," *Current Opinion in Insect Science,* vol. 2, pp. 26-32, 2014.

[12] P. S. Barton, C. Strong, M. J. Evans, A. Higgins, and M.-M. Quaggiotto, "Nutrient and moisture transfer to insect consumers and soil during vertebrate decomposition," *Food Webs,* vol. 18, p. e00110, 2019.

[13] M. A. Jervis, G. E. Heimpel, P. N. Ferns, J. A. Harvey, and N. A. C. Kidd, "Life-history strategies in parasitoid wasps: a comparative analysis of 'ovigeny'," *Journal of Animal Ecology,* vol. 70, no. 3, pp. 442-458, 2001, doi: https://doi.org/10.1046/j.1365-2656.2001.00507.x.

[14] S. Sharma, R. Kooner, and R. Arora, "Insect pests and crop losses," *Breeding insect resistant crops for sustainable agriculture,* pp. 45-66, 2017.

[15] H. E. Tonnang, B. M. Sokame, E. M. Abdel-Rahman, and T. Dubois, "Measuring and modelling crop yield losses due to invasive insect pests under climate change," *Current Opinion in Insect Science,* vol. 50, p. 100873, 2022.

[16] G. Biswas, "Insect pests of soybean (Glycine max L.), their nature of damage and succession with the crop stages," *Journal of the Asiatic Society of Bangladesh, Science*, vol. 39, no. 1, pp. 1-8, 2013.
[17] G. Dhaliwal, V. Jindal, and A. Dhawan, "Insect pest problems and crop losses: changing trends," *Indian Journal of Ecology*, vol. 37, no. 1, pp. 1-7, 2010.
[18] L. Ji, Z. Wang, X. Wang, and L. An, "Forest insect pest management and forest management in China: an overview," *Environmental Management*, vol. 48, pp. 1107-1121, 2011.
[19] K. R. Day and S. R. Leather, "Threats to forestry by insect pests in Europe," *Forests and insects*, pp. 177-205, 1997.
[20] E. D. Ivantsova, A. I. Pyzhev, and E. V. Zander, "Economic consequences of insect pests outbreaks in boreal forests: A literature review," *Журнал Сибирского федерального университета. Гуманитарные науки,* vol. 12, no. 4, pp. 627-642, 2019.
[21] H. Eidmann, "Impact of bark beetles on forests and forestry in Sweden 1," *Journal of Applied Entomology*, vol. 114, no. 1‐5, pp. 193-200, 1992.
[22] R. Seidl, W. Rammer, D. Jäger, and M. J. Lexer, "Impact of bark beetle (Ips typographus L.) disturbance on timber production and carbon sequestration in different management strategies under climate change," *Forest Ecology and Management*, vol. 256, no. 3, pp. 209-220, 2008.
[23] E. Christiansen and A. Bakke, *The spruce bark beetle of Eurasia* (Dynamics of forest insect populations). Springer, 1988, pp. 479-503.
[24] I. Statista. "Deadliest Animals Globally by Annual Number of Human Deaths 2022." In Statista. https://www.statista.com/statistics/448169/deadliest-creatures-in-the-world-by-number-of-human-deaths/ (accessed 2024-03-12.
[25] A. R. Magalhães, C. T. Codeço, J.-C. Svenning, L. E. Escobar, P. Van de Vuurst, and T. Gonçalves-Souza, "Neglected tropical diseases risk correlates with poverty and early ecosystem destruction," *Infectious Diseases of Poverty*, vol. 12, no. 1, p. 32, 2023/04/10 2023, doi: 10.1186/s40249-023-01084-1.
[26] A. Nigusie, Z. Gizaw, M. Gebrehiwot, and B. Destaw, "Vector-Borne Diseases and Associated Factors in the Rural Communities of Northwest Ethiopia: A Community-Based Cross-Sectional Study," (in eng), *Environ Health Insights*, vol. 15, p. 11786302211043049, 2021, doi: 10.1177/11786302211043049.
[27] J. Learish. "The 24 deadliest animals on Earth, ranked." https://www.cnet.com/pictures/the-24-deadliest-animals-on-earth-ranked/ (accessed Retrieved March 24, 2019, CNET. Archived from the original on March 24, 2019).
[28] M. A. Titley, J. L. Snaddon, and E. C. Turner, "Scientific research on animal biodiversity is systematically biased towards vertebrates and temperate regions," *PLOS ONE*, vol. 12, no. 12, p. e0189577, 2017, doi: 10.1371/journal.pone.0189577.
[29] H. Moersberger *et al.*, "Europa Biodiversity Observation Network: User and Policy Needs Assessment," *ARPHA Preprints*, vol. 3, 2022, doi: 10.3897/arphapreprints.e84517.

[30] A. Petrović, "Sizing the Knowledge Gap in Taxonomy: The Last Dozen Years of Aphidiinae Research," *Insects*, vol. 13, no. 2, p. 170, 2022. [Online]. Available: https://www.mdpi.com/2075-4450/13/2/170.

[31] G. Pérez-Lachaud and J.-P. Lachaud, "Hidden biodiversity in entomological collections: The overlooked co-occurrence of dipteran and hymenopteran ant parasitoids in stored biological material," *PLoS One*, vol. 12, no. 9, p. e0184614, 2017.

[32] J. T. Huber, "Biodiversity of hymenoptera," *Insect biodiversity: science and society*, pp. 419-461, 2017.

[33] S. Köthe *et al.*, "Recommendations for effective insect conservation in nature protected areas based on a transdisciplinary project in Germany," *Environmental Sciences Europe*, vol. 35, no. 1, p. 102, 2023/11/19 2023, doi: 10.1186/s12302-023-00813-5.

[34] G. A. Montgomery, M. W. Belitz, R. P. Guralnick, and M. W. Tingley, "Standards and Best Practices for Monitoring and Benchmarking Insects," (in English), *Frontiers in Ecology and Evolution*, Review vol. 8, 2021-January-15 2021, doi: 10.3389/fevo.2020.579193.

[35] Y. Basset *et al.*, "IBISCA-Panama, a large-scale study of arthropod beta-diversity and vertical stratification in a lowland rainforest: rationale, study sites and field protocols," *Bulletin de L'Institut Royal des Sciences Naturelles de Belgique Entomologie*, 2007.

[36] Y. Basset *et al.*, "Arthropod Distribution in a Tropical Rainforest: Tackling a Four Dimensional Puzzle," *PLOS ONE*, vol. 10, no. 12, p. e0144110, 2015, doi: 10.1371/journal.pone.0144110.

[37] Y. Basset *et al.*, "Arthropod Diversity in a Tropical Forest," *Science*, vol. 338, no. 6113, pp. 1481-1484, 2012, doi: doi:10.1126/science.1226727.

[38] K. M. Staunton, L. Usher, T. Prachar, S. A. Ritchie, N. Snoad, and B. J. Johnson, "A Novel Methodology For Recording Wing Beat Frequencies of Untethered Male and Female Aedes aegypti," *Journal of the American Mosquito Control Association*, vol. 35, no. 3, pp. 169-177, 2019, doi: 10.2987/18-6799.1.

[39] I. Potamitis, I. Rigakis, and K. Fysarakis, "The electronic McPhail trap," *Sensors*, vol. 14, no. 12, pp. 22285-22299, 2014. [Online]. Available: https://res.mdpi.com/d_attachment/sensors/sensors-14-22285/article_deploy/sensors-14-22285-v3.pdf.

[40] I. Potamitis, I. Rigakis, and K. Fysarakis, "Insect biometrics: Optoacoustic signal processing and its applications to remote monitoring of McPhail type traps," *PloS one*, vol. 10, no. 11, p. e0140474, 2015. [Online]. Available: https://www.ncbi.nlm.nih.gov/pmc/articles/PMC4636391/pdf/pone.0140474.pdf.

[41] I. Potamitis and I. Rigakis, "Measuring the fundamental frequency and the harmonic properties of the wingbeat of a large number of mosquitoes in flight using 2D optoacoustic sensors," *Applied Acoustics*, vol. 109, pp. 54-60, 2016.

[42] I. Potamitis, I. Rigakis, and N.-A. Tatlas, "Automated surveillance of fruit flies," *Sensors*, vol. 17, no. 1, p. 110, 2017.

[43] D. M. UNWIN and S. A. CORBET, "Wingbeat frequency, temperature and body size in bees and flies," *Physiological Entomology*, vol. 9, no. 1, pp. 115-121, 1984, doi: https://doi.org/10.1111/j.1365-3032.1984.tb00687.x.
[44] J. Oertli, "Relationship of wing beat frequency and temperature during take-off flight in temperate-zone beetles," *Journal of experimental biology*, vol. 145, no. 1, pp. 321-338, 1989.
[45] A. R. S. Parmezan, V. M. A. Souza, I. Žliobaitė, and G. E. A. P. A. Batista, "Changes in the wing-beat frequency of bees and wasps depending on environmental conditions: a study with optical sensors," *Apidologie*, vol. 52, no. 4, pp. 731-748, 2021/08/01 2021, doi: 10.1007/s13592-021-00860-y.
[46] M. Wang, J. Wang, P. Liang, and K. Wu, "Nutritional Status, Sex, and Ambient Temperature Modulate the Wingbeat Frequency of the Diamondback Moth Plutella xylostella," *Insects*, vol. 15, no. 2, p. 138, 2024. [Online]. Available: https://www.mdpi.com/2075-4450/15/2/138.
[47] J. Huang, G. Zhang, and Y. Wang, "Effects of age, ambient temperature and reproductive status on wing beat frequency of the rice leafroller Cnaphalocrocis medinalis (Guenée) (Lepidoptera: Crambidae)," *Applied Entomology and Zoology*, vol. 48, no. 4, pp. 499-505, 2013/11/01 2013, doi: 10.1007/s13355-013-0209-z.
[48] R.-B. Xu, S.-S. Ge, W.-H. Yu, X.-K. Li, and K.-M. Wu, "Physiological and Environmental Influences on Wingbeat Frequency of Oriental Armyworm, Mythimna separata (Lepidoptera: Noctuidae)," *Environmental Entomology*, vol. 52, no. 1, pp. 1-8, 2022, doi: 10.1093/ee/nvac101.
[49] D. N. Byrne, S. L. BUCHMANN, and H. G. SPANGLER, "Relationship between wing loading, wingbeat frequency and body mass in homopterous insects," *Journal of Experimental Biology*, vol. 135, no. 1, pp. 9-23, 1988.
[50] E. Feuerbacher, J. H. Fewell, S. P. Roberts, E. F. Smith, and J. F. Harrison, "Effects of load type (pollen or nectar) and load mass on hovering metabolic rate and mechanical power output in the honey bee Apis mellifera," *Journal of Experimental Biology*, vol. 206, no. 11, pp. 1855-1865, 2003, doi: 10.1242/jeb.00347.
[51] K. Rydhmer *et al.*, "Photonic sensors reflect variation in insect abundance and diversity across habitats," *Ecological Indicators*, vol. 158, p. 111483, 2024/01/01/ 2024, doi: https://doi.org/10.1016/j.ecolind.2023.111483.
[52] N. Guilcher. "Supplementary: Study of the variation of wing thickness among species of clear winged insect." https://github.com/BioBeamMeng/InsectWBF/blob/main/InsectWingProjectData.xls (accessed 16 April 2024).
[53] B. Kim, N. Jakob Bonde, S. Martin Videbæk, H.-N. Flemming, and H. Toke Thomas, "A light trap and computer vision system to detect and classify live moths (Lepidoptera) using tracking and deep learning," *bioRxiv*, p. 2020.03.18.996447, 2020, doi: 10.1101/2020.03.18.996447.
[54] K. Bjerge, J. Alison, M. Dyrmann, C. E. Frigaard, H. M. R. Mann, and T. T. Høye, "Accurate detection and identification of insects from camera trap images

with deep learning," *PLOS Sustainability and Transformation*, vol. 2, no. 3, p. e0000051, 2023, doi: 10.1371/journal.pstr.0000051.

[55] L. Wührl *et al.*, "DiversityScanner: Robotic handling of small invertebrates with machine learning methods," *Molecular ecology resources*, vol. 22, no. 4, pp. 1626-1638, 2022. [Online]. Available: https://onlinelibrary.wiley.com/doi/pdfdirect/10.1111/1755-0998.13567?download=true.

[56] K. Thenmozhi and U. S. Reddy, "Crop pest classification based on deep convolutional neural network and transfer learning," *Computers and Electronics in Agriculture*, vol. 164, p. 104906, 2019.

[57] D. Xia, P. Chen, B. Wang, J. Zhang, and C. Xie, "Insect detection and classification based on an improved convolutional neural network," *Sensors*, vol. 18, no. 12, p. 4169, 2018.

[58] O. L. P. Hansen *et al.*, "Species-level image classification with convolutional neural network enables insect identification from habitus images," *Ecology and Evolution*, vol. 10, no. 2, pp. 737-747, 2020, doi: https://doi.org/10.1002/ece3.5921.

[59] J. Ärje *et al.*, "Automatic image‐based identification and biomass estimation of invertebrates," *Methods in Ecology and Evolution*, vol. 11, no. 8, pp. 922-931, 2020.

[60] Y. Milián-García, C. Pyne, K. Lindsay, A. Romero, and R. H. Hanner, "Unveiling invasive insect threats to plant biodiversity: Leveraging eDNA metabarcoding and saturated salt trap solutions for biosurveillance," *PLOS ONE*, vol. 18, no. 8, p. e0290036, 2023, doi: 10.1371/journal.pone.0290036.

[61] Y. Milián‐García, R. Young, M. Madden, E. Bullas‐Appleton, and R. H. Hanner, "Optimization and validation of a cost‐effective protocol for biosurveillance of invasive alien species," *Ecology and Evolution*, vol. 11, no. 5, pp. 1999-2014, 2021.

[62] J. P. Newton *et al.*, "Monitoring the birds and the bees: Environmental DNA metabarcoding of flowers detects plant–animal interactions," *Environmental DNA*, vol. 5, no. 3, pp. 488-502, 2023, doi: https://doi.org/10.1002/edn3.399.

[63] T. Saito and H. Doi, "A Model and Simulation of the Influence of Temperature and Amplicon Length on Environmental DNA Degradation Rates: A Meta-Analysis Approach," (in English), *Frontiers in Ecology and Evolution*, Original Research vol. 9, 2021-March-19 2021, doi: 10.3389/fevo.2021.623831.

[64] "GBIF | Global Biodiversity Information Facility." https://www.gbif.org/ (accessed 17th April 2024).

[65] A. Bush *et al.*, "Studying ecosystems with DNA metabarcoding: Lessons from biomonitoring of aquatic macroinvertebrates," *Frontiers in Ecology and Evolution*, vol. 7, p. 434, 2019.

[66] A. Kirse, S. J. Bourlat, K. Langen, and V. G. Fonseca, "Metabarcoding Malaise traps and soil eDNA reveals seasonal and local arthropod diversity shifts," *Scientific reports*, vol. 11, no. 1, p. 10498, 2021.

[67] C. S. Svenningsen *et al.*, "Detecting flying insects using car nets and DNA metabarcoding," *Biology Letters*, vol. 17, no. 3, p. 20200833, 2021.

[68] A. Srivathsan *et al.*, "Rapid, large-scale species discovery in hyperdiverse taxa using 1D MinION sequencing," *BMC biology*, vol. 17, pp. 1-20, 2019.
[69] A. Srivathsan *et al.*, "ONTbarcoder and MinION barcodes aid biodiversity discovery and identification by everyone, for everyone," *BMC biology*, vol. 19, pp. 1-21, 2021.
[70] B. Bruderer, "The Study of Bird Migration by Radar," *Naturwissenschaften*, vol. 84, pp. 45-54, 02/01 1997, doi: 10.1007/s001140050348.
[71] V. A. Drake and D. R. Reynolds, *Radar entomology: observing insect flight and migration*. Cabi, 2012.
[72] J. Riley, P. Valeur, A. Smith, D. Reynolds, G. Poppy, and C. Löfstedt, "Harmonic radar as a means of tracking the pheromone-finding and pheromone-following flight of male moths," *Journal of Insect Behavior*, vol. 11, no. 2, pp. 287-296, 1998.
[73] A. Smith, D. Reynolds, and J. Riley, "The use of vertical-looking radar to continuously monitor the insect fauna flying at altitude over southern England," *Bulletin of Entomological Research*, vol. 90, no. 3, pp. 265-277, 2000.
[74] J. W. Chapman, D. R. Reynolds, and A. D. Smith, "Vertical-looking radar: a new tool for monitoring high-altitude insect migration," *Bioscience*, vol. 53, no. 5, pp. 503-511, 2003.
[75] O. Ovaskainen *et al.*, "Tracking butterfly movements with harmonic radar reveals an effect of population age on movement distance," *Proceedings of the National Academy of Sciences*, vol. 105, no. 49, pp. 19090-19095, 2008, doi: 10.1073/pnas.0802066105.
[76] J. W. Chapman, V. A. Drake, and D. R. Reynolds, "Recent insights from radar studies of insect flight," *Annual review of entomology*, vol. 56, pp. 337-356, 2011.
[77] V. A. Drake and H. Wang, "Ascent and descent rates of high-flying insect migrants determined with a non-coherent vertical-beam entomological radar," *International Journal of Remote Sensing*, pp. 1-22, 2018, doi: 10.1080/01431161.2018.1519283.
[78] J. R. Riley, "Radar cross section of insects," *Proceedings of the IEEE*, vol. 73, no. 2, pp. 228-232, 1985, doi: 10.1109/PROC.1985.13135.
[79] A. Noskov, S. Achilles, and J. Bendix, "Presence and biomass information extraction from highly uncertain data of an experimental low-range insect radar setup," *Diversity*, vol. 13, no. 9, p. 452, 2021.
[80] A. Noskov, J. Bendix, and N. Friess, "A review of insect monitoring approaches with special reference to radar techniques," *Sensors*, vol. 21, no. 4, p. 1474, 2021.
[81] M. Brydegaard, A. Gebru, and S. Svanberg, "Super resolution laser radar with blinking atmospheric particles----Application to interacting flying insects," *Progress In Electromagnetics Research*, vol. 147, pp. 141-151, 2014.
[82] M. Brydegaard, "Towards quantitative optical cross sections in entomological laser radar–potential of temporal and spherical parameterizations for identifying atmospheric fauna," *PLoS One*, vol. 10, no. 8, p. e0135231, 2015. [Online]. Available: https://www.ncbi.nlm.nih.gov/pmc/articles/PMC4546581/pdf/pone.0135231.pdf.

[83] E. Malmqvist, S. Jansson, S. Török, and M. Brydegaard, "Effective parameterization of laser radar observations of atmospheric fauna," *IEEE Journal of Selected Topics in Quantum Electronics,* vol. 22, no. 3, pp. 327-334, 2015.
[84] M. Brydegaard and S. Jansson, "Advances in Entomological Laser Radar," presented at the IET Intenstional Radar Cenference, Nanjing, China, 2018.
[85] M. Brydegaard and S. Svanberg, "Photonic Monitoring of Atmospheric and Aquatic Fauna," *Laser & Photonics Reviews,* vol. 12, no. 12, p. 1800135, 2018, doi: 10.1002/lpor.201800135.
[86] H. Månefjord, "Toward Accessible Biophotonics: Instrumentation for Insect and Vegetation Applications," Ph.D. Thesis, 2024.
[87] S. Jansson *et al.*, "Real-time dispersal of malaria vectors in rural Africa monitored with lidar," *PLOS ONE,* vol. 16, no. 3, p. e0247803, 2021, doi: 10.1371/journal.pone.0247803.
[88] V. Santos *et al.*, "Dual-Band Infrared Scheimpflug Lidar Reveals Insect Activity in a Tropical Cloud Forest," *Applied Spectroscopy,* vol. 77, no. 6, pp. 593-602, 2023, doi: 10.1177/00037028231169302.
[89] M. Brydegaard, B. Kouakou, S. Jansson, J. Rydell, and J. Zoueu, "High Dynamic Range in Entomological Scheimpflug Lidars," *IEEE Journal of Selected Topics in Quantum Electronics,* 2021, doi: 10.1109/JSTQE.2021.3062088.
[90] K. Rydhmer *et al.*, "Scheimpflug lidar range profiling of bee activity patterns and spatial distributions," *Animal Biotelemetry,* vol. 10, no. 1, p. 14, 2022/04/19 2022, doi: 10.1186/s40317-022-00285-z.
[91] Z. Song *et al.*, "Application of lidar remote sensing of insects in agricultural entomology on the Chinese scene," *Journal of Applied Entomology,* vol. 144, no. 3, pp. 161-169, 2020, doi: 10.1111/jen.12714.
[92] A. S.-D. Yamoa *et al.*, "Comparative lidar assessment of insect diversity at four Ivorian habitats," *(Draft),* 2024.
[93] E. Shevtsova, C. Hansson, D. H. Janzen, and J. Kjaerandsen, "Stable structural color patterns displayed on transparent insect wings," (in eng), *PNAS,* Research Support, Non-U.S. Gov't

Research Support, U.S. Gov't, Non-P.H.S. vol. 108, no. 2, pp. 668-73, Jan 11 2011, doi: 10.1073/pnas.1017393108.
[94] A. Genoud, Y. Gao, G. Williams, and B. Thomas, "Identification of gravid mosquitoes from changes in spectral and polarimetric backscatter cross-sections," *Journal of Biophotonics,* vol. 12, p. e201900123, 06/18 2019, doi: 10.1002/jbio.201900123.
[95] H. Månefjord *et al.*, "Hyperspectral lidar for monitoring high-resolution activity patterns of African stingless bee species," *Animal Biotelemetry,* vol. 12, no. 1, p. 15, 2024/05/29 2024, doi: 10.1186/s40317-024-00372-3.
[96] S. Gunderson and R. Schiavone, "The insect exoskeleton: A natural structural composite," *JOM,* vol. 41, no. 11, pp. 60-63, 1989/11/01 1989, doi: 10.1007/BF03220386.
[97] E. Cohen, "Chitin Biochemistry: Synthesis and Inhibition," *Annual Review of Entomology,* vol. 32, no. Volume 32, 1987, pp. 71-93, 1987, doi: https://doi.org/10.1146/annurev.en.32.010187.000443.

[98] M. Brydegaard, S. Jansson, M. Schulz, and A. Runemark, "Can the narrow red bands of dragonflies be used to perceive wing interference patterns?," *Ecology and evolution*, vol. 8, no. 11, pp. 5369-5384, 2018. [Online]. Available: https://www.ncbi.nlm.nih.gov/pmc/articles/PMC6010746/pdf/ECE3-8-5369.pdf.

[99] W. Song *et al.*, "Melanin: insights into structure, analysis, and biological activities for future development," *Journal of Materials Chemistry B*, 10.1039/D3TB01132A vol. 11, no. 32, pp. 7528-7543, 2023, doi: 10.1039/D3TB01132A.

[100] M. M. A. Whitten and C. J. Coates, "Re-evaluation of insect melanogenesis research: Views from the dark side," *Pigment Cell & Melanoma Research*, vol. 30, no. 4, pp. 386-401, 2017, doi: https://doi.org/10.1111/pcmr.12590.

[101] W. B. Watt, "ADAPTIVE SIGNIFICANCE OF PIGMENT POLYMORPHISMS IN COLIAS BUTTERFLIES. I. VARIATION OF MELANIN PIGMENT IN RELATION TO THERMOREGULATION1," *Evolution*, vol. 22, no. 3, pp. 437-458, 1968, doi: 10.1111/j.1558-5646.1968.tb03985.x.

[102] J. G. Kingsolver and D. C. Wiernasz, "Seasonal Polyphenism in Wing-Melanin Pattern and Thermoregulatory Adaptation in Pieris Butterflies," *The American Naturalist*, vol. 137, no. 6, pp. 816-830, 1991, doi: 10.1086/285195.

[103] M. Brenner and V. J. Hearing, "The protective role of melanin against UV damage in human skin," (in eng), *Photochem Photobiol*, vol. 84, no. 3, pp. 539-49, May-Jun 2008, doi: 10.1111/j.1751-1097.2007.00226.x.

[104] S. Jacques, "Optical Properties of Biological Tissues: A Review," *Physics in medicine and biology*, vol. 58, pp. R37-R61, 05/10 2013, doi: 10.1088/0031-9155/58/11/R37.

[105] omlc. "Optical Absorption of Water Compendium." https://omlc.org/spectra/water/abs/index.html (accessed July, 2024.

[106] A. P. Genoud, T. Saha, G. M. Williams, and B. P. Thomas, "Insect biomass density: measurement of seasonal and daily variations using an entomological optical sensor," *Applied Physics B*, vol. 129, no. 2, p. 26, 2023/01/17 2023, doi: 10.1007/s00340-023-07973-5.

[107] T. S. Le, R. Harper, and B. Dell, "Application of Remote Sensing in Detecting and Monitoring Water Stress in Forests," *Remote Sensing*, vol. 15, no. 13, p. 3360, 2023. [Online]. Available: https://www.mdpi.com/2072-4292/15/13/3360.

[108] V. Alistair Drake, D. Mirkovic, and M. J. Steinbauer, "Insects as radar targets: size, form, density and permittivity," *International Journal of Remote Sensing*, vol. 45, no. 9, pp. 2985-3002, 2024.

[109] C. R. Vaughn, "Birds and insects as radar targets: A review," *Proceedings of the IEEE*, vol. 73, no. 2, pp. 205-227, 1985, doi: 10.1109/PROC.1985.13134.

[110] M. J. O'Donnell, "A perspective on insect water balance," *Journal of Experimental Biology*, vol. 225, no. 7, 2022, doi: 10.1242/jeb.242358.

[111] D. J. Segelstein, "The complex refractive index of water," University of Missouri--Kansas City, 1981.

[112] D. G. Stavenga, H. L. Leertouwer, T. Hariyama, H. A. De Raedt, and B. D. Wilts, "Sexual dichromatism of the damselfly Calopteryx japonica caused by a melanin-chitin multilayer in the male wing veins," *PloS one*, vol. 7, no. 11, p. e49743,

2012. [Online]. Available: https://www.ncbi.nlm.nih.gov/pmc/articles/PMC3502265/pdf/pone.0049743.pdf.
[113] C. E. Pinheiro, A. V. Freitas, V. C. Campos, P. J. DeVries, and C. M. Penz, "Both Palatable and Unpalatable Butterflies Use Bright Colors to Signal Difficulty of Capture to Predators," (in eng), *Neotrop Entomol*, vol. 45, no. 2, pp. 107-13, Apr 2016, doi: 10.1007/s13744-015-0359-5.
[114] D. G. Stavenga, A. Matsushita, and K. Arikawa, "Combined pigmentary and structural effects tune wing scale coloration to color vision in the swallowtail butterfly Papilio xuthus," *Zoological Letters*, vol. 1, no. 1, p. 14, 2015/04/24 2015, doi: 10.1186/s40851-015-0015-2.
[115] T. E. White, J. Zeil, and D. J. Kemp, "Signal design and courtship presentation coincide for highly biased delivery of an iridescent butterfly mating signal," *Evolution*, vol. 69, no. 1, pp. 14-25, 2015, doi: 10.1111/evo.12551.
[116] C. W. Mason, "Structural colors in insects. II," *The Journal of Physical Chemistry*, vol. 31, no. 3, pp. 321-354, 2002.
[117] R. INSIGHTS. https://summitchemical.com/mosquitoes-lay-their-eggs-in-standing-water/ (accessed 2024-07-11.
[118] P. Kubelka, "New Contributions to the Optics of Intensely Light-Scattering Materials. Part I," *J. Opt. Soc. Am.*, vol. 38, no. 5, pp. 448-457, 1948/05/01 1948, doi: 10.1364/JOSA.38.000448.
[119] J. Qin and R. Lu, "Measurement of the optical properties of fruits and vegetables using spatially resolved hyperspectral diffuse reflectance imaging technique," *Postharvest Biology and Technology*, vol. 49, no. 3, pp. 355-365, 2008/09/01/ 2008, doi: https://doi.org/10.1016/j.postharvbio.2008.03.010.
[120] T. Svensson, E. Alerstam, D. Khoptyar, J. Johansson, S. Folestad, and S. Andersson-Engels, "Near-infrared photon time-of-flight spectroscopy of turbid materials up to 1400 nm," *Review of Scientific Instruments*, vol. 80, no. 6, 2009, doi: 10.1063/1.3156047.
[121] P. Vukusic, B. Hallam, and J. Noyes, "Brilliant Whiteness in Ultrathin Beetle Scales," *Science*, vol. 315, no. 5810, pp. 348-348, 2007, doi: doi:10.1126/science.1134666.
[122] M. Burresi *et al.*, "Bright-White Beetle Scales Optimise Multiple Scattering of Light," *Scientific Reports*, vol. 4, no. 1, p. 6075, 2014/08/15 2014, doi: 10.1038/srep06075.
[123] M. Rebora, G. Salerno, S. Piersanti, A. Kovalev, and S. N. Gorb, "The origin of black and white coloration of the Asian tiger mosquito Aedes albopictus (Diptera: Culicidae)," (in eng), *Beilstein J Nanotechnol*, vol. 14, pp. 496-508, 2023, doi: 10.3762/bjnano.14.41.
[124] D. Fukutomi, K. Ishii, and K. Awazu, "Determination of the scattering coefficient of biological tissue considering the wavelength and absorption dependence of the anisotropy factor," *Optical Review*, vol. 23, no. 2, pp. 291-298, 2016/04/01 2016, doi: 10.1007/s10043-015-0161-y.
[125] S. Jansson, "Entomological Lidar : Target Characterization and Field Applications," PhD Thesis, Department of Physics, Lund University, Lund University, Lund University, 2020.

[126] B. K. Kouakou, S. Jansson, M. Brydegaard, and J. T. Zoueu, "Entomological Scheimpflug lidar for estimating unique insect classes in-situ field test from Ivory Coast," *OSA Continuum,* vol. 3, no. 9, 07/22 2020, doi: 10.1364/osac.387727.
[127] S. Kinoshita, S. Yoshioka, and J. Miyazaki, "Physics of structural colors," *Reports on Progress in Physics,* vol. 71, no. 7, p. 076401, 2008.
[128] M. D. Shawkey *et al.*, "Electron tomography, three-dimensional Fourier analysis and colour prediction of a three-dimensional amorphous biophotonic nanostructure," *Journal of the Royal Society Interface,* vol. 6, no. suppl_2, pp. S213-S220, 2009.
[129] J. Walther *et al.*, "Optical coherence tomography in biomedical research," *Analytical and bioanalytical chemistry,* vol. 400, pp. 2721-2743, 2011.
[130] H. Yin *et al.*, "Iridescence in the neck feathers of domestic pigeons," *Physical Review E,* vol. 74, no. 5, p. 051916, 11/22/ 2006, doi: 10.1103/PhysRevE.74.051916.
[131] R. O. Prum and R. Torres, "Structural colouration of avian skin: convergent evolution of coherently scattering dermal collagen arrays," *Journal of Experimental Biology,* vol. 206, no. 14, pp. 2409-2429, 2003, doi: 10.1242/jeb.00431.
[132] D. G. Stavenga, "Thin film and multilayer optics cause structural colors of many insects and birds," *Materials Today: Proceedings,* vol. 1, pp. 109-121, 2014.
[133] E. Shevtsova and C. Hansson, "Species recognition through wing interference patterns (WIPs) in Achrysocharoides Girault (Hymenoptera, Eulophidae) including two new species," *Zookeys,* no. 154, p. 9, 2011.
[134] M. F. Hawkes *et al.*, "Sexual selection drives the evolution of male wing interference patterns," *Proceedings of the Royal Society B: Biological Sciences,* vol. 286, no. 1903, p. 20182850, 2019, doi: doi:10.1098/rspb.2018.2850.
[135] R. O. Prum, R. Torres, C. Kovach, S. Williamson, and S. M. Goodman, "Coherent light scattering by nanostructured collagen arrays in the caruncles of the malagasy asities (Eurylaimidae: aves)," *Journal of Experimental Biology,* vol. 202, no. 24, pp. 3507-3522, 1999, doi: 10.1242/jeb.202.24.3507.
[136] A. P. Genoud, R. Basistyy, G. M. Williams, and B. P. Thomas, "Optical remote sensing for monitoring flying mosquitoes, gender identification and discussion on species identification," *Applied Physics B,* vol. 124, no. 3, pp. 1-11, 2018.
[137] S. Jansson, P. Atkinson, R. Ignell, and M. Brydegaard, "First polarimetric investigation of malaria mosquitoes as lidar targets," *IEEE Journal of Selected Topics in Quantum Electronics,* vol. 25, no. 1, pp. 1-8, 2018.
[138] A. Yoshida, M. Motoyama, A. Kosaku, and K. Miyamoto, "Antireflective nanoprotuberance array in the transparent wing of a hawkmoth, Cephonodes hylas," *Zoological science,* vol. 14, no. 5, pp. 737-741, 1997.
[139] D. G. Stavenga, J. R. Wallace, and E. J. Warrant, "Bogong Moths Are Well Camouflaged by Effectively Decolourized Wing Scales," *Frontiers in physiology,* vol. 11, p. 95, 2020. [Online]. Available: https://www.ncbi.nlm.nih.gov/pmc/articles/PMC7026391/pdf/fphys-11-00095.pdf.

[140] P. O. Vidal and L. Suesdek, "Comparison of wing geometry data and genetic data for assessing the population structure of Aedes aegypti," *Infection, Genetics and Evolution*, vol. 12, no. 3, pp. 591-596, 2012/04/01/ 2012, doi: https://doi.org/10.1016/j.meegid.2011.11.013.
[141] M. Nixon, A. Orr, and P. Vukusic, "Wrinkles enhance the diffuse reflection from the dragonfly Rhyothemis resplendens," *Journal of the Royal Society Interface*, vol. 12, no. 103, p. 20140749, 2015.
[142] S. A. Combes and T. L. Daniel, "Flexural stiffness in insect wings I. Scaling and the influence of wing venation," *Journal of experimental biology*, vol. 206, no. 17, pp. 2979-2987, 2003.
[143] T. R. Neil, Z. Shen, D. Robert, B. W. Drinkwater, and M. W. Holderied, "Moth wings are acoustic metamaterials," *Proceedings of the National Academy of Sciences*, vol. 117, no. 49, pp. 31134-31141, 2020. [Online]. Available: https://www.pnas.org/content/pnas/117/49/31134.full.pdf.
[144] X. Wang, Q. Cong, J. Zhang, and Y. Wan, "Multivariate coupling mechanism of NOCTUIDAE moth wings' surface superhydrophobicity," *Chinese Science Bulletin*, vol. 54, no. 4, pp. 569-575, 2009/02/01 2009, doi: 10.1007/s11434-009-0071-0.
[145] C. Munnerlyn and M. Latta, "Rough surface interferometry using a CO_2 laser source," *Applied Optics*, vol. 7, no. 9, pp. 1858-1859, 1968.
[146] O. Kwon, J. Wyant, and C. Hayslett, "Rough surface interferometry at 10.6 μm," *Applied optics*, vol. 19, no. 11, pp. 1862-1869, 1980.
[147] R. Basistyy, A. Genoud, and B. Thomas, "Backscattering properties of topographic targets in the visible, shortwave infrared, and mid-infrared spectral ranges for hard-target lidars," *Applied optics*, vol. 57, no. 24, pp. 6990-6997, 2018.
[148] S. Berthier, *Iridescence*. Springer, 2007.
[149] F. Stanco, S. Battiato, and G. Gallo, *Digital imaging for cultural heritage preservation: Analysis, restoration, and reconstruction of ancient artworks*. CRC Press, 2017.
[150] J. Shell, "Bidirectional reflectance: An overview with remote sensing applications & measurement," 2004.
[151] P. Vukusic, J. Sambles, and C. Lawrence, "Structurally assisted blackness in butterfly scales," *Proceedings of the Royal Society of London. Series B: Biological Sciences*, vol. 271, no. suppl_4, pp. S237-S239, 2004.
[152] E. K. Robertson, "Goniometric investigation of scattering from insect wings in near infrared," 2024.
[153] A. P. Willmott and C. P. Ellington, "The mechanics of flight in the hawkmoth Manduca sexta. I. Kinematics of hovering and forward flight," *Journal of experimental Biology*, vol. 200, no. 21, pp. 2705-2722, 1997, doi: 10.1242/jeb.200.21.2705.
[154] E. Malmqvist *et al.*, "The bat–bird–bug battle: daily flight activity of insects and their predators over a rice field revealed by high-resolution Scheimpflug Lidar," *Royal Society open science*, vol. 5, no. 4, p. 172303, 2018, doi: 10.1098/rsos.172303.

[155] T. D. Schultz and O. M. Fincke, "Structural colours create a flashing cue for sexual recognition and male quality in a Neotropical giant damselfly," *Functional Ecology*, vol. 23, no. 4, pp. 724-732, 2009.
[156] H. Cong and W. Cao, "Thin film interference of colloidal thin films," *Langmuir*, vol. 20, no. 19, pp. 8049-8053, 2004.
[157] A. N. Bashkatov and E. A. Genina, "Water refractive index in dependence on temperature and wavelength: a simple approximation," in *Saratov Fall Meeting 2002: Optical Technologies in Biophysics and Medicine IV*, 2003, vol. 5068: SPIE, pp. 393-395.
[158] S. Jansson and M. Brydegaard, "Passive kHz lidar for the quantification of insect activity and dispersal," *Animal Biotelemetry*, vol. 6, no. 1, p. 6, 2018/05/30 2018, doi: 10.1186/s40317-018-0151-5.
[159] A. Gebru, S. Jansson, R. Ignell, C. Kirkeby, J. Prangsma, and M. Brydegaard, "Multiband modulation spectroscopy for determination of sex and species of mosquitoes in flight," *J. Biophotonics*, vol. 11, no. 8, 2018.
[160] A. Moore and R. H. Miller, "Automated Identification of Optically Sensed Aphid (Homoptera: Aphidae) Wingbeat Waveforms," *Annals of the Entomological Society of America*, vol. 95, no. 1, pp. 1-8, 2002, doi: 10.1603/0013-8746(2002)095[0001:Aioosa]2.0.Co;2.
[161] K. Bjerge, J. B. Nielsen, M. V. Sepstrup, F. Helsing-Nielsen, and T. T. Høye, "An automated light trap to monitor moths (Lepidoptera) using computer vision-based tracking and deep learning," *bioRxiv*, p. 2020.03.18.996447, 2020, doi: 10.1101/2020.03.18.996447.
[162] C. Kirkeby *et al.*, "Advances in automatic identification of flying insects using optical sensors and machine learning," *Scientific Reports*, vol. 11, no. 1, p. 1555, 2021/01/15 2021, doi: 10.1038/s41598-021-81005-0.
[163] K. Rydhmer *et al.*, "Automating insect monitoring using unsupervised near-infrared sensors," *Scientific Reports*, vol. 12, no. 1, pp. 1-11, 2022.
[164] M. E. Sinka *et al.*, "HumBug–An Acoustic Mosquito Monitoring Tool for use on budget smartphones," *Methods in Ecology and Evolution*, vol. 12, no. 10, pp. 1848-1859, 2021.
[165] R. J. Bomphrey, T. Nakata, N. Phillips, and S. M. Walker, "Smart wing rotation and trailing-edge vortices enable high frequency mosquito flight," *Nature*, vol. 544, no. 7648, pp. 92-95, 2017/04/01 2017, doi: 10.1038/nature21727.
[166] M. L. May, "Wingstroke frequency of dragonflies (Odonata: Anisoptera) in relation of temperature and body size," *Journal of comparative physiology*, vol. 144, no. 2, pp. 229-240, 1981.
[167] T. Saha, A. P. Genoud, J. H. Park, and B. P. Thomas, "Temperature Dependency of Insect's Wingbeat Frequencies: An Empirical Approach to Temperature Correction," *Insects*, vol. 15, no. 5, p. 342, 2024. [Online]. Available: https://www.mdpi.com/2075-4450/15/5/342.
[168] V. Drake, "Distinguishing target classes in observations from vertically pointing entomological radars," *International Journal of Remote Sensing*, vol. 37, no. 16, pp. 3811-3835, 2016.

[169] M. Brydegaard, E. Malmqvist, S. Jansson, J. Larsson, S. Török, and G. Zhao, "The Scheimpflug lidar method," *Lidar Remote Sensing for Environmental Monitoring 2017*, vol. 10406, p. 104060I, 2017, doi: 10.1117/12.2295982.
[170] M. Brydegaard *et al.*, "Short-wave infrared atmospheric Scheimpflug lidar," in *EPJ Web of Conferences*, 2018, vol. 176: EDP Sciences, p. 01012.
[171] A. Runemark, M. Wellenreuther, H. H. Jayaweera, S. Svanberg, and M. Brydegaard, "Rare events in remote dark-field spectroscopy: an ecological case study of insects," *IEEE Journal of Selected Topics in Quantum Electronics*, vol. 18, no. 5, pp. 1573-1582, 2012.
[172] G. Zhao *et al.*, "Inelastic Hyperspectral Lidar for Profiling Aquatic Ecosystems," *Laser & Photonics Reviews*, vol. 10, no. 5, pp. 807–813, 2016.
[173] B. E. Saleh and M. C. Teich, *Fundamentals of photonics*. john Wiley & sons, 2019.
[174] V. V. Tuchin, "Tissue optics and photonics: light-tissue interaction," *Journal of Biomedical Photonics & Engineering*, vol. 1, no. 2, pp. 98-134, 2015.
[175] V. V. Tuchin, "Polarized light interaction with tissues," *Journal of biomedical optics*, vol. 21, no. 7, pp. 071114-071114, 2016.
[176] S. L. Jacques and J. C. Ramella-Roman, "Polarized light imaging of tissues," *Lasers and Current Optical Techniques in Biology*, vol. 4, pp. 591-607, 2004.
[177] S. L. Jacques, J. R. Roman, and K. Lee, "Imaging superficial tissues with polarized light," *Lasers in Surgery and Medicine: The Official Journal of the American Society for Laser Medicine and Surgery*, vol. 26, no. 2, pp. 119-129, 2000.
[178] S. L. Jacques, J. C. Ramella-Roman, and K. Lee, "Imaging skin pathology with polarized light," *Journal of biomedical optics*, vol. 7, no. 3, pp. 329-340, 2002.
[179] K. Järrendahl and H. Arwin, "Polarizing Natural Nanostructures," *Ellipsometry of Functional Organic Surfaces and Films*, pp. 247-268, 2018.
[180] N. Shashar, R. Hagan, J. G. Boal, and R. T. Hanlon, "Cuttlefish use polarization sensitivity in predation on silvery fish," *Vision research*, vol. 40, no. 1, pp. 71-75, 2000.
[181] V. Pignatelli, S. E. Temple, T.-H. Chiou, N. W. Roberts, S. P. Collin, and N. J. Marshall, "Behavioural relevance of polarization sensitivity as a target detection mechanism in cephalopods and fishes," *Philosophical Transactions of the Royal Society B: Biological Sciences*, vol. 366, no. 1565, pp. 734-741, 2011.
[182] C. W. Hawryshyn, "Mechanisms of ultraviolet polarization vision in fishes," *Sensory processing in aquatic environments*, pp. 252-265, 2003.
[183] F. Lou *et al.*, "How mantis shrimp compound eye recognizes circularly polarized light," *Authorea Preprints*, 2023.
[184] D. BRUNNER and T. LABHART, "Behavioural evidence for polarization vision in crickets," *Physiological entomology*, vol. 12, no. 1, pp. 1-10, 1987.
[185] M. Dacke, D.-E. Nilsson, C. H. Scholtz, M. Byrne, and E. J. Warrant, "Insect orientation to polarized moonlight," *Nature*, vol. 424, no. 6944, pp. 33-33, 2003.
[186] M. Dacke, "Polarized light orientation in ball-rolling dung beetles," in *Polarized Light and Polarization Vision in Animal Sciences*: Springer, 2014, pp. 27-39.

[187] B. el Jundi, J. Smolka, E. Baird, M. J. Byrne, and M. Dacke, "Diurnal dung beetles use the intensity gradient and the polarization pattern of the sky for orientation," *Journal of experimental biology*, vol. 217, no. 13, pp. 2422-2429, 2014.
[188] S. A. Jewell, P. Vukusic, and N. W. Roberts, "Circularly polarized colour reflection from helicoidal structures in the beetle Plusiotis boucardi," *New Journal of Physics*, vol. 9, no. 4, p. 99, 2007/04/23 2007, doi: 10.1088/1367-2630/9/4/099.
[189] H. Arwin, R. Magnusson, J. Landin, and K. Järrendahl, "Chirality-induced polarization effects in the cuticle of scarab beetles: 100 years after Michelson," *Philosophical Magazine*, vol. 92, no. 12, pp. 1583-1599, 2012.
[190] P. Brady and M. Cummings, "Differential response to circularly polarized light by the jewel scarab beetle Chrysina gloriosa," *The American Naturalist*, vol. 175, no. 5, pp. 614-620, 2010.
[191] L. Mei and P. Guan, "Development of an atmospheric polarization Scheimpflug lidar system based on a time-division multiplexing scheme," *Optics letters*, vol. 42, no. 18, pp. 3562-3565, 2017, doi: 10.1364/OL.42.003562.
[192] S. Zhu *et al.*, "Insect abundance over Chinese rice fields in relation to environmental parameters, studied with a polarization-sensitive CW near-IR lidar system," *Applied Physics B*, vol. 123, no. 7, p. 211, 2017/07/10 2017, doi: 10.1007/s00340-017-6784-x.
[193] S. Zhu *et al.*, "Insect remote sensing using a polarization sensitive cw lidar system in chinese rice fields," *EPJ Web of Conferences*, vol. 176, p. 07001, 01/01 2018, doi: 10.1051/epjconf/201817607001.
[194] E. Malmqvist, "From Fauna to Flames."
[195] N. J. Butterworth, T. E. White, P. G. Byrne, and J. F. Wallman, "Love at first flight: wing interference patterns are species‐specific and sexually dimorphic in blowflies (Diptera: Calliphoridae)," *Journal of Evolutionary Biology*, vol. 34, no. 3, pp. 558-570, 2021. [Online]. Available: https://onlinelibrary.wiley.com/doi/pdfdirect/10.1111/jeb.13759?download=true.
[196] F. Mattia *et al.*, "The effect of surface roughness on multifrequency polarimetric SAR data," *IEEE Transactions on Geoscience and Remote Sensing*, vol. 35, no. 4, pp. 954-966, 1997.
[197] D. Kasilingam, D. Schuler, and J.-S. Lee, "The depolarization of radar backscatter from rough surfaces due to surface roughness and slopes," in *IGARSS 2001. Scanning the Present and Resolving the Future. Proceedings. IEEE 2001 International Geoscience and Remote Sensing Symposium (Cat. No. 01CH37217)*, 2001, vol. 2: IEEE, pp. 925-927.
[198] S. Hong, "Surface roughness and polarization ratio in microwave remote sensing," *International Journal of Remote Sensing*, vol. 31, no. 10, pp. 2709-2716, 2010.
[199] U. Persson, "Measurement of surface roughness using infrared scattering," *Measurement*, vol. 18, no. 2, pp. 109-116, 1996/06/01/ 1996, doi: https://doi.org/10.1016/S0263-2241(96)00047-4.

[200] C. J. Tay, S. H. Wang, C. Quan, and H. M. Shang, "In situ surface roughness measurement using a laser scattering method," *Optics Communications*, vol. 218, no. 1, pp. 1-10, 2003/03/15/ 2003, doi: https://doi.org/10.1016/S0030-4018(03)01102-7.
[201] W. G. Egan, "Polarization and surface roughness," in *Scattering and Surface Roughness II*, 1998, vol. 3426: SPIE, pp. 144-152.
[202] H. L. Leertouwer, B. D. Wilts, and D. G. Stavenga, "Refractive index and dispersion of butterfly chitin and bird keratin measured by polarizing interference microscopy," *Optics Express*, vol. 19, no. 24, pp. 24061-24066, 2011/11/21 2011, doi: 10.1364/OE.19.024061.
[203] D. G. Stavenga, H. L. Leertouwer, D. C. Osorio, and B. D. Wilts, "High refractive index of melanin in shiny occipital feathers of a bird of paradise," *Light: Science & Applications*, vol. 4, no. 1, pp. e243-e243, 2015/01/01 2015, doi: 10.1038/lsa.2015.16.
[204] A. R. Parker, D. R. Mckenzie, and M. C. Large, "Multilayer reflectors in animals using green and gold beetles as contrasting examples," *Journal of experimental biology*, vol. 201, no. 9, pp. 1307-1313, 1998.
[205] J. A. Noyes, P. Vukusic, and I. R. Hooper, "Experimental method for reliably establishing the refractive index of buprestid beetle exocuticle," *Optics express*, vol. 15, no. 7, pp. 4351-4358, 2007.
[206] A. I. Lvovsky, "Fresnel equations," *Encyclopedia of Optical Engineering*, vol. 27, pp. 1-6, 2013.
[207] M. Born and E. Wolf, *Principles of optics: electromagnetic theory of propagation, interference and diffraction of light*. Elsevier, 2013.
[208] V. Lucarini, J. J. Saarinen, K.-E. Peiponen, and E. M. Vartiainen, *Kramers-Kronig relations in optical materials research*. Springer Science & Business Media, 2005.
[209] J. S. Toll, "Causality and the Dispersion Relation: Logical Foundations," *Physical Review*, vol. 104, no. 6, pp. 1760-1770, 12/15/ 1956, doi: 10.1103/PhysRev.104.1760.
[210] T. Sai, M. Saba, E. R. Dufresne, U. Steiner, and B. D. Wilts, "Designing refractive index fluids using the Kramers–Kronig relations," *Faraday Discussions*, 10.1039/D0FD00027B vol. 223, no. 0, pp. 136-144, 2020, doi: 10.1039/D0FD00027B.
[211] V. Lucarini, J. Saarinen, K. Peiponen, and E. Vartiainen, "Kramers-Kronig Relations in Optical Materials Research," *Kramers-Kronig Relations in Optical Materials Research, by V. Lucarini, J. Saarinen, K. Peiponen, and E. Vartiainen. X, 162 p. 37 illus. 3-540-23673-2. Berlin: Springer, 2005.*, vol. 110, 01/01 2005, doi: 10.1007/b138913.
[212] A. Paar. "Basics of refractometry." https://wiki.anton-paar.com/de-de/grundlagen-der-refraktometrie/ (accessed.
[213] D. G. Stavenga, H. L. Leertouwer, and B. D. Wilts, "Coloration principles of nymphaline butterflies–thin films, melanin, ommochromes and wing scale stacking," *Journal of Experimental Biology*, vol. 217, no. 12, pp. 2171-2180, 2014.

[214] M. Giraldo and D. Stavenga, "Brilliant iridescence of Morpho butterfly wing scales is due to both a thin film lower lamina and a multilayered upper lamina," *Journal of Comparative Physiology A*, vol. 202, no. 5, pp. 381-388, 2016. [Online]. Available: https://www.ncbi.nlm.nih.gov/pmc/articles/PMC4841846/pdf/359_2016_Article_1084.pdf.

[215] M. Khan, M. Alam, M. Masud, and A. Amin, "Importance of high order high pass and low pass filters," *World Applied Sciences Journal*, vol. 34, no. 9, pp. 1261-1268, 2016.

[216] S. M. Villarreal, O. Winokur, and L. Harrington, "The impact of temperature and body size on fundamental flight tone variation in the mosquito vector Aedes aegypti (Diptera: Culicidae): implications for acoustic lures," *Journal of medical entomology*, vol. 54, no. 5, pp. 1116-1121, 2017. [Online]. Available: https://www.ncbi.nlm.nih.gov/pmc/articles/PMC5850351/pdf/tjx079.pdf.

[217] I. E. Hendriks, "Spectrally resolved insect flashes by sunlight," 2024 2024.

[218] G. Zhao *et al.*, "Dual-band continuous-wave lidar system employed for particle classification," *To appear*, 2017.

[219] M. Zucco, V. Caricato, A. Egidi, and M. Pisani, "A hyperspectral camera in the UVA band," *IEEE Transactions on Instrumentation and Measurement*, vol. 64, no. 6, pp. 1425-1430, 2015.

[220] J. Yang, Q. Xue, J. Li, B. Han, Y. Wang, and H. Bai, "Deep ultraviolet high-resolution microscopic hyperspectral imager and its biological tissue detection," *Applied Optics*, vol. 62, no. 13, pp. 3310-3319, 2023.

[221] HySpex. "HySpex Classic SWIR-384." https://www.hyspex.com/hyspex-products/hyspex-classic/hyspex-swir-384/ (accessed 07 Jun, 2021).

[222] M. Li *et al.*, "Potential for identification of wild night-flying moths by remote infrared microscopy," *Journal of The Royal Society Interface*, vol. 19, no. 191, p. 20220256, 2022, doi: doi:10.1098/rsif.2022.0256.

[223] S.-E. Qian, "Hyperspectral satellites, evolution, and development history," *IEEE Journal of Selected Topics in Applied Earth Observations and Remote Sensing*, vol. 14, pp. 7032-7056, 2021.

[224] M. Govender, K. Chetty, V. Naiken, and H. Bulcock, "A comparison of satellite hyperspectral and multispectral remote sensing imagery for improved classification and mapping of vegetation," *Water sa*, vol. 34, no. 2, pp. 147-154, 2008.

[225] E. Bedini, "The use of hyperspectral remote sensing for mineral exploration: A review," *Journal of Hyperspectral Remote Sensing*, vol. 7, no. 4, pp. 189-211, 2017.

[226] V. E. Brando and A. G. Dekker, "Satellite hyperspectral remote sensing for estimating estuarine and coastal water quality," *IEEE transactions on geoscience and remote sensing*, vol. 41, no. 6, pp. 1378-1387, 2003.

[227] A. Bjorgan, M. Milanic, and L. L. Randeberg, "Estimation of skin optical parameters for real-time hyperspectral imaging applications," *Journal of biomedical optics*, vol. 19, no. 6, pp. 066003-066003, 2014.

[228] M. Denstedt, B. S. Pukstad, L. A. Paluchowski, J. E. Hernandez-Palacios, and L. L. Randeberg, "Hyperspectral imaging as a diagnostic tool for chronic skin ulcers," in *Photonic Therapeutics and Diagnostics IX*, 2013, vol. 8565: SPIE, pp. 71-84.

[229] L. L. Randeberg, "Hyperspectral characterization of tissue in the SWIR spectral range: a road to new insight?," in *Optical Biopsy XVII: Toward Real-Time Spectroscopic Imaging and Diagnosis*, 2019, vol. 10873: SPIE, pp. 125-140.

[230] H. P. La, Y. D. Eo, A. Chang, and C. Kim, "Extraction of individual tree crown using hyperspectral image and LiDAR data," *KSCE Journal of Civil Engineering*, vol. 19, pp. 1078-1087, 2015.

[231] Y. Shi *et al.*, "Tree species classification using plant functional traits from LiDAR and hyperspectral data," *International Journal of Applied Earth Observation and Geoinformation*, vol. 73, pp. 207-219, 2018.

[232] J. M. Medina, S. M. C. Nascimento, and P. Vukusic, "Hyperspectral optical imaging of two different species of lepidoptera," *Nanoscale research letters*, vol. 6, pp. 1-5, 2011.

[233] J. Carpenter, "Improvements in enlarging or like cameras, 1901," *British patent GB*, vol. 1139, 1901.

[234] T. Scheimpflug, "Improved method and apparatus for the systematic alteration or distortion of plane pictures and images by means of lenses and mirrors for photography and for other purposes," *GB patent*, vol. 1196, 1904.

[235] S. Svanberg, *Atomic and molecular spectroscopy: basic aspects and practical applications*. Springer Science & Business Media, 2012.

[236] E. Malmqvist, M. Brydegaard, M. Aldén, and J. Bood, "Scheimpflug Lidar for combustion diagnostics," *Optics Express*, vol. 26, no. 12, pp. 14842-14858, 2018/06/11 2018, doi: 10.1364/OE.26.014842.

[237] S. Jansson, E. Malmqvist, M. Brydegaard, S. Akesson, and J. Rydell, "A Scheimpflug lidar used to observe insect swarming at a wind turbine," *Ecological Indicators*, vol. 117, p. 106578, 10/01 2020, doi: 10.1016/j.ecolind.2020.106578.

[238] L. Mei and M. Brydegaard, "Development of a Scheimpflug lidar system for atmospheric aerosol monitoring," in *EPJ Web of Conferences*, 2016, vol. 119: EDP Sciences, p. 27005.

[239] R. Clawges, K. Vierling, L. Vierling, and E. Rowell, "The use of airborne lidar to assess avian species diversity, density, and occurrence in a pine/aspen forest," *Remote sensing of environment*, vol. 112, no. 5, pp. 2064-2073, 2008.

[240] J. Müller and R. Brandl, "Assessing biodiversity by remote sensing in mountainous terrain: the potential of LiDAR to predict forest beetle assemblages," *Journal of Applied Ecology*, vol. 46, no. 4, pp. 897-905, 2009.

[241] G. Sun, K. J. Ranson, Z. Guo, Z. Zhang, P. Montesano, and D. Kimes, "Forest biomass mapping from lidar and radar synergies," *Remote sensing of environment*, vol. 115, no. 11, pp. 2906-2916, 2011.

[242] A. Ansmann and D. Müller, "Lidar and atmospheric aerosol particles," in *Lidar: range-resolved optical remote sensing of the atmosphere*: Springer, 2005, pp. 105-141.

[243] S. R. Pal, W. Steinbrecht, and A. I. Carswell, "Automated method for lidar determination of cloud-base height and vertical extent," *Applied optics*, vol. 31, no. 10, pp. 1488-1494, 1992.
[244] A. Piroli, V. Dallabetta, M. Walessa, D. Meissner, J. Kopp, and K. Dietmayer, "Detection of Condensed Vehicle Gas Exhaust in LiDAR Point Clouds," in *2022 IEEE 25th International Conference on Intelligent Transportation Systems (ITSC)*, 8-12 Oct. 2022 2022, pp. 600-606, doi: 10.1109/ITSC55140.2022.9922475.
[245] L. Mei, T. Ma, Z. Kong, Z. Gong, and H. Li, "Comparison studies of the Scheimpflug lidar technique and the pulsed lidar technique for atmospheric aerosol sensing," *Applied Optics*, vol. 58, no. 32, pp. 8981-8992, 2019/11/10 2019, doi: 10.1364/AO.58.008981.
[246] L. Xing, W. Dai, and Y. Zhang, "Scheimpflug camera-based technique for multi-point displacement monitoring of bridges," *Sensors*, vol. 22, no. 11, p. 4093, 2022.
[247] J. Larsson *et al.*, "Atmospheric CO2 sensing using Scheimpflug-lidar based on a 1.57um fiber source," *Optics Express*, vol. 27, no. 12, pp. 17348-17358, 2019/06/10 2019, doi: 10.1364/OE.27.017348.
[248] Y. Li, K. Wang, R. Quintero-Torres, R. Brick, A. V. Sokolov, and M. O. Scully, "Insect flight velocity measurement with a CW near-IR Scheimpflug lidar system," *Optics Express*, vol. 28, no. 15, pp. 21891-21902, 2020/07/20 2020, doi: 10.1364/OE.394992.
[249] L. Müller, "Elastic hyperspectral lidar for detecting coherent backscatter from insects," Master Thesis, 2022.
[250] P. R. Hemmer *et al.*, "Standoff spectroscopy via remote generation of a backward-propagating laser beam," *Proceedings of the National Academy of Sciences*, vol. 108, no. 8, pp. 3130-3134, 2011.
[251] A. Dogariu, J. B. Michael, M. O. Scully, and R. B. Miles, "High-gain backward lasing in air," *Science*, vol. 331, no. 6016, pp. 442-445, 2011.
[252] V. Letokhov and S. Johansson, *Astrophysical Lasers* Oxford University Press, 2009, p. 304.
[253] P. Polynkin and Y. Cheng, "Air Lasing," ed: Springer, 2018.
[254] U. Westblom, S. Agrup, M. Aldén, H. Hertz, and J. Goldsmith, "Properties of laser-induced stimulated emission for diagnostic purposes," *Applied Physics B*, vol. 50, no. 6, pp. 487-497, 1990.
[255] P. Ding, M. Ruchkina, Y. Liu, M. Alden, and J. Bood, "Femtosecond two-photon-excited backward lasing of atomic hydrogen in a flame," *Opt. Lett.*, vol. 43, no. 5, pp. 1183-1186, 2018.
[256] J. Kasparian *et al.*, "White-Light Filaments for Atmospheric Analysis," *Science*, vol. 301, no. 5629, pp. 61-64, July 4, 2003 2003, doi: 10.1126/science.1085020.
[257] J. Kasparian and J.-P. Wolf, "Physics and applications of atmospheric nonlinear optics and filamentation," *Opt. Express*, vol. 16, no. 1, pp. 466-493, 2008.
[258] J.-P. Wolf, "Short-pulse lasers for weather control," *Reports on Progress in Physics*, vol. 81, no. 2, p. 026001, 2017.

[259] M. Goerke *et al.*, "Characterizing ice particles using two-dimensional reflections of a lidar beam," *Applied optics*, vol. 56, no. 19, pp. G188-G196, 2017.
[260] M. Vollmer and J. A. Shaw, "Brilliant colours from a white snow cover," *Physics Education*, vol. 48, no. 3, p. 322, 2013.
[261] U. Platt and J. Stutz, "Differential absorption spectroscopy," in *Differential Optical Absorption Spectroscopy*. Berlin, Heidelberg: Springer, 2008, pp. 135-174.
[262] M. T. Zuber *et al.*, "The Lunar Reconnaissance Orbiter Laser Ranging Investigation," *Space Science Reviews*, vol. 150, no. 1-4, pp. 63-80, 2009, doi: 10.1007/s11214-009-9511-z.
[263] R. R. Neely *et al.*, "Properties of horizontally oriented ice crystals observed by polarization lidar over summit, Greenland," in *EPJ Web of Conferences*, 2018, vol. 176: EDP Sciences, p. 05007.
[264] R. M. Schotland, K. Sassen, and R. Stone, "Observations by lidar of linear depolarization ratios for hydrometeors," *Journal of Applied Meteorology and Climatology*, vol. 10, no. 5, pp. 1011-1017, 1971.
[265] A. Tsekeri *et al.*, "Polarization lidar for detecting dust orientation: system design and calibration," *Atmos. Meas. Tech.*, vol. 14, no. 12, pp. 7453-7474, 2021, doi: 10.5194/amt-14-7453-2021.
[266] G. David *et al.*, "UV polarization lidar for remote sensing new particles formation in the atmosphere," *Optics Express*, vol. 22, no. 103, pp. A1009-A1022, 2014.
[267] J. A. Shaw *et al.*, "Polarization lidar measurements of honey bees in flight for locating land mines," *Optics express*, vol. 13, no. 15, pp. 5853-5863, 2005. [Online]. Available: https://www.osapublishing.org/oe/fulltext.cfm?uri=oe-13-15-5853&id=85242.
[268] G. Zhao *et al.*, "Particle profiling and classification by a dual-band continuous-wave lidar system," *Applied Optics*, vol. 57, no. 35, pp. 10164-10171, 2018/12/10 2018, doi: 10.1364/AO.57.010164.
[269] J. Sun *et al.*, "Evaluation of hyperspectral LiDAR for monitoring rice leaf nitrogen by comparison with multispectral LiDAR and passive spectrometer," *Scientific Reports*, vol. 7, no. 1, p. 40362, 2017.
[270] T. Hakala, J. Suomalainen, S. Kaasalainen, and Y. Chen, "Full waveform hyperspectral LiDAR for terrestrial laser scanning," *Optics express*, vol. 20, no. 7, pp. 7119-7127, 2012.
[271] Y. Chen *et al.*, "Feasibility Study of Ore Classification Using Active Hyperspectral LiDAR," *IEEE Geoscience and Remote Sensing Letters*, vol. 15, pp. 1-5, 07/31 2018, doi: 10.1109/LGRS.2018.2854358.
[272] T. Malkamäki, S. Kaasalainen, and J. Ilinca, "Portable hyperspectral lidar utilizing 5 GHz multichannel full waveform digitization," *Optics express*, vol. 27, no. 8, pp. A468-A480, 2019.
[273] H. Månefjord *et al.*, "3D-Printed Fluorescence Hyperspectral Lidar for Monitoring Tagged Insects," *IEEE Journal of Selected Topics in Quantum Electronics*, vol. 28, no. 5, pp. 1-9, 2022, doi: 10.1109/JSTQE.2022.3162417.
[274] X. Wang, Z. Duan, M. Brydegaard, S. Svanberg, and G. Zhao, "Drone-based area scanning of vegetation fluorescence height profiles using a miniaturized

hyperspectral lidar system," *Applied Physics B*, journal article vol. 124, no. 11, p. 207, October 09 2018, doi: 10.1007/s00340-018-7078-7.
[275] O. Shoshanim and A. Baratz, "Daytime measurements of bioaerosol simulants using a hyperspectral laser-induced fluorescence LIDAR for biosphere research," *Journal of Environmental Chemical Engineering*, vol. 8, no. 5, p. 104392, 2020.
[276] R. Boateng *et al.*, "Remote Vegetation Diagnostics in Ghana with a Hyperspectral Fluorescence Lidar," *IEEE Journal of Selected Topics in Quantum Electronics*, vol. 29, no. 4: Biophotonics, pp. 1-7, 2023 2023, doi: 10.1109/JSTQE.2023.3234022.
[277] M. Brydegaard *et al.*, "Lidar reveals activity anomaly of malaria vectors during pan-African eclipse," *Science Advances*, vol. 6, 05/13 2020, doi: 10.1126/sciadv.aay5487.
[278] F. Murtagh and P. Contreras, "Algorithms for hierarchical clustering: an overview," *Wiley Interdisciplinary Reviews: Data Mining and Knowledge Discovery*, vol. 2, no. 1, pp. 86-97, 2012.
[279] I. Dokmanic, R. Parhizkar, J. Ranieri, and M. Vetterli, "Euclidean distance matrices: essential theory, algorithms, and applications," *IEEE Signal Processing Magazine*, vol. 32, no. 6, pp. 12-30, 2015.
[280] M. Brydegaard *et al.*, "Towards global insect biomonitoring with frugal methods," *Philosophical Transactions of the Royal Society B: Biological Sciences*, vol. 379, no. 1904, p. 20230103, 2024, doi: doi:10.1098/rstb.2023.0103.
[281] K. Dyba *et al.*, *How Spectral Properties and Machine Learning Can Categorize Twin Species - Based on Diachrysia Genus*. 2021.
[282] T. T. Høye *et al.*, "Deep learning and computer vision will transform entomology," *Proceedings of the National Academy of Sciences*, vol. 118, no. 2, 2021.

Appendix

Guide to pinning insects for optical scanning

Here's a detailed guide on how to pin insects for the BIOSPACE scan. Remember, we need the wings flattened out to get the best normal incidence reflection when scanned at the right angle. For more visual help, we have a lot of videos on insect pinning and lidar assembly on our group YouTube channel, *@biophotonicslund653*. To the new Ph.D. and PostDoc of the lidar group, please help keep this channel alive after we leave. If you need the logins, contact me.

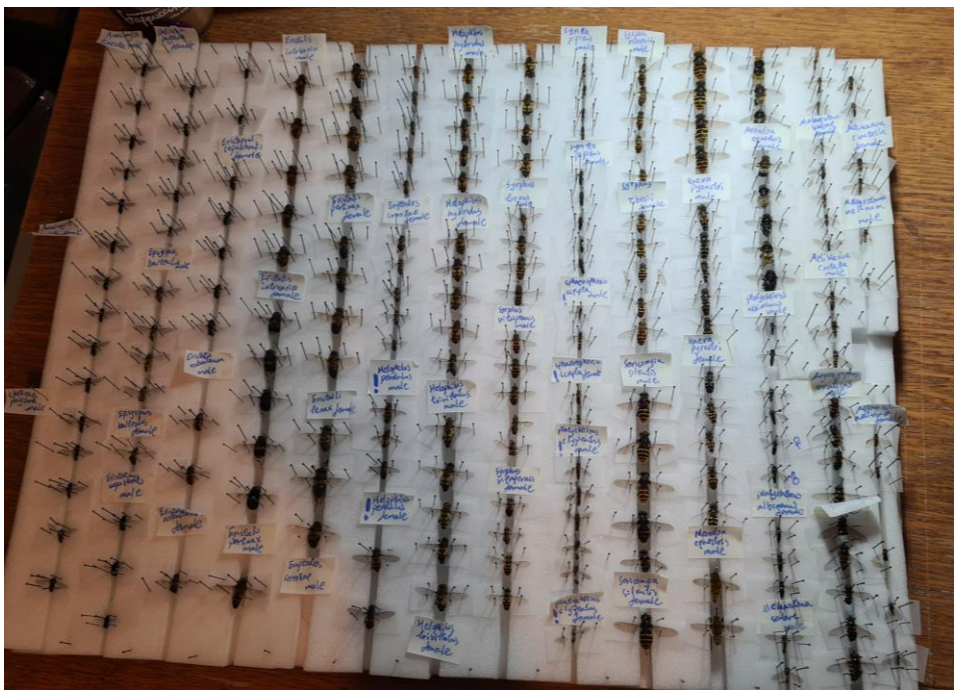

Fig. S1: Example of a finished pinning board. When borrowing samples from a museum, it is important to carefully track which individual specimen is which.

Acquisition:

Obtain insect specimens from museums, or catch them yourself, or acquire them from insect breeders. If your specimens are dry, you need to soften them in a wet chamber first.

Preparation of a Wet Chamber:

1. Build a wet chamber using a box with a lid, wet tissue paper, plastazote foam, pins, scissors, and a knife.
2. Add water to the box and place tissue paper inside. Pin the specimen onto the plastazote foam, and place the insect and flastazote foam in the box, ensuring it does not touch the water of the wet tissue paper. Close the lid and let it sit for a day.

Softening the Specimen:

After a day, check the specimen's flexibility. If it has been moistened sufficiently, the specimen will be flexible enough for further handling.

Building a Pinning Board:

1. Cut two long rectangles from plastazote foam and place them parallel to each other on a larger piece of foam.
2. Position the specimen between these rectangles, leaving a gap approximately the width of the insect's body.
3. Fix the two long rectangles with insect pins, and then push the specimen into the gap and leave the wing outside the gap and on the same plane as the two rectangle boards upper surface.

Pinning the Wings:

1. Use wing-setting tape (preferably made from baking paper) at least double or triple the size of the wing area.
2. Gently move the wings onto the side of the rectangle board and secure them with the wing-setting tape and pins. Ensure the pins do not pierce the wings themselves.

Drying:

Place the board in a dry, stable location away from direct sunlight. Allow at least two days for the specimen to dry in the desired position. This drying period ensures the wings remain in the desired configuration permanently.

Handling Beetles with Elytra:

1. Place beetles in a wet chamber for a day. No direct touch of water or wet tissue.

2. Use a needle or tweezers to gently open the elytra (hardened wing covers) to expose the wings underneath.
3. Follow the same wing-pinning procedure as with other insects.
4. When pinning beetle wings, extra care is needed due to the complex folding within the elytra, requiring patience to avoid damaging the wings.

Re-pinning for Different Scans:

1. For most museum specimen collection, the pin is through the specimen's thorax.
2. For scans requiring the frontal plane view, remove the pin from the thorax and re-pin the specimen through its anteroposterior.

Handling Fresh Specimens:

1. Freeze fresh or live insects for at least half a day.
2. After freezing, place them on dry tissue to prevent moisture absorption.
3. Since these specimens do not require a wet chamber, proceed with pinning directly.













Printed by Media-Tryck, Lund 2024
NORDIC SWAN ECOLABEL 3041 0903

LUND UNIVERSITY

Department of Physics

LRCP 257
ISBN 978-91-8104-153-8
ISSN 1102-8718
ISRN LUTFD2/TFCP-257-SE